Identification of Cancer-Specific Essential Genes in Glioblastoma Multiforme

Christopher G. Hubert

A dissertation

submitted in partial fulfillment of the

requirements for the degree of

Doctor of Philosophy

University of Washington

2012

Reading Committee:

James Olson, Chair

Patrick Paddison

Dusty Miller

Program Authorized to Offer Degree:

Molecular and Cellular Biology

University of Washington

Abstract

Identification of Cancer-Specific Essential Genes in Glioblastoma Multiforme

Christopher G. Hubert

Chair of the Supervisory Committee:

Professor James M. Olson

Pediatrics, Division of Hematology/Oncology, FHCRC

Glioblastoma multiforme (GBM) is the most common and aggressive type of brain cancer and is notoriously drug and radiation resistant. Current therapies and trials have repeatedly failed to substantially increase the survival of patients over the last two decades. Although new therapeutic approaches are urgently needed, sophisticated strategies to identify novel GBM therapies have been precluded by several biological and technical barriers. First, established GBM cell lines poorly represent human glioblastoma. Second, powerful gene discovery and manipulation tools were not yet developed or applied to GBM. To overcome these historic challenges, we have applied both focused and genome-wide functional genetic screening

techniques to multiple primary glioma stem cell (GSC) cultures that accurately model essential elements of this disease, as well as normal neural stem cells (NSCs).

From these unbiased screens, we show that GSCs have an added requirement for the mitotic spindle checkpoint BUB1B to suppress lethal consequences of altered kinetochore function. Specifically, the activity of the Gle2-binding-sequence (GLEBS) domain within BUB1B is required to suppress lethal kinetochore-microtubule attachment defects in GBM isolates and genetically transformed cells. We also identified the pre-mRNA splicing protein PHF5A as a key GSC-specific essential gene. PHF5A knockdown or pharmacologic inhibition of its complex triggers a G2/M arrest in GSCs but not in NSCs or other untransformed cells. We show that PHF5A facilitates recognition of exons with unusual C-rich 3' splice sites and its suppression results in the cancer-specific mis-splicing of thousands of genes. PHF5A suppression compromises GBM tumor formation and maintenance in vivo and results in the regression of established GBM tumors. Rather than being isolated to GSCs, this sensitivity to splicing inhibition is conferred by Ras-mediated transformation of multiple normal cell types, suggesting that a therapy targeting PHF5A may be applicable to a wide range of cancer types.

Table of Contents

List of Figures

List of Tables

ACKNOWLEDGEMENTS

This thesis work has been truly collaborative and I am grateful to so many people who have helped me along the way.

I have been lucky enough to have two excellent advisors mentoring me throughout most of my time in graduate school. First, my primary mentor, Jim Olson, has been a miraculous combination of scientific advisor, critic, cheerleader, role model, and friend. I am so fortunate that I stumbled into his lab in my first year and that I have had the chance to learn from and experience how Jim bridges the medical, research, and corporate fields. In another wonderful stroke of serendipity, my co-mentor, Patrick Paddison, joined the Hutchinson Center part way through my graduate career. With Jim's enthusiastic support, I seized the chance to work with him, and rather than a simple collaborator Patrick became a true second mentor for me. I appreciate the time he has dedicated to teaching me scientific strategies that are both deep and broad, then how to raise those findings to the next level. I hope I can one day learn to emulate his ability to build collaborative research projects and to make novel and unbiased discoveries in the field.

All my labmates in both the Olson and Paddison labs have been a great source of support. In particular, I am hugely indebted to Yu Ding for his knowledge, experience, patience, and advice throughout this project work. He cheerfully and tirelessly led the screening work in our lab, paving a road for the rest of us to follow, and he solidly and tenaciously led the work on BUB1B. Thanks to Rob Bradley for joining our team and for lifting our work to a higher level through his hard work analyzing RNA isoforms. Thanks to Chad Toledo for his assistance, humor, encouragement, and good cheer. Thanks to Rich Klinghoffer, Andy Strand, Beth Villavicencio, and especially Jason Berndt for your repeated lessons and good advice through my graduate career. Finally, many thanks to the excellent Olson lab mouse team, especially Sally Ditzler, Stacey Hansen, Emily Girard, Kyle Pedro, and Andrew Richards for your training, advice, and help over many years.

Thank you to my thesis advisory committee members, Dusty Miller, Jon Cooper, Bruce Clurman, and Rick Morrisson, for all of their time, encouragement, and useful advice.

I big piece of my enjoyment and success through grad school has come from the support, advice, and companionship of my friends here. Thank you all for both your scientific help when I needed it for work, and for the coffee, tea, movies, dinners, and hiking trips when I needed to get away from work. A special thanks to Stephanie Bush for her friendship, kindness, and cheer through so many days and holidays since our beginning here.

Thanks to all my family, who have had to trade hugs for phone calls, for your understanding and support during my graduate career. I hope we will be visiting you much more now!

Finally thank you to my lovely wife Erin for all the days she waited without complaint while I finished experiments, for taking care of me, and for all the fun we've had together. I appreciate her support and love more than anything.

DEDICATION

To Mary Glover

October 12, 1964 - November 20, 1996

The death of my cousin Mary at age 32 to advanced astrocytoma is part of the reason that I became interested in cancer research. I am proud to continue her fight against this disease.

Chapter 1 – Introduction

I. A Stem Cell Origin of Glioblastoma

Over the past decade, multiple mouse models of glioblastoma have been developed by altering components of RTK/Ras/PI3K, p53, and Rb signaling (Fomchenko and Holland, 2006; Holland, 2001). In vivo and in vitro experiments have suggested that these alterations force either neural stem cells (NSCs), neural progenitors, or astrocytic cells into an undifferentiated NSC-like state as well as driving continued growth (Bachoo et al., 2002; Zheng et al., 2008a, b). Although it may be possible for differentiated cells to dedifferentiate and become stem-like (Bachoo et al., 2002; Takahashi et al., 2007; Yu et al., 2007), the known hierarchical organization of adult and pediatric brain tumors is suggestive of a cancer stem cell origin (Galli et al., 2004; Hemmati et al., 2003; Singh et al., 2003; Singh et al., 2004). The concept that stem cells underlie some types of cancer was initially studied in leukemias (reviewed in Huntly and Gilliland, 2005; Lapidot et al., 1994; Wang and Dick, 2005). More recently, increasing evidence has suggested that many solid tumors including glioma (Singh et al., 2003) and cancers of the breast (Al-Hajj et al., 2003), pancreas (Li et al., 2007), and other origins harbor a subset of highly tumorigenic cancer cells that share many of the developmental programs and features of their normal stem cell counterparts. Cancers are not always driven by a rare stem cell subpopulation (Kelly et al., 2007; Quintana et al., 2008) but the view of cancer as a disease of stem and progenitor cells has put a greater focus on the putative cell of origin from which brain tumors are thought to arise.

The two opposing views in the field are that glioblastomas arise either: a) from a primitive neural stem or progenitor cell that loses the ability to control its proliferation, or b)

from a relatively mature and committed astrocytic cell that becomes transformed and dedifferentiates into a more primitive stem-like state (Dietrich et al., 2008; Dirks, 2008; Stiles and Rowitch, 2008; Vescovi et al., 2006). Recent mouse studies have helped to address these diverging views. Deletion of the key tumor suppressor genes PTEN, p53, and/or NF1 specifically in NSCs causes aggressive glioblastoma with high frequency (Alcantara Llaguno et al., 2009; Kwon et al., 2008; Llaguno et al., 2008; Zheng et al., 2008b; Zhu et al., 2005) and viral induction of glioblastoma in vivo showed that these cancers originate from areas of the brain containing NSCs and rarely from stem cell poor areas (Alcantara Llaguno et al., 2009; Llaguno et al., 2008; Marumoto et al., 2009). Whether an NSC is the *exclusive* cell of origin for glioblastoma is a burning question in the field that is still debated, but the *most likely* source of most glioblastoma is a normal NSC whose progeny accumulate genetic mutations promoting their overall proliferation and survival. The salient point, regardless of the exact cell of origin of an individual patient's or mouse's tumor, is that glioblastoma-initiating cells are functionally and pathologically stem cell like.

II. GBM Models

Much of what we know about biology, cancer, and disease treatments has come from studying human and animal cells cultured in the lab. Tissue culture cell lines, including most cell lines established from glial tumors, are traditionally grown in a buffered saline medium such as DMEM, with the addition of antibiotics and serum. It is unknown exactly what nutrients and stimuli are presented to the cells by each varying batch of serum, nor how well this recapitulates a cell's in vivo environment. Through the selection and evolution, many cancer cells are able to

adapt to in vitro growth and become established cell lines. This process presents a greater challenge to some cell types than others and is an especially higher barrier to cells of the nervous system, which are normally protected from the influence of serum compounds by the blood brain barrier. This presents a barrier to establishing neural and GBM cultures because stem cells from the nervous system tend to terminally differentiate and senesce rather than proliferate upon exposure to serum (Gage et al., 1995).

Despite the challenges in adapting to serum culture growth, many astrocytoma and glioblastoma cell lines have been established to date and continue to yield valuable information about glioma biology. Recently, however, scientists have begun to question how faithfully these culture models represent the original tumors. A series of studies from the Howard Fine's lab at the NIH has shed light on the genetic aberrations present in serum cultured glioblastoma cell lines and the changes that occur when cells isolated from primary glioblastomas are cultured under either a) conditions optimal for the propagation of normal NSCs (defined medium culture utilizing serum free neurobasal media supplemented with growth factors) or b) standard conditions for growth of established glioma and many other cell lines (DMEM containing 10% fetal bovine serum). Hierarchical analysis of gene expression and principal component analysis found that both neural stem cells and the primary glioblastoma cells grown in defined media clustered closely with the parental tumors. In contrast, established GBM cell lines and primary GBM isolates cultures in serum clustered away from the parent tumors (Lee et al., 2006). Very low passage primary serum cultured glioblastoma cells were found to be in an intermediate state between the two indicating a change over time as the cells adapted to serum culture. Whereas the primary GBM cultures in defined media maintained a near-diploid chromosome count, their serum cultured counterparts displayed complex karyotypes and were predominantly

pseudotriploid or tetraploid (Lee et al., 2006). Serum-cultured glioblastoma cells were in fact found to have more similarity to a panel of cultured lung, breast, bone, and skin cancer cell lines than to a panel of 83 clinical glioblastomas (Li et al., 2008).

An important advance in glioma research is the recent establishment of tumor-initiating GBM stem cells (GSCs) isolated from patients. These primary cultures retain the developmental potential and specific genetic alterations found in the original tumor (Hemmati et al., 2003; Lee et al., 2006; Pollard et al., 2009; Singh et al., 2003). Accordingly, there is less chance that the underlying molecular signals have changed compared to the original primary glioblastoma. Also, GSCs are grown adherently, allowing them to be used for chemical or genetic screens. Importantly, both GSCs and neural stem cells (NSCs) can be grown and faithfully maintained under these conditions (Pollard et al., 2009; Sun et al., 2008) and mirror each other's characteristics including the expression of neural markers Nestin and Sox2 (Gangemi et al., 2009; Mangiola et al., 2007), migration within the brain (Sanai et al., 2005), self-renewal and multilineage differentiation (Fael Al-Mayhani et al., 2009; Galli et al., 2004), similar gene expression profiles (Lee et al., 2006) and responsiveness to similar signaling cues (Piccirillo et al., 2006). Moreover, NSCs represent a possible cell of origin for GBM (Al-Hajj et al., 2003; Alcantara Llaguno et al., 2009; Dietrich et al., 2008; Dirks, 2008; Sanai et al., 2005; Vescovi et al., 2006). NSCs are isolated and grown in the same serum-free conditions, have similar expansion rates and developmental potential as GSCs, but retain a normal karyotype and are not tumorigenic (Sun et al., 2008). These attributes create an ideal screening system for the identification of specific glioblastoma-lethal gene targets (Goidts et al., 2012).

III. Synthetic lethal screening

Glioblastoma and NSCs rely on similar molecular signaling pathways, especially RTK/Ras/PI3K signaling, for their growth. The high-level proliferative signaling present in many cancer cells gives rise to elevated pro-apoptotic signaling in that cell, the effects of which must be in turn suppressed by the overwhelming oncogenic survival signaling for the cancer cell to survive. This creates a scenario, often termed "oncogene addiction" where the cancer cells require continuation of their proliferative signaling for survival, whereas normal cells do not (reviewed in Luo et al., 2009b). The cancer cells are therefore more sensitive to loss of their addictive proliferative signal than normal cells would be, creating an ideal target for treatment. The concept of synthetic lethality can provide a framework to identify and exploit such unique differences between cancers such as GBM and normal cells. Two conditions are considered to be "synthetic lethal" if either one alone is tolerable but their combination leads to cell death (Kaelin, 2005). In cancer therapy, the goal is to identify a synthetic lethal relationship that comes into play only in the cancer cells and avoids lethality in normal tissues. Such a combination may yield an increased therapeutic window when treating a patient compared to the standard additive effects of drugs that hit all cells equally. Examples of synthetic-lethal relationships in cancer therapy include BRCA deficiency combined with PARP inhibition (Bryant et al., 2005) and PTEN loss combined with mTOR inhibition (Neshat et al., 2001).

Synthetic lethal interactions can be discovered and explored through hypothesis-driven research based on known functions of proteins. However, to make novel discoveries in a systematic and unbiased way we must turn to an alternate approach such as functional genomic screening. High throughput screens can be performed in either arrayed or pooled format. Arrayed screens are usually performed in multi-well plates and have the great advantage that each experimental test is distinct and separate. This enables a direct readout for each drug, siRNA, or

virus tested on the cells. Since the number of wells in a multi-well plate is relatively small, the scale of the screen is constrained by the number of plates that can be manipulated at one time. This number is usually limited by lab infrastructure, available robotics, and cost. Conversely, pooled screens utilizing shRNA-expressing viruses can be performed with tens-of-thousands of silencing constructs in parallel. This is done by infecting the target cells with approximately one construct per cell and growing the cells together in large culture plates. Here, in addition to biological noise, statistical noise generated from random events in the population can become significant. To ensure the success of the screen, a critical minimum fold-representation of each construct must be maintained throughout the screening process. This number dictates the necessary scale of a pooled screen. The major difficulty of pooled screening strategies is often deconvoluting the results after the screen is completed. However, this can be accomplished by examining unique genetic sequences in each construct either through the use of DNA microarrays (Paddison et al., 2004; Silva et al., 2005; Silva et al., 2008) or through next-generation DNA sequencing technologies (Erlich et al., 2009).

Systemic cancer therapies must target molecular vulnerabilities that neoplastic cells differentially rely upon due to some property of their transformed state such as growth rate, metabolism, or oncogene/non-oncogene addictions. Recently, multiple studies have attempted to define such cancer-lethal targets through large scale loss-of-function screens in either wide panels of cancer cell lines or engineered isogenic cancer line pairs (Barbie et al., 2009; Brough et al., 2011; Cheung et al., 2011; Luo et al., 2009a; Marcotte et al., 2012; Scholl et al., 2009). To reduce the number of identified hits simply required for the growth and proliferation of all cells, screening studies generally compare the effect of a potential hit between defined populations of cultured cancer cells and select genes whose loss is harmful to some of the cancers tested but not

harmful to others. Here the essential goal of identifying a target differentially required for cancer cell growth but not by similar normal cells has been lost.

Studies performing primary screen comparisons between cancer and related unimmortalized normal cells are exceedingly rare (Goidts et al., 2012), and none have done so on a genome-wide scale. There are many reasons for this discrepancy including the scarcity and growth difficulties of untransformed unimmortalized human cells. However, comparison based on the relative change in fitness between subtypes of cancer cells *must* choose targets that are *not lethal* to many cancer samples. This strategy also makes it difficult to define whether an observed requirement for a gene is due to vulnerability in one group versus resistance in the other. This uncertainty leaves in question the possibility for a therapeutic window in a patient.

Here, I have identified novel and essential glioblastoma gene and protein targets with an increased potential for a therapeutic window. I have employed functional genomic screens utilizing two differing strategies to accomplish this goal. First, since PI3-kinase inhibitors show some specificity for GBM, I investigated kinase genes whose inhibition could be synthetic-lethal in the context of PI3K inhibition. From these genes, I identified HSP90 as a target whose inhibition enhances the efficacy of targeted PI3-kinase drugs. Second, I and colleagues performed both focused and genome-wide loss-of-function screens to compare genes that are essential in primary glioblastoma stem cell cultures with those that are essential in normal neural stem cell cultures. The extreme similarity of these control and cancer cell types has allowed me to identify genes whose necessity is highly specific to the transformed state of a glioblastoma cell. I and collaborators led by Yu Ding in Patrick Paddison's lab utilized a focused kinome-screen in GSC isolates and NSCs to identify the mitotic spindle kinase BUB1B/BUBR1 as a cancer-lethal target. We show that in transformed cells, but not normal cells, BUB1B's GLEBS

domain activity is required to suppress lethal kinetochore-microtubule instability. Finally, through multiple focused and genome-wide functional screens in GSCs and NSCs, I and collaborators have identified the pre-mRNA splicing factor PHF5A whose expression is differentially required for GSC growth and survival both in vitro and in vivo. PHF5A is necessary for the splicing machinery of a transformed cell to recognize an unusual class of C-rich 3' splice sites present in many essential genes and cell cycle regulators. Loss of PHF5A results in G2/M cell cycle arrest and subsequent cell death only in GSCs or Ras-transformed cells and not NSCs or normal cell controls.

Chapter 2 – Identification of PI3-kinase and HSP90 combination therapy for glioblastoma multiforme

I. ABSTRACT

Glioblastoma is the most deadly form of brain cancer with an average survival time of 12-14 months after diagnosis. Current therapies have done little to improve the survival of patients in part because parallel signaling pathways and redundancies present in cells allow their continued viability even when one piece is compromised. Although these molecular signaling "work-arounds" can confer drug resistance upon cancer cells, they could also, if properly exploited, render the cancer cells vulnerable to combination therapies.

We have utilized functional genomic screening to determine kinases whose inhibition enhances the therapeutic strategy of PI3-kinase inhibition in glioblastoma cells. From these candidate hits, we identified the molecular chaperone protein HSP90 whose inhibition had additive or supra additive antitumor effects in vitro and in vivo. In vivo studies revealed that although PI3-kinase and HSP90 dual inhibition had clear therapeutic benefit in terms of tumor size, dose limiting toxicity prevented this combination strategy from having any increased benefit over higher-dose single agents. The lack of differential effect of dual PI3-kinase and HSP90 inhibition between primary GBM cultures and normal neural stem cells suggests that this combination is unlikely to be effective against clinical glioblastoma in general.

II. INTRODUCTION

Malignant glioma is the most common and lethal form of brain cancer (CBTRUS, 2011). Glioblastoma multiforme (GBM) is the most invasive and aggressive grade of glioma and is notoriously drug and radiation resistant. Current therapies and trials using single agents have repeatedly failed to substantially increase the survival of patients over the last two decades (Asbury). New combination therapies could have the potential to affect treatment efficacy by exploiting synergies between drugs. However, it is crucial to develop therapies that are effective against the tumor but also have little negative effect in the body's normal cells, giving clinicians the maximum possible therapeutic window between the necessary effective dose and toxicity. The ideal treatment would be a pairing of drugs that function synergistically only within a glioblastoma cell but not in the rest of the body.

Finding such cancer specific combinations requires identifying unique molecular differences between tumor cells and normal cells. The molecular signaling mechanisms that drive glioblastoma growth are also conserved across a wide range of cells in many organisms. On the cell membrane, receptor tyrosine kinases (RTKs) are activated upon growth factor binding and in turn activate downstream signaling proteins, including Ras and PI3K, which instruct a cell to grow and survive (Shaw and Cantley, 2006). The tumor suppressor PTEN opposes this activation of PI3-kinase (PI3K) and its deletion causes hyperproliferation through overactive PI3K signaling (Groszer et al., 2001). PI3K in turn activates AKT which signals for cell cycle progression, resists apoptotic death signals, and activates numerous other proteins, including mTOR. mTOR activation increases a cell's protein synthesis ability and supports proliferative signaling (Shaw and Cantley, 2006). Recently, two independent groups performed full genomic sequencing and characterization of more than 200 glioblastoma tumor samples (Parsons et al., 2008; TCGA, 2008). These unbiased analyses found genetic alterations in the

RTK/Ras/PI3K signaling cascade and the p53 and Rb tumor suppressor pathways in 88%, 87%, and 78% of tumor samples, respectively (TCGA, 2008). The formation and stability of many of these signal transduction complexes is supported by the chaperone HSP90 which serves to increase their interaction ability and protects them from degradation (Whitesell and Lindquist, 2005). Although its function is not required for normal cell survival, HSP90 has the capacity to serve as a buffer for signaling complexes, allowing them to continue functioning in less than ideal circumstances like cellular stress or in the presence of mutations. Thus, in addition to its role buffering normal cell interactions, it can also facilitate the stability and interaction of oncogenic signaling in a variety of cancers (reviewed in Whitesell and Lindquist, 2005).

Our increasing knowledge of these oncogenic signaling cascades has presented a variety of potential targets to attack with cancer therapies but has also emphasized the complexity that makes successful cancer treatment so difficult. Parallel signaling pathways and redundancies present in cells allow their continued viability even when one piece is compromised. In the case of cancer therapies, this can mean that a potent and specific drug may be effective against its one target but ineffective at shutting down the overall oncogenic signal driving proliferation. For instance, suppression of mTOR, a downstream target of PI3K, has the paradoxical effect of increasing PI3K signaling by removing an mTOR dependent negative feedback loop (Cloughesy et al., 2008; Peterson et al., 2009; Sabatini, 2006). Such notions have stimulated interest in inhibitors of signaling network hubs, such as PI3K, as well as drugs specific to multiple targets.

The drug PI-103 is a dual-specificity inhibitor of PI3K and mTOR that has shown significant efficacy against several cancers in vitro and in vivo, including glioblastoma (Fan et al., 2007; Fan et al., 2006; Fan and Weiss, 2006; Raynaud et al., 2007). Use of this dually-specific drug also eliminates the negative feedback loop between PI3K and mTOR which can

severely blunt targeted therapies against this pathway (Cloughesy et al., 2008; Fan and Weiss, 2006). When a panel of 38 popular kinase inhibitors was quantitatively tested against a library of 317 human kinases, PI-103 was found to be one of the most specific and selective for its targets, showing significantly better specificity than even many drugs in approved clinical use (Karaman et al., 2008). In addition, several preclinical trials have proven PI103 an effective, although likely cytostatic rather than cytotoxic, therapy against glioblastoma cell lines including PTEN mutant glioblastoma. In these studies dosing was well tolerated by mice at levels sufficient to suppress xenograft growth (Fan et al., 2007; Fan et al., 2006).

To discover genes synthetic-lethal with PI3K inhibition in GBM, we performed pooled chemical-genetic screening using a viral shRNA library in glioblastoma cells treated with a low dose of the PI3K inhibitor PI-103. We identified a set of candidate gene targets whose inhibition was only detrimental to GBM cells in the context of PI3K inhibition, not in control cells. These targets included HSP90 and were further enriched for genes known to bind HSP90. HSP90 inhibition was validated pharmacologically to enhance the effect of PI3K inhibition in vitro. PI3Kinase and HSP90 inhibitors likewise had additive effects in vivo tumor xenografts, but also showed increased toxicity. Further in vitro experiments in primary glioblastoma stem cell isolates demonstrated a consistent but small increased effect from PI3K and HSP90 inhibitor combination. These data suggest that PI3-Kinase and HSP90 combination therapy is unlikely to be effective in clinical glioblastoma.

III. RESULTS

An RNAi kinome screen for genes that sensitize glioblastoma cells to PI3-kinase inhibition

It is not known what genes may be synthetic lethal with PI3k inhibition in glioblastoma. We therefore chose to use pooled functional genetic screening as an unbiased approach to target identification. To begin the screen, we produced a viral pool containing an shRNA library targeting the set of human kinase genes. The screen was carried out on a scale that represented each hairpin approximately 800 times in the target cell population, well in excess of the minimum level necessary to silence statistical noise below the threshold of our microarray detection method. We productively infected U87-MG cells at an MOI below 0.3 to ensure a high probability that infected target cells will contain no more than one integrated construct and selected stable integrants with puromycin. Triplicate populations of cells with or without a GI50 dose of PI-103 were passaged and maintained under selective conditions for two weeks, encompassing approximately 10 cell doublings. After this selective phase, we isolated DNA from the remaining cells and amplified the viral inserts containing each barcode by PCR. The resultant PCR fragments were purified by gel electrophoresis and sent to the FHCRC array facility for fluorescent labeling and hybridization with barcode arrays. (Figure 2.1)

Since our chosen dose of drug partially but non-lethally suppresses the PI3-kinase pathway through its key effector PI3K, and since the suppression of additional PI3K signaling members by shRNA is likely to decrease total PI3K pathway beyond this sub-lethal threshold, we expected to find enrichment for known members of the RTK/Ras/PI3K signaling pathway. We indeed did see a large number of these expected "positive control" canonical signaling proteins in our set of primary screen hits. (Figure 2.2A) These included 11 receptor tyrosine kinases and 12 known members of the Ras-MAPK signaling cascade, some of which may be successful candidates for increasing the potency of PI3K inhibition, as has already been

demonstrated for EGFR (Fan et al., 2007). Since most of these are highly conserved pathway members, it is likely that their dual-inhibition will affect the growth and survival of many cells in addition to glioblastoma, greatly reducing the likelihood of a potential therapeutic window targeting these proteins.

HSP90 inhibition has additive effects with PI3K inhibition in glioma cells in vitro

One synthetic lethal hit in particular, HSP90, holds promise for a selective combination therapy. HSP90 is necessary for buffering within stressed and mutated cancer cells, but is expendable, at least temporarily, in normal cells. Furthermore, suppression of HSP90 function can increase the degradation of activated signaling complexes by the proteasome (Whitesell and Lindquist, 2005). Such an increased decay of active oncogenic signaling, combined with inhibition of an "addicted" oncogenic pathway, could increase any subsequent apoptotic response beyond removal of the addictive growth signal alone (Kaelin, 2005). To determine if our set of primary screen hits was significantly enriched for genes encoding proteins known to interact with HSP90, we compared this gene set to the set of known HSP90 interaction partners maintained by the Picard lab (Picard). The overlap between these sets was highly significant (p-value = 0.00478, Figure 2.2B). Since HSP90 often serves to maintain the expression level and function of its client proteins, this raises the possibility that in addition to enhancing the effect of PI3K inhibition on its own, HSP90 inhibition could have a ripple effect able to invoke multiple other synthetic lethal interactions with PI3K inhibition.

As an orthogonal method of validation, and because shRNA silencing sequences can have off target effects, we next chose to validate the potential combination of HSP90 suppression with PI-103 treatment using the well characterized pharmacologic inhibitor of HSP90, 17-AAG.

To do this we first determined the approximate effective dose range for each drug in U87-MG cells and then tested the drugs alone or in combination over this range. We observed a clear additive effect from PI3K + HSP90 dual-inhibition throughout the dose range, determined an EC50 dose of the combination at approximately 1/3 the dose of either individual drug, and achieved a maximal inhibitory dose at approximately 1/3 that needed from either individual drug (Figure 2.2C). These results pharmacologically validate HSP90 as a PI3K-sensitizing screen hit. We further tested the same drug combination over the same dose range in the karyotypically normal fibroblast line IMR90 (Nichols et al., 1977). In these untransformed cells there was no increased effect from the combination compared to PI-103 alone (Figure 2.2D). There was also strikingly little effect over most of the dose range from 17-AAG alone, however the lack of any additive effect does not stem from a complete lack of 17-AAG effect in IMR90s. Even at the maximal dose of 17-AAG where the cells experience a 40% viability loss, there was no detectable decrease in viability from the combination treatment compared to PI-103 alone (Figure 2.2D). This suggests that the additive drug effects are specific to the glioma cells and may not be generalizable to normal cells such as fibroblasts.

The combination of HSP90 and PI3K inhibitors has increased anti-tumor effects in vivo

Given our promising results from PI3K and HSP90 inhibitor combinations in vitro, and given the fact individual HSP90 and PI3K inhibtors are undergoing human clinical trials for various malignancies (ClinicalTrials.gov, 2009), we wanted to ask whether PI3K + HSP90 dual-inhibition had greater antitumor activity in vivo compared to either drug alone. To determine whether such a treatment had merit, we began a small pilot study utilizing xenografts of U87-MG cells bearing a luciferase reporter in the flanks of nude mice.

Two weeks after the initial injection of xenograft cells obvious flank tumors were palpable. After taking caliper measurements of each tumor, mice were injected with luciferin and imaged for luminescent signal. The mice then began treatment regimens of high-dose 17-AAG alone, high-dose PI-103 + 17-AAG, half-dose PI-103 + 17-AAG, or vehicle control. After 4-weeks of treatment the tumors were measured and imaged again. (Figure 2.3A) Whereas the tumors of vehicle-treated mice increased in size considerably and the 17-AAG treated tumors increased in size moderately, mice treated with high dose combination therapy exhibited little tumor growth or in one case a moderate reduction in size. (Figure 2.3A-B) Measurements by luciferase quantification and by caliper measurement were roughly comparable and mice treated with the half-dose combination had tumor measurements that clustered similarly to high-dose 17-AAG alone. (Figure 2.3B) Because caliper measurements correlated more closely to excised tumor mass (data not shown), we continued to use this method to quantify tumor mass in subsequent experiments.

Our initial findings demonstrated the potential of PI3K + HSP90 combination therapy to improve upon the efficacy of the HSP90 inhibitor alone. Based on this, we began a trial to definitively evaluate the effect of PI3K + HSP90 combination against both single agents in larger cohorts of mice. For this work we used the same doses as in our previous pilot study but reduced the dosing schedule to three days per week. This schedule gave us a moderate antitumor effect from 17-AAG and little detectable effect from PI-103, allowing us to efficiently evaluate any increased effect from their combination. We observed an increased anti-tumor effect from the inhibitor combination therapy where mice in this cohort both had smaller average tumors and the longest survival times. (Figure 2.3C) Strikingly, PI3K+HSP90 dual-inhibition showed this increased effect even using a dose and dosing regimen where the PI3K inhibitor had no effect

compared to control. (Figure 2.3C) In contrast to in vitro experiments, this demonstrated an increase in efficacy from the combination that was clearly more than additive.

PI3K and HSP90 combination has increased toxicity compared to single agents

In addition to increased anti-tumor effects, we also observed increased toxicity from the combination of PI-103 and 17-AAG at high dose compared to high dose single drugs alone. Life expectancy of mice on the high dose combination treatment exhibited a bimodal distribution where the life of some mice was extended due to decreased tumor burden, but other mice developed distended bowels and had to be sacrificed within the first two weeks of treatment. Upon autopsy, these mice exhibited visible gut and kidney toxicity (data not shown). We therefore administered the combination therapy at half the given high dose therapy in another cohort of mice and compared these to 17-AAG high dose alone. Although dose limiting toxicities were not seen at this lower combination dose, the anti-tumor effects were slightly decreased from high dose 17-AAG alone, which also did not show dose limiting toxicity. Differences between these cohorts were not significant. (Figure 2.3D) In order to determine whether this toxicity was due to on or off target effects, and to rule out toxicity specific to the intraperitoneal injection route, we began a small pilot study utilizing the oral HSP90 inhibitor 17-DMAG instead of 17-AAG, and the recently developed orally available derivative of PI-103, GDC-0941. Both of these drugs have entered human clinical trials as oral agents (ClinicalTrials.gov, 2009). Again we saw similar toxic symptoms and identical gut and kidney toxicities compared to the previous intraperitoneally administered drug combination. (Data not shown.) This suggests the combination of PI3K and HSP90 inhibition exhibits on-target toxicity in normal tissues that, like U87 glioblastoma, are sensitive to PI3K+HSP90 combination inhibition.

Dual inhibition of PI3K and HSP90 affects both glioma primary cultures and untransformed normal neural stem cells.

For a drug combination to be an effective therapeutic, its effective dose range must be below the maximally tolerated combination dose that we have defined. Although U87-MG cells are a widely used model of GBM, such serum cultured GBM lines can differ from clinical GBM (Lee et al., 2006; Li et al., 2008) and may be more or less responsive to perturbations due to their evolution in culture. There are also multiple subtypes of GBM which feature different mutations and signaling activity (Verhaak et al., 2010), raising the question of whether some types of clinical GBM may be more responsive to dual PI3K + HSP90 inhibition than U87-MG. We therefore investigated several patient-derived GBM cultures to define whether primary GBM are more or less responsive to dual PI3k+HSP90 inhibition than either normal neural stem cells (NSCs) or our U87-MG model.

Recently, a new method for deriving and maintaining glioma stem cells (GSCs) was developed that allows adult GSCs to be isolated and grown in serum-free, defined monolayer culture (Lee et al., 2006; Pollard et al., 2009). Importantly, these cells faithfully represent patient tumors (Lee et al., 2006; Li et al., 2008) and mirror the characteristics of normal neural stem cells cultured under the same conditions (Pollard et al., 2009; Sun et al., 2008). To investigate the differential effects of PI3K + HSP90 dual inhibition in primary GBM, we repeated our dose-response studies (Figure 2.2C-D) utilizing several primary GSC cultures and compared the results both to our previous findings and to normal NSCs.

Across the three GSC isolates tested, we observed a similar additive effect in the combination therapy as we previously demonstrated in the U87-MG cells. However, to achieve a growth-inhibitory effect similar to that observed in U87-MG, GNS cells required an

approximately 3-fold higher dose. (compare Figure 2.2C with 2.4A-C) This suggests that our U87-MG findings underestimate the dose of drug necessary to achieve effects in primary GBM. Furthermore, our normal NSC control (CB660) response was nearly identical to that of the primary GSC cultures. (Figure 2.4D) This is perhaps not surprising since GSCs and NSC are known to be highly similar in both gene expression and phenotypic responses. However this result is in direct contrast to our findings utilizing human fibroblasts showing a lack of additive effects from PI3K + HSP90 inhibitor combination in normal untransformed cells (Figure 2.2D). Taken together, these results support our in-vivo findings that some but not all normal cells are sensitive to PI3K + HSP90 dual-inhibition at levels necessary to negatively affect glioma cell growth. This makes it unlikely that such a drug combination will have a sufficient therapeutic window to yield clinical benefit.

IV. DISCUSSION

Here we utilized functional genetic screening of the human kinome to identify genes whose inhibition enhances the effects of PI3-kinase inhibition. From these screen hits, HSP90 emerged as a likely candidate to amplify the antiproliferative effects of PI3K-targeted therapy. We demonstrated that dual-inhibition of PI3K and HSP90 results in additive or supra-additive antiproliferative effects in GBM both in vitro and in vivo. However, other normal cells of the body are also affected by the same dual-inhibition, resulting in unacceptable toxicity at doses necessary to affect tumor growth.

Primary GSC isolates show reduced sensitivity to PI3K + HSP90 combination therapy compared to U87-MG. Since PI3K +HSP90 combination therapy at a dose free of toxicities was

not more effective than single agent therapy in the most sensitive cell model, and since the more resistant primary isolates are currently the best representation of clinical tumors, we conclude that combination therapy against these gene targets is unlikely to be effective in clinical GBM patients.

Recently, multiple functional genomic screens have been performed seeking to identify gene targets or molecular compounds that are lethal to cancer cells. These works frequently use normal human fibroblasts either as a counter screen or during target validation to deselect screen hits which are likely to be generally cell-lethal and therefore likely to have toxic effects in normal tissues. Although this is likely to be an effective technique for some hits, our current work demonstrates that while fibroblasts can be a representative of normal cell types, they cannot represent the myriad of normal tissues in a whole organism. There is currently no substitute for whole animal studies to model potential therapies.

Our results show marked differences in drug response between our normal "control" cell types both with regard to the drug combination and to each individual drug. There are many potential reasons for this discrepancy including cell background, proliferation rate, gene expression profiles, and culture conditions. No single normal cell, nor even several normal cell cultures, can be a true surrogate for the normal tissues of an organism. However, we still believe that negative screening indicators are a vital part of refining novel screen hits. We suggest that by removing variables between the screened cancer cells and the normal comparison cells, screen hits can become more likely to yield a therapeutic window. In our case, GSCs and NSCs are extremely similar in terms of their gene expression profiles, growth rates, differentiation capabilities, tissue origin, and culture conditions. Gene knockdowns or drug treatments that do exert a differential effect between these two populations are likely to be highly specific to the

transformed state of the GSCs, and therefore less likely to exert effects upon other untransformed cells of the body (Ding et al., 2012). The lack of difference from dual PI3-kinase and HSP90 inhibition between these cells, and the corresponding drug toxicity at effective anti-tumor doses, suggests that this combination strategy is unlikely to be effective against clinical glioblastoma.

V. METHODS

Cell culture

U87-MG cells were obtained from ATCC and cultured according to ATCC guidelines. BTIC and NSC lines were grown in N2B27 neural basal media (Stemcell Technologies) supplemented with EGF and FGF-2 (20 ng/ml each) (Peprotech) on laminin (Sigma) coated polystyrene plates according and passaged according to Pollard (Pollard et al., 2009). PI-103 was obtained from Cayman chemical and LC Laboratories and dissolved in DMSO.

ShRNA Bar-code screens and array analysis

For shRNA screen and Bar-code array analysis U87-MG cells were infected with a pool of retroviral shRNAs targeting approximately 700 human kinases at a representation of ~800 fold (MOI<0.3). The population was selected with puromycin (Sigma) (1 μg/ml) to remove uninfected cells. Afterwards, cells were expanded briefly and separated into two cohorts of triplicate culture populations. Cells propagated in culture for an additional 14 days in the presence or absence of a GI50 dose of PI-103 in their media. For each passage a minimal representation of 800 fold was maintained and cellular DNA was sampled for BC array analysis at 14 days. For each corresponding sample, shRNA barcodes were PCR-recovered from genomic

samples, labeled with Cy5 or Cy3, and competitively hybridized to a microarray containing the corresponding probes (Agilent Technologies). Replicate array results were analyzed using the BioConductor package limma. The change in the relative abundance of each shRNA in the library over time was measured using the normalized Cy3/Cy5 ratio of its probe signal. Barcode probes depleted in the BTIC samples were considered candidate genes using the following criteria: 1) adjusted p-value ≤ 0.05 and 2) $|\log2(\text{ratio})| \geq 0.585$.

Cell proliferation studies

Cells were plated in 96-well plates at a density of 3000 cells per well in standard culture media. Cells were refed with drug-containing media 24 hours after plating, allowed to grow another 72 hours in the presence of drug, then analyzed for cell viability using the CellTiter-Glo assay (Promega).

RNAi and lentiviral production

ShRNAs were obtained from the RNAi Shared Resource (FHCRC) in the MLP retroviral vector. For virus production MLP-shRNA plasmids were transfected into ΦNX cells along with packaging and VSV-G plasmids to produce retrovirus. Approximately 24 hours after transfection, new medium was added to replace original growth medium. Virus was harvested 24 and 48 hours after medium change, filtered, and stored at -80°C.

Xenograft studies

U87-MG cells from culture were resuspended in a single cell suspension in PBS and 50% matrigel (BD). 10^6 cells were implanted subcutaneously into the flanks of nude mice (JAX). Tumors were monitored by caliper measurement and allowed to grow to ~75 mm^3 before

commencing drug treatments. PI-103 (LC Labs) and 17-AAG (LC Labs) were administered intraperitoneally at up to 50mg/kg and 80mg/kg, respectively. GDC-0941 (Sigma) and 17-DMAG (LC Labs) were solubilized in dilute Methylcellulose-Tween80-Dextrose solution and administered orally by gavage at 50 mg/kg and 37.5 mg/kg, respectively.

VI. FIGURES

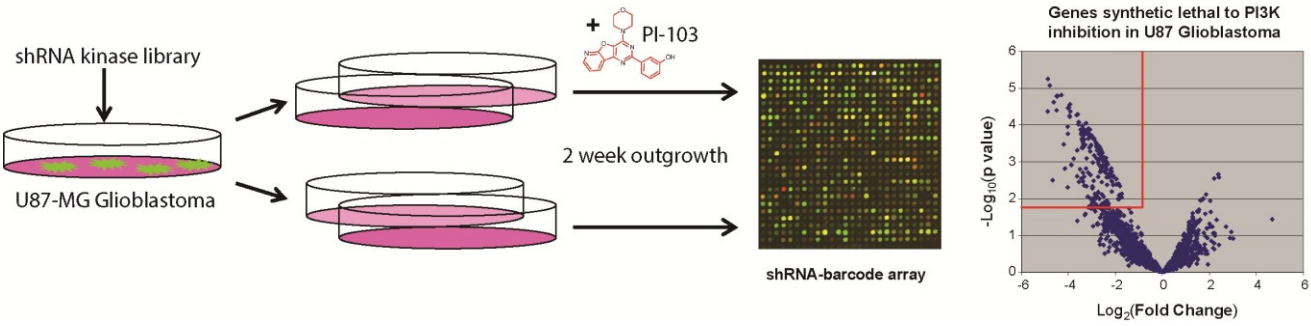

2.1 Schematic diagram of human kinome screen for genes synthetic-lethal to PI3-kinase inhibition in glioblastoma. The shRNA screening approach used to initially identify HSP90 as a drug sensitizing target for PI3K inhibition. Pooled shRNA viruses targeting human kinases were used in outgrowth screens in human U87-MG glioblastoma cells with or without a low dose of the PI3-kinase inhibitor PI-103. Candidate genes differentially required for GSC expansion over 14-days of outgrowth were identified through hybridization of viral DNA barcodes to custom microarrays.

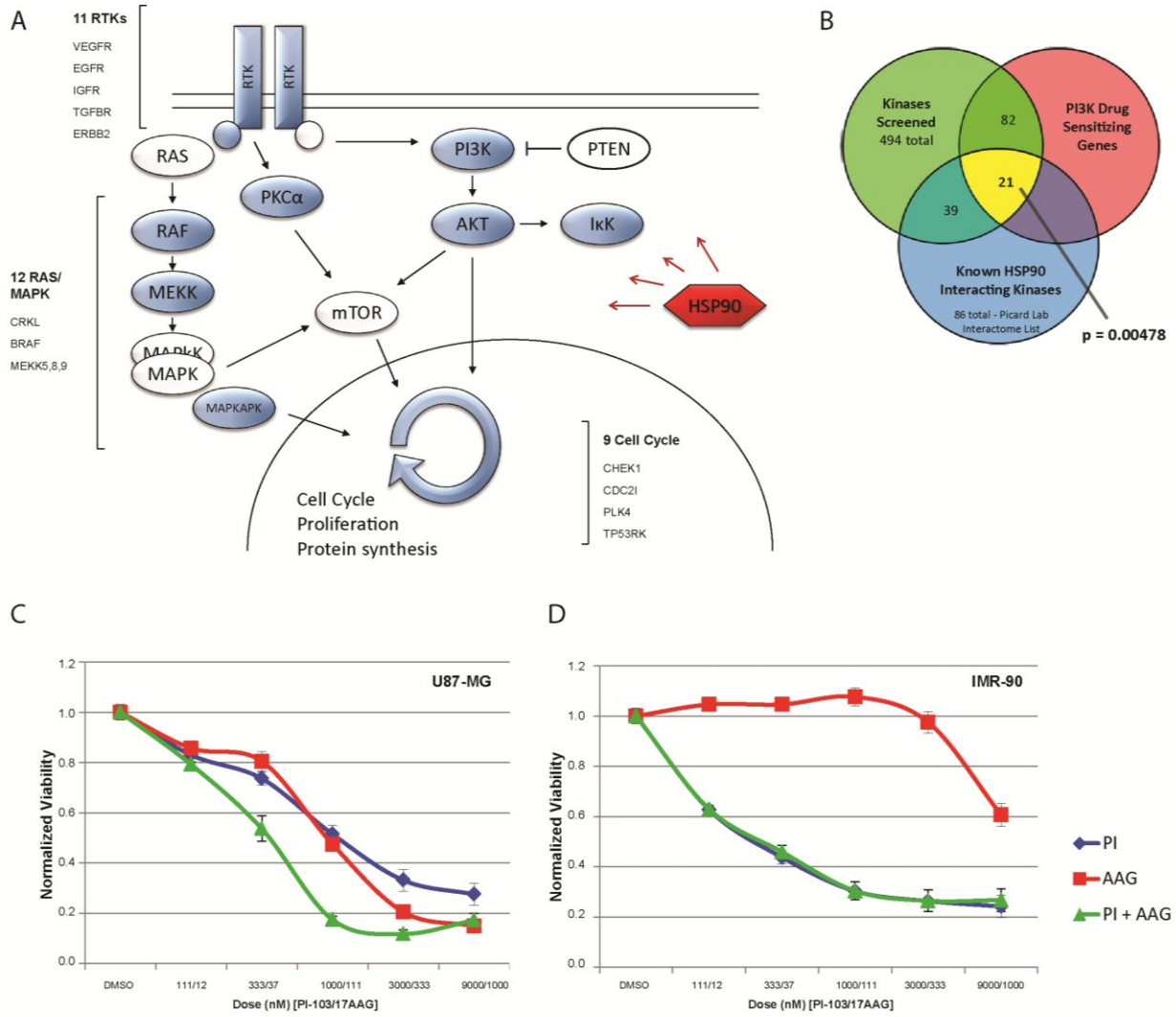

2.2 HSP90 inhibition sensitizes glioblastoma but not normal fibroblasts to PI3K inhibition

(A) Diagram of PI3K sensitizing hits from our screen with characterized roles in receptor signaling.
(B) Venn diagram depicting the overlap between kinases in our screen and known HSP90 interacting kinases. p-value for overlapping genes was determined by hypergeometric calculation.
(C) Viability of U87-MG glioblastoma cells treated with increasing doses of PI-103, 17-AAG, or both inhibitors.
(D) Viability of normal IMR-90 fibroblasts treated with increasing doses of PI-103, 17-AAG, or both inhibitors.

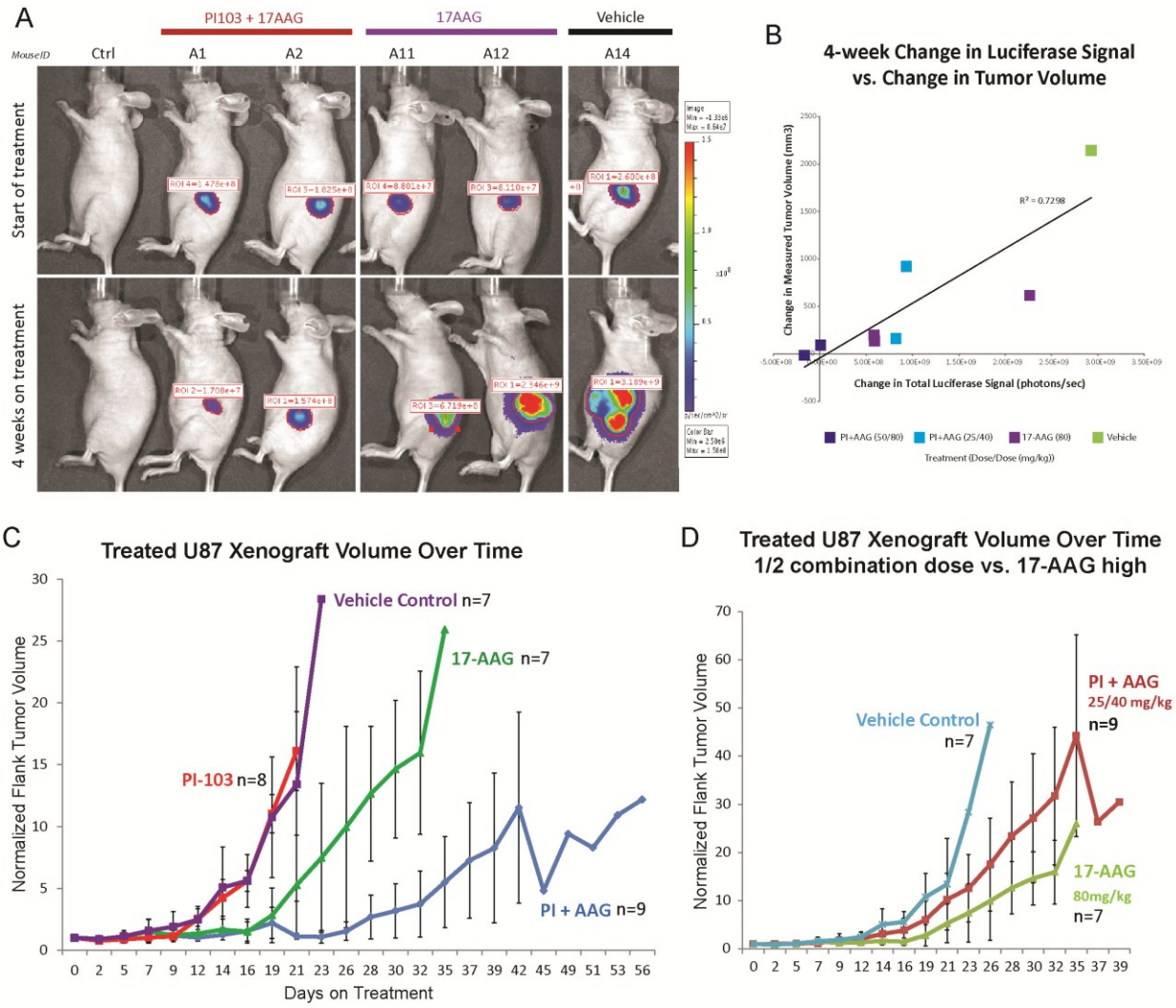

2.3 PI3K and HSP90 inhibitor combination has increased anti-tumor effects compared to single drug therapies in vivo.

(A) Luciferase imaging of mice with glioblastoma flank xenografts before and after treatment with the indicated inhibitors. Control mouse on left did not receive a xenograft.
(B) Change in tumor size over 4 weeks as measured by luciferase signal or caliper measurement.
(C) Flank xenograft tumor volume over time after commencement of treatment 3x weekly with PI-103 (50mg.kg), 17-AAG (80mg/kg) or combination therapy (50+80mg/kg). The number of mice in each cohort bearing a flank xenograft at the start of treatment is indicated.
(D) Flank xenograft tumor volume over time after commencement of treatment with either 17-AAG (80mg/kg) or half-dose combination (PI-103 25mg/kg + 17-AAG 40mg/kg).

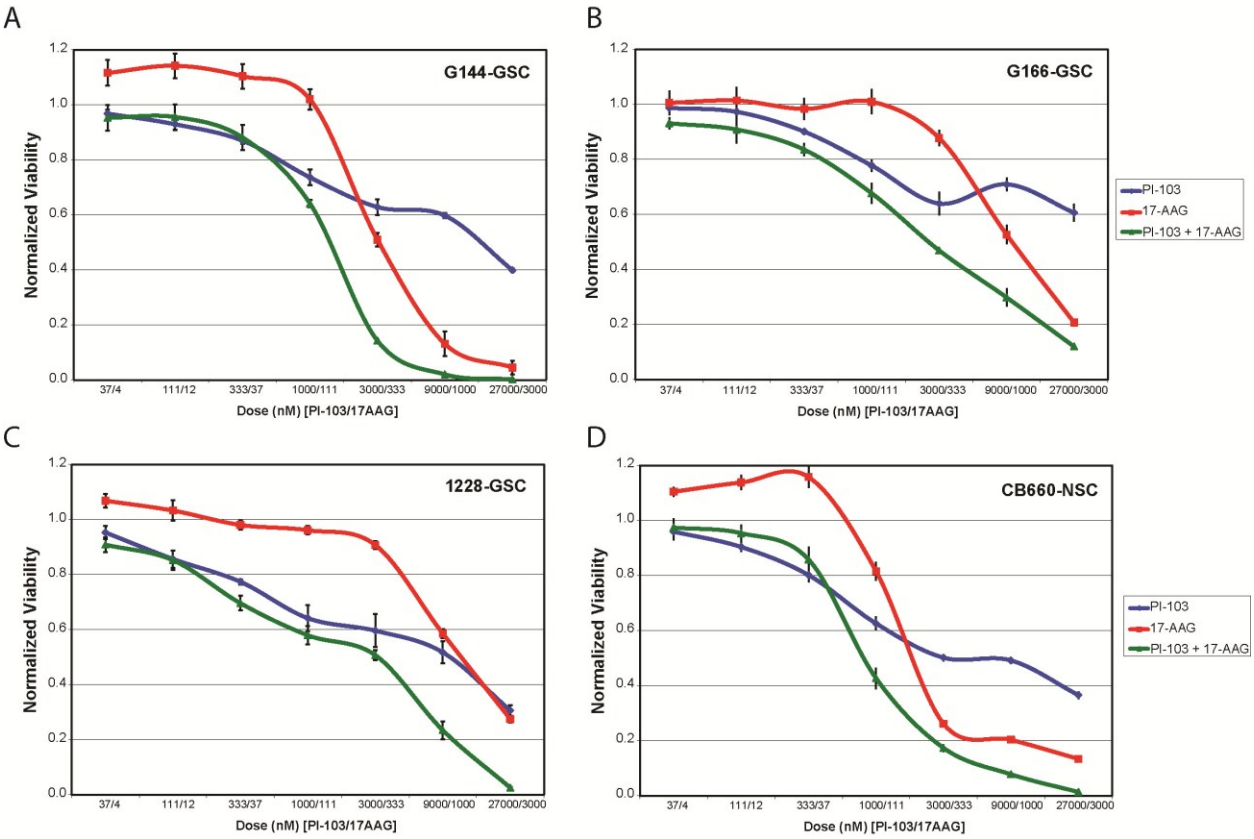

2.4 Primary glioma stem cell cultures and normal neural stem cell cultures respond similarly to PI3K + HSP90 drug combination.

(A-D) Viability of primary glioma stem cell (GSC) or normal neural stem cell (NSC) cultures after treatment with increasing doses of PI-103, 17-AAG, or both inhibitors.

Chapter 3 – A cancer-specific requirement for BUB1B/BubR1 in human brain tumor isolates and genetically transformed cells?

Adapted from an article published in Cancer Discovery (Ding et al., 2012).

Yu Ding, Christopher G. Hubert, Jacob Herman, Philip Corrin, Chad M. Toledo, Kyobi Skutt-Kakaria, Julio Vazquez, Ryan Basom, Bin Zhang, Jennifer K. Risler, Steven M. Pollard, Do-Hyun Nam, Jeffery J. Delrow, Jun Zhu, Jeongwu Lee, Jennifer DeLuca, James M. Olson, and Patrick J. Paddison

I. ABSTRACT

To identify new candidate therapeutic targets for Glioblastoma multiforme (GBM), we combined functional genetics and GBM network modeling to identify kinases required for the growth of patient-derived brain tumor initiating cells (BTICs), but which are dispensable to proliferating human neural stem cells (NSCs). This approach yielded BUB1B/BUBR1, a critical mitotic spindle checkpoint player, as the top scoring GBM-lethal kinase. Knockdown of BUB1B inhibited expansion of BTIC isolates, both in vitro and in vivo, without affecting proliferation of NSCs or astrocytes. Mechanistic studies revealed that BUB1B's GLEBs domain activity is required to suppress lethal kinetochore-microtubule (KT-MT) attachment defects in GBM isolates and genetically transformed cells with altered sister KT dynamics, which likely favor KT-MT instability. These results indicate that GBM tumors have added requirement for BUB1B to suppress lethal consequences of altered KT function. They further suggest that sister KT measurements may predict cancer-specific sensitivity to BUB1B inhibition and perhaps other mitotic targets that affect KT-MT stability.

Significance

There are currently no effective therapies for GBM, the most frequent and aggressive brain tumor. Our results suggest that targeting BUB1B's GLEBs domain activity may provide a therapeutic window for GBM, since the GLEBs domain is non-essential in untransformed cells. Moreover, the results further suggest that sister KT distances at metaphase may predict sensitivity to anti-cancer therapeutics targeting KT function.

II. INTRODUCTION

Glioblastoma multiforme (GBM) is the most aggressive and common form of brain cancer in adults (American Cancer Society). There are currently no effective therapies for GBM. Even with standard of care treatments, such as surgery, radiation, and chemotherapy, ~90% of adult patients die within 2 years of diagnosis (Stupp et al., 2005). Both adult and pediatric brain tumors appear to be hierarchically organized suggestive of a cancer stem cell origin (Galli et al., 2004; Hemmati et al., 2003; Singh et al., 2003; Singh et al., 2004). Consistent with this notion, brain tumor-initiating cells (BTICs) have recently been isolated that retain the development potential and specific genetic alterations found in the patient's tumor (Hemmati et al., 2003; Lee et al., 2006; Pollard et al., 2009; Singh et al., 2003). When implanted into the cortex of rodents, BTICs give rise to GBM-like tumors with patient-specific molecular signatures and histological features (Galli et al., 2004; Lee et al., 2006; Pollard et al., 2009; Singh et al., 2004). Expression of neural progenitor molecular networks may contribute to the aggressive behavior of GBM tumors through enhancing self-renewal or developmental programs (Stiles and Rowitch, 2008),

DNA repair pathways (Bao et al., 2006a), angiogenesis (Bao et al., 2006b), and/or invasiveness (Liu et al., 2009). Given the likelihood of BTIC-driven maintenance and spread of GBM, effective cell-based therapies will likely have to target the stem cell.

Recently, a new method for deriving and maintaining BTICs was developed in which adult BTICs can be isolated and grown in serum-free, defined monolayer culture (Lee et al., 2006; Pollard et al., 2009). By this method BTICs can retain tumor-initiating potential and tumor-specific genetic and epigenetic signatures over extended outgrowth periods (Sawin et al., 1992). Here, we sought to take advantage of this BTIC culture system to find evidence for the cancer-lethal hypothesis: that transformed cells harbor novel molecular vulnerabilities compared to "normal" cells as a direct consequence of cancer-causing genetic alterations (Hartwell et al., 1997). Although multiple studies have addressed the question of cancer lethality in serum-derived cell lines (Barbie et al., 2009; Luo et al., 2009a), there remain lingering questions of applicability to human cancers, since serum-derived lines may not faithfully represent the primary cancer (Lee et al., 2006).

By combining the results of shRNA kinome screens in BTICs and NSCs for genes required for progenitor expansion with a GBM bionetwork created from patient molecular signatures, we identified BUB1B, a critical mitotic checkpoint kinase (Musacchio and Salmon, 2007), as the top GBM-specific hit. Our results suggest that GBM tumors and genetically transformed cells have added requirement for BUB1B to suppress lethal consequences of altered KT function. Importantly, these studies demonstrate that non-transformed cells do not require BUB1B/BubR1 for chromosome alignment, nor do they require the GLEBs domain to maintain the spindle assembly checkpoint. They further suggest that altered KT conformations apparent in

GBM and genetically transformed cells may predict cancer-specific sensitivity to BUB1B inhibition and perhaps other mitotic targets that affect KT-MT stability.

III. RESULTS

An RNAi kinome screen for genes differentially required for BTIC expansion

To discover candidate therapeutic targets for GBM, we performed an shRNA screen targeting 713 human kinases to identify gene activities required for *in vitro* expansion of BTICs. To enrich for BTIC-specific hits, a parallel screen was conducted in human fetal NSC-CB660 cells (Fig. 3.1A) (Sun et al., 2008). NSCs share molecular and phenotypic features with BTICs, including: identical isolation and growth in serum-free conditions, similar doubling times, overlapping expression profiles, and similar developmental potential (Sun et al., 2008). However, they retain a normal karyotype and are not tumorigenic (Sun et al., 2008), and, thereby, represent ideal controls for BTICs.

This screening approach (see Methods for details) revealed ~53 candidate kinase targets with shRNAs underrepresented in BTICs relative to NSCs (Table 2.1). To prioritize these hits, we examined whether hits could be parsed into distinct pathways and/or complexes using protein-protein interaction networks (Lens et al., 2010). By this analysis, most hits were connected in a single, large subnetwork, enriched for 248 GO biological processes (multiple testing adjusted p-value<0.01), such as protein kinase cascade (p-value= 5.6e-085) and protein amino acid phosphorylation (p-value=1.1e-082). This lack of specific biological processes likely

reflected the fact that these kinases are well studied and involved in many biological processes and, thus, did not provide any useful information for prioritizing of candidate hits.

As an alternative strategy, we examined the occurrence of screen hits in GBM specific regulatory network, constructed *de novo* from over 421 TCGA GBM tumor samples (Cancer Genome Atlas Research Network, 2008) by integrating gene expression and DNA copy number variation data (Tran et al., 2011; Zhu et al., 2008) (Supplemental Information). By this analysis, 37 of 48 shRNA candidate hits appeared as nodes in the GBM network. Examination of subnetworks in the GBM network, revealed 15 biological processes significantly enriched (5 cell cycle related, 9 general phosphorylation related), including the M phase of mitotic cell cycle (p-value=1.64e-5). The largest GBM-specific subnetwork contained four screen hits, including AURKB, BUB1B, MELK, and PLK1 (Fig. 3.1B). Based on key driver node analysis (Yang et al., 2009), BUB1B scored as the top ranked screen hit (Fig. 3.1C).

To control for GBM network comparisons, we also examined screen hits in a normal brain network constructed from 160 non-dementia human prefrontal cortex samples. Only 20 of the 48 candidate hits appeared in the normal brain network, and produced smaller subnetworks enriched for general phosphorylation related GO biological processes (data not shown). Although BUB1B appeared in this network, it was connected to only one gene and had no down nodes (Fig. 3.1B), and, thus, was not a key driver node.

BUB1B is differentially required for BTIC expansion

Retests of AURKB, BUB1B, MELK, and PLK1 revealed that BUB1B inhibition gave the largest differential effect on BTICs from multiple GBM isolates, including common developmental subtypes (Verhaak et al., 2010), without observable toxicity in proliferating NSCs

or astrocytes (Figs. 3.2A-D). In these studies, shRNA expressing cells were subjected to short- and long-term out growth assays (Fig. 3.2D and Supplementary Fig. 3.3A-B). Knockdown of KIF11 was used as a positive control. KIF11 encodes a microtubule motor protein required for mitotic progression in proliferating mammalian cells (Sawin et al., 1992). During short and long term outgrowth shKIF11 blocked the growth of BTICs, NSCs, and astrocytes. Since shKIF11 only inhibits cycling cells entering mitosis, shKIF11-dependent growth inhibition indicates similar division rates for various cells used and that they have comparable RNAi pathway activity. However, BUB1B knockdown only triggered significant growth inhibition in BTIC lines (Figs. 3.2A & D). During longer-term outgrowth shBUB1B inhibited the growth of SSEA1+ BTIC subpopulations, which are enriched for tumor initiating cell activity (Son et al., 2009) (Supplementary Fig. 3.3C-D). BUB1B knockdown was also deleterious to BTIC tumor sphere formation, which may reflect tumor initiating cell activity (Galli et al., 2004; Singh et al., 2004), in both BTICs and primary tumor samples (Fig. 3.2E). However, knockdown did not profoundly alter expression of SSEA1 or other progenitor markers, including SOX2 and NESTIN, or neural lineage markers, including GFAP and TUJ1 (data not shown).

By contrast, PLK1 knockdown had a partial effect; MELK knockdown had no effect; and inhibition of AURKB was equally toxic to BTICs and NSCs (Supplementary Fig. 3.4). Based on these results, we further pursued BUB1B as a candidate BTIC-lethal gene.

BUB1B is overexpressed in GBM isolates and its checkpoint activity is compromised by shBUB1B in both BTICs and NSCs

BUB1B encodes a highly conserved BUB1-like kinase, BubR1, whose activity is essential for mitotic spindle checkpoint signaling (Musacchio and Salmon, 2007). The mitotic spindle checkpoint monitors the attachment of kinetochores to the plus ends of spindle

microtubules and prevents anaphase onset until chromosomes are aligned and kinetochores are under tension at the metaphase plate (Musacchio and Salmon, 2007). Due to its role in maintaining chromosome stability, mitotic spindle checkpoint activity has been touted as a mechanism for tumor suppression (Cahill et al., 1998; Musacchio and Salmon, 2007). In rare instances partial loss of function mutations in checkpoint genes have been reported for certain cancers (Cahill et al., 1998). However, many late-stage cancers, including glioma, exhibit high BUB1B expression (Bie et al., 2011; Yuan et al., 2006), suggestive of hyperactivity.

To begin to reconcile these observations with our results, we analyzed BUB1B expression patterns and activity in BTICs and NSCs. We observed that BUB1B and other spindle checkpoint genes were up regulated in BTIC isolates and also Ras-transformed astrocytes as judged by mRNA and protein abundance (Supplementary Fig. 3.5). Moreover, BTICs and NSCs both had normal mitotic spindle arrest responses after taxol treatment, which were abrogated by BUB1B knockdown (Supplementary Fig. 3.6). Thus, BUB1B knockdown achieves a similar level of suppression BUB1B mRNA, protein, and activity in both BTICs and NSCs. The results suggest that BUB1B knockdown produces a hypomorphic state to which BTICs, but not NSCs or astrocytes, are sensitive. Below we provide further evidence to support this conclusion, by addressing BUB1B's essential and non-essential functions in BTICs, transformed, and untransformed cells.

Shortened inter-kinetochore distances are indicative of sensitivity to shBUB1B in BTICs and genetically transformed cells

One possible explanation for BTIC's observed sensitivity to hypomorphic BUB1B activity is that KT-MT dynamics could be altered to favor MT detachment. In order to properly segregate chromosomes during mitosis, stable attachments must occur between the “plus” end of

mitotic spindle MTs and KTs, which are formed at centromeres of each sister chromatid as cells enter mitosis (Santaguida and Musacchio, 2009). Early in mitosis, KT-MT attachments are unstable and dynamic, allowing chromosomes to be towed toward MT plus ends during congression and improperly attached chromosomes to be released and re-attached to spindle MTs until they are bi-oriented and under tension (Lens et al., 2010; Santaguida and Musacchio, 2009). The distance between KTs on sister chromatids can range from ~0.6 μm in prophase to >1 μm in metaphase, when sister KTs achieve stable MT attachment and are pulled toward opposing spindle poles (Fig. 3.7A) (DeLuca et al., 2002). In the prevailing model, this KT movement prevents outer kinetochore proteins from being phosphorylated by Aurora B kinase, which promotes KT-MT detachment (e.g., for error correction), by physically removing them from centromere-embedded Aurora B activity (Santaguida and Musacchio, 2009).

To examine KT-MT dynamics, we first investigated the possibility that KT dynamics may be altered in GBM cells. To this end, we measured inter-kinetochore distance (IKD): the maximum distance achieved between sister KTs when stable end-on MT attachment has occurred (DeLuca et al., 2006). We first measured IKDs for shBUB1B insensitive NSCs (CB660) and two shBUB1B sensitive BTIC isolates (G166 and 0131). The results were surprising. We found that IKDs were significantly shorter in both BTIC isolates (1.23 μm for CB660 vs. 1.13 μm for G166 and 1.09 μm for 0131) (Figs. 3.7B & C). Thus, BTICs IKDs were short by 100-140nm, or 50-70nm for each sister KT. This represents a significant change, since, for example, the outer kinetochore protein Hec1 moves ~40 nm toward the spindle pole as KTs come under tension (Maresca et al., 2009; Uchida et al., 2009).

Next, we examined IKDs in two GBM patient isolates, 0827and 1502, that we had observed were completely insensitive to shBUB1B. These isolates were insensitive despite

having similar knockdown efficiencies to shBUB1B sensitive lines and among the fastest doubling times and tumor initiation rates (data not shown). Measuring IKDs in these cells revealed that they were indistinguishable from NSCs (1.23 μm), suggesting the possibility that IKDs may predict BUB1B sensitivity (Figs. 3.7B & C).

To further examine this possibility, we tested a hypothesis: that shortened IKDs and added BUB1B requirement arise as a result of oncogenic transformation and, specifically, oncogenic signaling. It was recently shown that expression of activated Ras oncogene can lead to mitotic stress and induce chromosome instability in mammalian cell, through an as yet undefined mechanism (Luo et al., 2009a). Thereby, we examined IKDs in p53-/- mouse embryo fibroblasts with or without RasV12 expression. In p53-/- control MEFs, IKDs averaged 1.25 μm similar to NSCs and 827 cells. Surprisingly, RasV12 expression converted long IKDs to short, averaging 1.13μm, indistinguishable from G166 and 0131 cells (Fig. 3.7D). Moreover, RasV12 transformation also converted MEFs from being resistant to BUB1B inhibition to being profoundly sensitive, which was also true for human astrocytes (Fig. 3.7D) as well (both experiments are presented below in Fig. 3.10 & Fig. 3.13). Importantly, all of the IKD measurements for BTICs, NSCs, and MEFs IKDs were scored blindly to avoid experimenter bias.

Since most BUB1B/BubR1 experimentation has been performed in HeLa cells, which are derived from a cervical carcinoma (Luo et al., 2009a), we next measured IKDs in these cells. As a control, we used immortalized retinal pigment epithelial (RPE-1) cells, which are untransformed. Hela cells showed IKDs similar to other BUB1B sensitive cells (1.11 μm), while RPE cells showed long IKD similar to insensitive cells (1.22 μm). Repeating the pattern above BUB1B knockdown only affected chromosome dynamics in Hela cells (detailed below).

These results suggest: 1) that IKDs occur in discrete intervals: long (~1.24 μm) and short (~1.12 μm); 2) that short IKDs predict sensitivity to BUB1B inhibition; and 3) that RasV12 transformation is sufficient to induce short IKDs and sensitivity to BUB1B.

GBM isolates with short Inter-kinetochore distances require BUB1B to suppress severe KT-MT attachment defects

We next wished to determine whether BTICs with short IKDs have altered KT-MT dynamics that favor detachment. To this end, we used a metaphase chromosome alignment assay, in which KT-MT attachment defects are visualized as misaligned chromosomes during metaphase arrest induced by proteasome inhibition (Lampson and Kapoor, 2005). By this assay, knockdown of BUB1B resulted in dramatic chromosome alignment defects only in BTICs with short IKDs, but did not affect alignment in NSCs, 0827 cells (Figs. 3.8A & 4B; Supplementary Fig. 3.9A) or astrocytes (see below). The alignment defects in G166 cells were accompanied by profound loss of KT-MT attachment, as indicated by lack of co-localization KTs with cold resistant MTs (Supplementary Fig. 3.9B). Moreover, examination of phospho-Ser44-Hec1/Ndc80 at KTs revealed that after BUB1B knockdown, G166 cells retain Ser44-P (DeLuca et al., 2011) (Supplementary Fig. 3.9C). This phosphorylation is dependent upon centromere-embedded Aurora B kinase activity, and has a KT-MT destabilizing effect (Santaguida and Musacchio, 2009). These results suggest that cells with short IKDs have KT-MT attachment defects, which BUB1B is required to suppress.

Consistent with this notion, G166 cells also displayed overt differences in chromosome dynamics during mitosis, with significantly more lagging chromosomes in anaphase compared to NSCs (Fig. 3.8C). BUB1B knockdown dramatically exacerbated these defects (Fig. 3.8D). In control experiments in NSCs, shBUB1B did not affect lagging chromosome frequency or

karyotype after extended outgrowth (Fig. 3.8C; Supplementary Fig. 3.9D), again suggesting that cells with long IKDs do not utilize BUB1B in the same way.

Genetic dissection of added requirement of BUB1B in RasV12-expressing fibroblasts and BTIC cells

BUB1B has multiple functional domains that have been implicated in mitotic checkpoint control, mitotic timing, and stable kinetochore-microtubule attachment (Musacchio and Salmon, 2007; Santaguida and Musacchio, 2009). These include: N- and C-terminal KEN box domains required for Cdc20 binding and APC inhibition (Davenport et al., 2006; Malureanu et al., 2009; Tang et al., 2001); a C-terminal kinase domain involved in checkpoint control (Harris et al., 2005; Mao et al., 2005); and a GLEBS-like motif necessary for KT localization during mitosis (Harris et al., 2005; Wang et al., 2001) (Fig. 3.10A). While BUB1B is essential for mammalian development (Wang et al., 2004), its essential function is contained solely within the N-terminal KEN box (Malureanu et al., 2009), which enables Bub1b to act as a pseudo-substrate inhibitor of APC/C^{Cdc20} during G2 and pre-anaphase mitosis, preventing a precocious anaphase (Malureanu et al., 2009).

The above results suggested that BTICs with short IKDs have added requirement for BUB1B that helps facilitate KT-MT attachment. BUB1B's GLEBS domain is necessary for its KT localization, interaction with Bub3, and helps facilitate KT-MT attachment (Harris et al., 2005; Wang et al., 2001). Recently, Maulureanu et al (2009) demonstrated that this domain is non-essential for stable end-on KT-MT attachment and viability in mouse embryo fibroblasts (MEFs). Their results, however, were not consistent with previous work in HeLa cells that clearly demonstrated that the GLEBs domain is essential for KT-MT attachment (Elowe et al., 2010). Intriguingly, our data sets inform these seemingly incompatible results with the following

thesis: BUB1B's GLEB domain is required in cells with abnormal KT conformations (e.g., Helas) to suppress lethal KT-MT instability. Furthermore, since our results above, demonstrate that RasV12 transformation can convert long IKDs to short, it would follow that oncogenic transformation gives rise to added BUB1B requirement.

To directly address this notion, we next performed allelic complementation studies using mouse Bub1b alleles (Fig. 3.10A) in mouse embryo fibroblasts (MEFs) harboring bi-allelic deletion of Bub1b (Malureanu et al., 2009), which were also transformed by H-RasV12. For these experiments, we used full-length mBub1b, the N-terminal deletion mutant and the E406K GLEB domain mutant allele, which cannot bind to KTs. Expression of each allele was verified by western blotting (Supplementary Fig. 3.11). For non-transformed MEFs, the viability pattern was the same as previously published (Malureanu et al., 2009): both FL and E406K alleles fully complemented Bub1b-/- and only the N-terminal KEN box domain was required for Bub1b-/- cell growth (Fig. 3.10B). However, after Ras-dependent transformation of these cells, the results changed dramatically. The GLEBs domain became essential for viability, as evidenced by the complete failure of the E406K allele to complement (Fig. 3.10B). RasV12 activity, however, did not alter requirement N-terminal KEN box domain. These results demonstrate that RasV12 transformation leads to profound requirement for BUB1B's GLEBs domain activity.

To further examine this result, we performed a similar set of complementation experiments in BTIC-G166 cells, using mouse Bub1b alleles to complement knockdown of endogenous human BUB1B. In this case, kinase defective and internal KEN box deletion alleles were also included (Fig. 3.10C). Expression of each allele was confirmed by western blotting (Supplementary Fig. 3.11). Knockdown efficiency of endogenous BUB1B was also shown to be unaffected by expression of mouse Bub1b (shBUB1B is not predicted to target mouse Bub1b)

(Supplementary Fig. 3.11). As shown in Figure 3.10C, expression of full length and KD2 mBub1b alleles achieved near-complete rescue of the viability defects of BUB1B knockdown in G166 cells, indicating that the shBUB1B phenotype is due to on-target silencing of BUB1B, and that BUB1B's kinase activity is not required in BTICs. By contrast the ΔN and E406K alleles, failed to complement viability, behaving exactly as the vector control, while ΔM showed a partial rescue (Fig. 3.10C). None of the alleles were able to complement control KIF11 knockdown. Thus, these results phenocopy those observed in RasV12-transformed MEFs.

To further investigate these results, we performed KT-MT attachment using chromosome alignment assays as described above. All alleles showed complete or partial suppression of alignment defects, except for E406K, which failed to complement (Figures 3.10D & 3.10E). This demonstrates that BUB1B's GLEBs domain is essential for both viability and stable-end on attachment of MTs to KTs in BTICs with short IKDs.

Since BUB1B's essential function is to prevent precocious anaphase through inhibiting APC^{Cdc20} activity, we also examined mitotic transit times in the same series of complementation experiments. BUB1B knockdown causes significant reduction in transit times in BTICs, which all alleles were able to complement, except for ΔN (ΔM was not determined) (Supplementary Fig. 3.12). Since the E406K allele restored mitotic timing, but not viability or KT-MT attachment, this would suggest that requirement for BUB1B-GLEBs domain activity is distinct from BUB1B-dependent APC regulation.

To provide additional evidence for transformation dependent changes in BUB1B function in human cells, we examined viability and KT-MT attachment requirements for BUB1B in normal human astrocytes with and without expression of RasV12. Knockdown of BUB1B in

RasV12- NHA, but not NHA controls, resulted in loss of viability and severe KT-MT defects (Supplementary Fig. 3.13). These results were, again, consistent with the notion that oncogenic transformation leads to added requirement for BUB1B to stabilize KT-MT attachments. A similar pattern was observed in HeLa cells and non-transformed RPE cells. ~93% of HeLa cells treated with siBUB1B have severe KT-MT attatchment defects (n>100), compared to only 17% for control; while KT-MT attachment was similar regardless of siBUB1B treatment (n>150) (Supplementary Fig. 3.13).

Several key conclusions can be drawn from these studies: 1) BUB1B is the relevant target of shBUB1B in BTICs; 2) BUB1B's kinase activity is dispensable for added BUB1B requirement in BTICs; 3) promotion of KT-MT attachment, rather than restoration of BTIC-mitotic delay/timing, is a key BTIC-lethality suppressing activity; 4) GBM cells differ in their requirement for BUB1B's GLEBS domain as compared to cells with long IKDs; and 5) that oncogenic transformation drives added requirement for BUB1B's GLEBs domain.

shBUB1B inhibits BTIC-driven tumor formation

Lastly, to ensure that the above results are applicable to patient tumor formation, we examined BUB1B requirement during BTIC tumor formation, for a BTIC line with short IKDs. We performed two different assays. In the first, shRNA-GFP+ 0131 cells competed against non-shRNA control 0131 cells at ~9:1 ratio (Fig. 3.14A) for injection into the cortex of immunodeficient mice. The end point was relative representation of shBUB1B. After 4 or 7 weeks post-injection, control cells had dramatically outcompeted shBUB1B-GFP+ cells (Fig. 3.14A). This was not simply due to inviability of injected cells at Day 0, since the most shBUB1B-GFP+ cells in the injection bolus could attach to laminin-coated dishes. For the

second assay, survival was the end point for mice injected with either shControl or shBUB1B expressing 0131 cells (Fig. 3.14B). This assay ended at 250 days post-injection when 90% of control mice had succumbed to tumors. During this time none of the shBUB1B-0131 mice died. These results suggest that knockdown of BUB1B is deleterious to GBM tumor formation and that the *in vivo* tumor environment does not suppress requirement for BUB1B.

IV. DISCUSSION

Here we attempted to identify kinases differentially required for the expansion of GBM-derived BTICs by combining a functional genetic approach with a GBM bionetwork derived from patient sample molecular data sets (Park and Rich, 2009). This approach produced BUB1B as the top-scoring screen hit. Validation studies bore out this prediction: knockdown of BUB1B differentially blocked expansion of 9 of 11 BTIC isolates examined, without effecting growth of human NSCs and astrocytes, which are both candidate cell types of origin for GBM (Park and Rich, 2009).

BUB1B encodes a highly conserved BUB1-like kinase, BubR1, whose activity is essential for mitotic spindle checkpoint signaling (Musacchio and Salmon, 2007). The mitotic spindle checkpoint monitors the attachment of kinetochores to the plus ends of spindle microtubules and prevents anaphase onset until chromosomes are aligned and kinetochores are under tension at the metaphase plate (Musacchio and Salmon, 2007). To pursue the mechanism of BUB1B requirement in GBM cells, we tested a hypothesis: that KT-MT dynamics are fundamentally altered in GBM cells to favor KT-MT detachment, which BUB1B is required to suppress.

This hypothesis was supported by multiple observations (summarized in Fig. 3.15). First, in examining sister KT dynamics at metaphase, we demonstrated that GBM and other cancer cells sensitive to BUB1B inhibition have significantly shorter IKDs, indicating that KT dynamics are dramatically altered. Second, in BTICs with short IKDs, BUB1B activity is required to suppress lethal KT-MT instability and to directly or indirectly inhibit centromere-embedded Aurora B activity on outer KT proteins. Third, expression of the RasV12 oncogene is sufficient to induce the same changes in sister KTs observed in BTICs. Fourth, RasV12 also triggered requirement for BUB1B's GLEBs domain for both viability and KT-MT attachment. Fifth, genetic dissection of BUB1B function in BTICs with short IKDs revealed the same requirement for BUB1B's GLEBs domain to suppress lethal KT-MT instability.

These results support a model whereby oncogenic signaling alters KT regulation, resulting in short IKDs and KT-MT instability. As a direct result, BUB1B's GLEBs domain activity becomes essential for KT-MT attachment (Fig. 3.15). Our studies demonstrate that non-transformed cells do not require BUB1B/BubR1 for chromosome alignment, nor do they require the GLEBs domain to maintain the spindle assembly checkpoint.

One key implication of this work is that short IKDs may be predictive of requirement for BUB1B's GLEBs domain and sensitivity to disruption of KT function in cancer cells. For example, we have found patient GBM isolates (i.e., 0827, 1502) that are resistant to BUB1B knockdown and have IKDs indistinguishable from untransformed cells. Thus, it is conceivable that anti-cancer therapies targeting KT or mitotic checkpoint function (e.g., (Sudakin and Yen, 2007; Wood et al., 2010)) would benefit from using IKDs as a biomarker or companion diagnostic. However, additional studies are required to determine the extent to which IKDs are

shorter in cancer cells and also the mechanisms through which KT conformations become perturbed.

One possibility is that RTK-Ras signaling directly affects KT function. There is evidence that Ras effector kinases Erk1/2 can directly phosphorylate the C-terminal domain of CENPE, a key KT protein, which is predicted to decrease its MT binding ability (Liao et al., 1994; Zecevic et al., 1998). Intriguingly, we observed that in both BTIC-G166 and RasV12-transformed astrocytes, which have short IKDs, there is significant up regulation of Erk1/2 activity in prophase and mitosis (Fig. 3.16). Thus, it is conceivable that inappropriate regulation of RTK-Ras pathway in mitosis could directly effect KT-MT attachments and/or KT conformational states. Future work is required to examine this possibility.

Our results also shed light on a recent study that identified genes differentially required in cancer cell lines overexpressing the activated KRAS oncogene (Luo et al., 2009a). Their results suggest that activated Ras oncogene activity triggers differential requirement for a PLK1-kinase-associated mitotic network (Luo et al., 2009a), which they proposed resulted from Ras-induced "mitotic stress". Our results suggest that these phenotypes likely result from KT-MT attachment defects arising from KT conformational abnormalities.

Lastly, our studies also inform the use of large collection of cancer patient molecular signatures. We used >300 GBM patient molecular signatures to create a Bayesian bionetwork, which when combined with our functional genetic data, predicted BUB1B inhibition to be differentially lethal for GBM cells. To our knowledge this is the first time a bionetwork derived solely from patient data has been used to successfully predict a gene activity specifically required for cancer cells. Intriguingly, integrating our BTIC kinome data set into bionetwork for breast

cancer also yielded BUB1B as the top scoring hit (J. Zhu, personal communication), suggesting that our results should prove useful for other cancers.

In summary, our results suggest that GBM tumors and genetically transformed cells have added requirement for BUB1B to suppress lethal consequences of altered KT function. They further suggest that IKDs may predict cancer-specific sensitivity to BUB1B inhibition and perhaps other mitotic targets that affect KT-MT stability.

V. METHODS

ShRNA Bar-code screens and array analysis

For shRNA screen and Bar-code array analysis cells were infected with a pool of lentiviral shRNAs targeting 713 human kinases at a representation of ~1,000 fold (MOI<1). At day 3 post-infection an initial Day-0 sample was taken. The rest of the population was selected with puromycin (Sigma) (2 μg/ml) to remove uninfected cells. Afterwards, cells were propagated in culture for an additional 21 days and sampled for BC array analysis at 21 days. For each passage a minimal representation of 1000 fold was maintained. For each corresponding sample, shRNA barcodes was PCR-recovered from genomic samples, labeled with Cy5 or Cy3, and competitively hybridized to a microarray containing the corresponding probes (Agilent Technologies). Replicate array results were analyzed using the BioConductor package limma. The change in the relative abundance of each shRNA in the library over time was measured using the normalized Cy3/Cy5 ratio of its probe signal. Barcode probes depleted in the BTIC samples were considered candidate genes using the following criteria: 1) adjusted p-value ≤ 0.05 and 2) $|\log2(\text{ratio})| \geq 0.585$.

Cell culture

BTIC and NSC lines were grown in N2B27 neural basal media (Stemcell Technologies) supplemented with EGF and FGF-2 (20 ng/ml each) (Peprotech) on laminin (Sigma) coated polystyrene plates according and passaged according to Pollard (Pollard et al., 2009). Immortalized neural stem cells, CX and VM, were maintained in ReNcell maintenance medium with EGF and FGF-2 (20 ng/ml each) (Peprotech) and also grown on laminin coated tissue culture treated plates and passaged according to Pollard (Pollard et al., 2009). NHA and NHA-Ras cells were grown in astrocyte growth medium (Clonetics) according to the manufacturer's instructions and published protocols (Sonoda et al., 2001).

RNAi

ShRNAs were obtained from the RNAi Shared Resource (FHCRC) or Open Biosystems (Huntsville, AL) in the pGIPZ lentiviral vector. Target sequences for shRNAs are as follows: BUB1B, #1, CDS:1417, CCTACAAAGGAGACAACTA; BUB1B, #2, CDS:1547, AGGAACAACCTCATTCTAA; and KIF11, CDS:571, AAGAGAGGAGTGATAATTA. For virus production pGIPZ-shRNA plasmids were transfected into 293T cells along with psPAX and pMD2.G packaging plasmid to produce lentivirus. ~24 hours after transfection, neural stem cell expansion medium was added to replace original growth medium. Virus was harvested 24 hours after medium change and stored at -80°C. BTICs and NSCs were infected at MOI<1 and selected with 2-4 μg of puromycin for 2-4 days.

RT-qPCR

Quantitect RT-qPCR primer sets and QuantiFast SYBR Green PCR Kits (Qiagen) were used according to the manufacturer's instructions with the ABI Prism 7900 sequence detection system

(Genomics Resource, FHCRC). Relative transcript abundance was analyzed using $2^{-\Delta\Delta Ct}$ method. TRIZOL (Invitrogen) extraction was used to collect total RNA from cells.

Western Blot

Western Blots were carried out using standard laboratory practices (www.cshprotocols.org), except that a modified RIPA buffer was used for protein extraction (150 mM NaCl, 50 mM Tris, 2 mM $MgCl_2$, 0.1% SDS, 0.4% DOC, 0.4% Triton-X 100, 2mM DTT, and complete protease inhibitors (Roche)) followed by a 15 min digestion with 125 U of Benzonase (Merck) at RT. The following antibodies were used for detection: Bub1B (1:1000, Sigma), Actin (1:1000, Cell signal) and cleaved Parp (1:1000, Cell signal). An Odyssey infrared imaging system was used to visualize blots (Li-cor) following manufacture's instruction.

Growth Assays

For short-term outgrowth assays, post-selection, shRNA transduced cells were harvested, counted (Nucleocounter, NBS), and plated onto a 96-well plate. After 7 days under standard growth conditions, cell proliferative rate was measured using Alamar blue reagent (Invitrogen). For long-term outgrowth assays, post-selection, shRNA transduced cells were mixed with non-transduced cells (9:1) and outgrown for 14-24 days using our standard passaging protocol. The GFP+ fraction, which marks shRNA containing cells, of each population was measured by FACS (BD LSR2 flow cytometer; FHCRC Shared Resources) at 5-8 day intervals.

Spindle checkpoint arrest

For image based assessment, cells were plated in a 96 well plate and then treated with paciltaxol (Sigma) and nocodozole (Sigma) for various time points (6-18 hrs). After treatment, cells were

fixed with 2% paraformaldehyde for 30 minutes, permeabilized with 0.25% Triton X-100, and blocked in PBS containing 3% BSA and 5% goat serum. After 3 washes with PBS, cells were stained with MPM-2 (1:300, Millipore) at room temperature for 1 hour. Next, cells were washed and incubated with Alexaflour-568 secondary antibody (Invitrogen) and DAPI for 1 hour in dark. Staining was visualized by Nikon eclipse Ti microscope. For FACS-based assessment, cells were then collected and fixed in 70% ethanol for 1 h at 4°C, then rinsed with ice-cold PBS+2% FCS, and stained with anti-MPM-2 (1:300, Millipore), anti-mouse Alexafluor-568 (1:200, Invitrogen), and DAPI (1 μg/ml). Cells were washed, re-suspended in PBS and filtered. Mitotic index was measured by BD LSR2 flow cytometer (FHCRC Shared Resources).

Mitotic transit time

NSC and BTIC cells were transduced with Control and BUB1B hairpins, respectively. After selection, cells were plated into a 96 well plate for time-lapse microscopy. During imaging, the atmosphere was maintained at a temperature of 37°C and 5% CO2. Imaging was performed using a Nikon Eclipse Ti microscope equipped with a live imaging system. Nikon elements software was used to collect and process data. Images were captured at 5.3 minute intervals for 16 hours.

Lagging chromosome assay

For one-step arrest in prometaphase, cells were treated overnight with the Eg5 kinesin inhibitor monastrol (100μM final concentration) overnight. DAPI staining was performed to visualize abnormal anaphase frequency. Monastrol inhibits the mitotic kinesin Eg5/Kif11, a motor protein required for spindle bipolarity, and specifically arrest cells in G2/M (26, 34). Cells were washed and released into fresh media for 2 hours and then fixed (4% PF), permeabilized, stained with

DAPI, and visualized using a Nikon Eclipse E800 (Scientific Imaging, FHCRC). >400 nuclei will be counted for each trial (n=5) and student's t-test will determine significance. For asynchronous populations, cells were additionally stained with an MPM-2 antibody (Millipore), which marks mitotic cells, and counter stained with DAPI (Sigma). Approximately one third of MPM-2 positive cells in asynchronous cultures where in anaphase/telophase, while the other two thirds where in prometaphase or metaphase.

Chromosome alignment assays

For metaphase staining, Cells were treated by 10 μM MG-132 (TOCRIS Bioscience) for 2 hours to arrest them at metaphase and then fixed for 20 min at room temperature with 4% formaldehyde in PBS and 0.2% Triton X-100. For cold stable microtubules, cells were incubated on ice for 15 min prior to fixation. After fixation, cells were blocked and stained with α-tubulin (Sigma, DM1A; 1:1000) and CREST anti-serum (Immunovision; 1:1000) at room temperature for 1 hour. Cells were washed and incubated with secondary antibody and DAPI for 1 hour in the dark. Immunolabeled cells were imaged on a Deltavision RT deconvolution microscope (Applied Precision Inc., Issaquah, WA). Optical sections were acquired at 0.2 micron spacing with an Olympus 100x/1.4 NA UPLS Apo objective. 3-D image stacks were deconvolved with Applied Precision's proprietary software Softworx, using a constrained iterative algorithm. Deconvolved 3-D data were loaded into the visualization software Velocity (PerkinElmer, Waltham MA). The number of misaligned microtubule-attached kinetochores were counted based on CREST staining on 3-D rendered images, and confirmed by visual inspection of maximum intensity projections of whole cells. Misaligned kinetochores were defined as those with normalized distance <0.2. At least 30 cells were analyzed for each RNAi experiment.

Xenotransplantation

131 BTIC cells were infected with pGIPZ-shRNA virus and selected for 3 days in puromycin (2μg/mL), such that >80% of cells were GFP+. Cells were then harvested using Accutase (Sigma), counted, resuspended in an appropriate volume of culture media, and kept on ice prior to immediate transplantation. NOD-scid IL2Rgammanull mice (Jackson Labs #005557) were anesthetized by IP injection of 0.2ml/10 grams 1.25% Avertin Solution and kept at 37°C. A small bore hole was made in the skull using a hand drill with a Meisinger #009 steel burr bit (Hager & Meisinger GmbH). 2x10^5 cells were slowly injected by pipet into the right frontal cortex approximately 2 mm rostral to Bregma, 2 mm lateral and 3 mm deep through a 0.2-10μl disposable sterile aerosol barrier tip (Fisher Scientific #02-707-30). The burr hole was closed using SURGIFOAM (Johnson & Johnson) and the skin rejoined using TISSUMEND II (Veterinary Product Laboratories, Phoenix AZ).

Brain Tumor Imaging

Seven weeks after initial transplantation mice were injected intravenously with 50μl of 40μM Chlorotoxin: Cy5.5 conjugate (Veiseh et al., 2007) 2 hours prior to sacrifice by carbon dioxide inhalation. The brain and tumor were removed from the skull and imaged for Cy5.5 and GFP fluorescence using the Xenogen IVIS Spectrum imaging system (Caliper Life Sciences).

BTIC classifications

In order to classify BTIC isolates by tumor subtypes according epigenetic signatures produced by The Cancer Genome Atlas (i.e., classical, mesenchymal, neural, and proneural) (Phillips et

al., 2006; Verhaak et al., 2010), we first performed RNA-seq on all BTICs presented in Fig 3.1 (n=3) using an Illumina HiSeq 2000 according to the manufacturer's instructions (FHCRC Genomics Shared Resource). RNA-Seq reads were aligned to the GRCh37/hg19 assembly using Tophat (Trapnell et al., 2012) and counted for gene associations against the UCSC genes database with HTSeq, a python package for analysis of high-throughput sequencing data (Anders, 2010). The R language of statistical computing was used for further analysis (R Development Core Team, 2011). All data was combined and normalized using a trimmed mean of M-values (TMM) method from the R package, edgeR (Robinson et al., 2010; Robinson and Smyth, 2007, 2008). Normalized counts were then log transformed, and the means across all the cell lines were used to calculate relative gene expression levels. The BTIC line data was clustered using a Manhattan distance complete-linkage method to establish leaflets. Previously 173 glioma cell lines were subtyped using the expression of 840 signature genes (Verhaak et al., 2010). Our samples were clustered using 790 of these genes. The associations of our cell lines to those in publication were determined by minimum Manhattan distance to expression centroids produced by ClaNC. If a gene was expressed consistently in a particular subtype by absolute distance than that was counted as a 1 and the number of associated genes in each category were summed. As a validation, the four subtypes are clearly distinguished when the method is applied to the 173 glioma lines described previously (Verhaak et al., 2010).

Construction of GBM Bayesian Network

The Bayesian network is one type of probabilistic causal network, providing a natural framework for integrating diverse types of data (where a joint probability can be decomposed to several conditional probabilities as $p(X_1,...,X_n) = \prod_{i=1}^{n} p(X_i \mid Pa(X_i))$). Bayesian networks have

been successfully used for modeling complex human diseases such as diabetes and obesity in different models (Schadt et al., 2005; Schadt et al., 2008; Yang et al., 2009; Zhu et al., 2004). Because the edges in Bayesian networks are directed, they not only represent interactions among genes, but also, when such information is available, they can represent causal associations between genes especially when genetic information is used as priors (Schadt et al., 2005; Zhu et al., 2007; Zhu et al., 2008).

To accurately construct a Bayesian network *de novo*, a large number of heterogeneous samples are needed (Zhu et al., 2007). As a result of The Cancer Genome Atlas (TCGA), gene expression data for over 300 GBM has been generated using standardized isolation techniques and data collection platforms (Cancer Genome Atlas Research Network, 2008). To begin building the network, we selected genes from 319 brain tumor expression profiles which could be robustly detected. Gene expression, which is a continuous variable, was discretized into one of three possible states (i.e., down-regulated, up-regulated, or no change relative to the reference channel) guided by k-means clustering (Zhu et al., 2007), modified to discourage extremely unbalanced classes. From this process, 8451 genes were identified and put into a Bayesian network construction software program based on a previously described algorithm (Zhu et al., 2004; Zhu et al., 2007).

The fitting of a network model M given observed data D is evaluated by the Bayes formula to determine the probability as a function of our prior belief that the model is correct and the probability of the observed data given the model: $P(M \mid D) \sim P(D|M) * P(M)$. The number of possible network structures grows exponentially with the number of nodes, so an exhaustive search of all possible structures to find the one best supported by the data is not feasible, even for a relatively small number of nodes. We employed Monte Carlo Markov Chain

(MCMC)(Madigan and York, 1995) simulation to identify potentially thousands of different plausible networks, which are then combined to obtain a consensus network (see below). Each reconstruction uses a random seed. Random local changes are then made by flipping, adding, or deleting individual edges, ultimately accepting those changes that lead to an overall improvement in the fit of the network to the data. We assess whether a change improves the network model using the Bayesian Information Criterion (BIC) (Schwarz, 1978), which avoids over-fitting by imposing a cost on the addition of new parameters. This is equivalent to imposing a lower prior probability P(M) on models with larger numbers of parameters.

We reconstructed 1000 Bayesian networks starting with 1000 different randomly seeds. Markov Chain Monte Carlo simulation was then employed to identify the most plausible networks. For each seed, $12*N^2$ iterations of MCMC were run, where N is the number of nodes in the network. From the 1000 reconstructed networks we determined the consensus network by retaining only those edges represented in a percentage of the individual networks. From the resulting set of 1000 networks generated by this process, edges that appeared in greater than 30% of the networks were used to define a consensus network. Edges in this consensus network were removed if 1) the edge was involved in a loop, and 2) the edge was the most weakly supported of all edges making up the loop. The resulting network consists of 14,349 links. Since this network is solely created from expression profiles, it represents nodes that are transcriptionally regulated within GBM tumors.

Screen hit prioritization

The shRNA kinome screen revealed 48 candidate genes differentially required for BTIC-G166 growth, as compared to NSC-CB660 cells (Supplemental Table S1). The 48 candidates

comparing to random 48 candidates drawing from the kinome library were significantly enriched for GO biological processes histone phosphorylation, integrin-mediated signaling pathway, protein amino acid phosphorylation, and regulation of cell cycle with permutation-based p-values 0.002, 0.001, 0.005, and 0.009.

In an attempt to refine this analysis, we next examined whether hits could be parsed into distinct pathways and/or complexes using protein-protein interaction networks similar as outlined by ref. 20. By this analysis, most of hits were connected in a single, large subnetwork, enriched for 248 GO biological processes (multiple testing adjusted p-value<0.01), such as protein kinase cascade (p-value= 5.57881e-085) and protein amino acid phosphorylation (p-value=1.10068e-082). This lack of specific biological processes likely reflected the fact that these kinases are well studied and involved in many biological processes and thus did not provide any useful information for prioritizing of candidate hits.

As an alternative strategy, we examined the occurrence of screen hits in GBM specific regulatory network, constructed de novo from over 421 TCGA GBM tumor samples (Cancer Genome Atlas Research Network, 2008) by integrating gene expression and DNA copy number variation data (Tran et al., 2011; Zhu et al., 2008). 37 of 48 shRNA candidate hits appeared as nodes in the GBM network. Analysis of subnetworks in the GBM network, revealed 15 biological processes significantly enriched (5 cell cycle related, 9 general phosphorylation related), including the M phase of mitotic cell cycle (p-value=1.64e-5). For GBM, the largest subnetwork contained four screen hits, including AURKA, BUB1B, MELK, and PLK1 (Fig. 3.4). By a key driver node analysis, a metric that helps predict the relative importance of nodes (Yang et al., 2009; Yang et al., 2011b), BUB1B scored as the top ranked screen hit (p-value = 0.003). We further checked shRNA candidate hits in a normal brain transcriptional network

constructed 160 non-dementia normal human prefrontal cortex samples. By contrast, there are only 20 of 48 candidate hits in the normal brain network, candidate hit subnetworks in the normal brain network are smaller. These subnetworks are only enriched for general phosphorylation related GO biological processes (data not shown). And BUB1B is connected only one gene in the network (Fig. 3.1B).

ACKNOWLEDGEMENTS

We thank: Sue Biggins for critical reading of this manuscript; Jan van Deursen, Howard Fine, Russell Pieper, Xiao-Nan Li, Julian Simon, and Austin Smith for providing cell lines and/or reagents; Stacey Hansen and Sally Ditzler for technical help; Pam Lindberg and Laima Abele for administrative support; members of the Paddison and Olson labs for helpful discussions. This work was supported by grants from: the PEW scholar program (PP), the Accelerate Brain Cancer Cure foundation (PP), a UK-US Stem Cell Collaboration Development Award program

VI. FIGURES

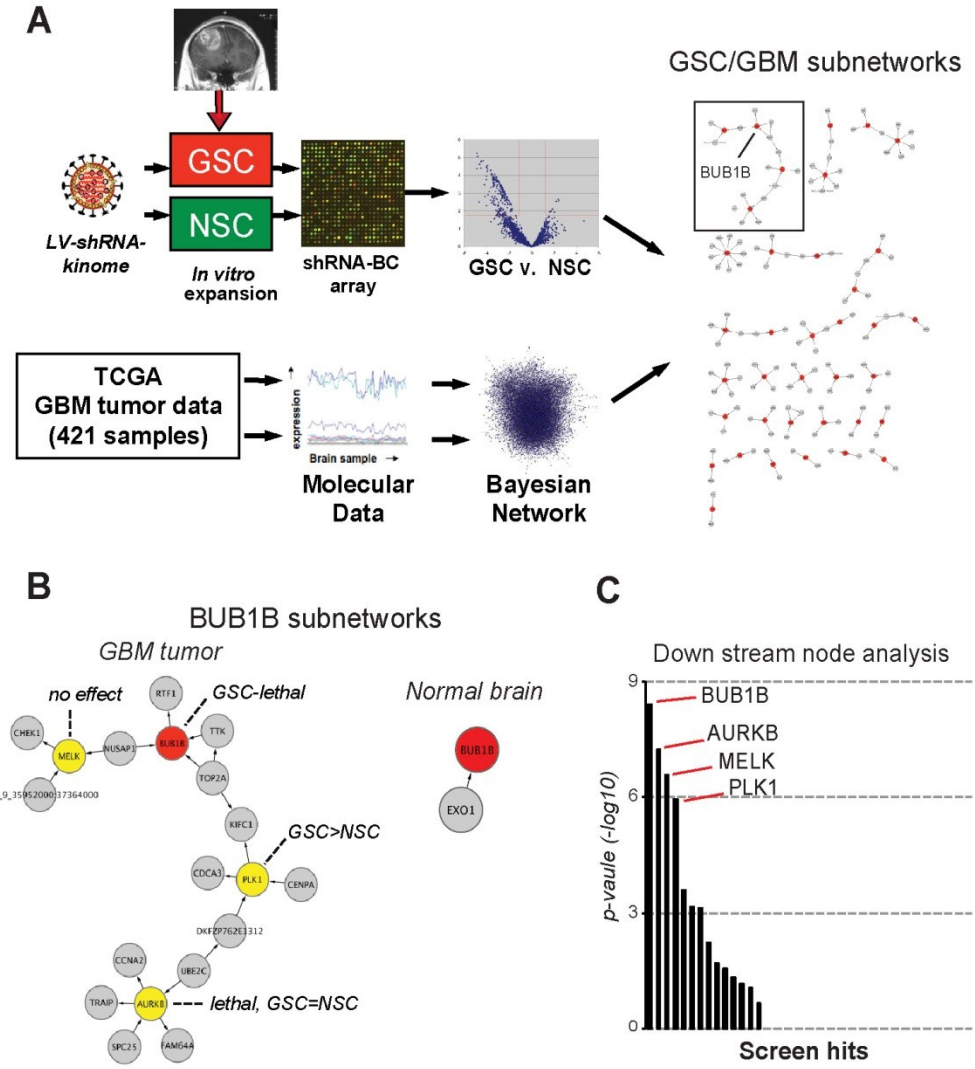

Figure 3.1. Integration of RNAi screens in patient-derived BTICs and GBM bionetworks
(A) Overview of shRNA screens, GBM network generation, and results of seeding screen hits into GBM network (see Methods for further details on GBM network construction and screen comparisons).
(B) BUB1B subnetworks from GBM tumors and also from normal brain networks. Also indicated are the node inhibition BTIC and NSC growth phenotypes.
(C) Down steam node analysis, a metric that helps predict the relative importance of nodes (14, 23) of BTIC-specific screen hits which appear in the GBM Bayesian network. Figure by Yu Ding.

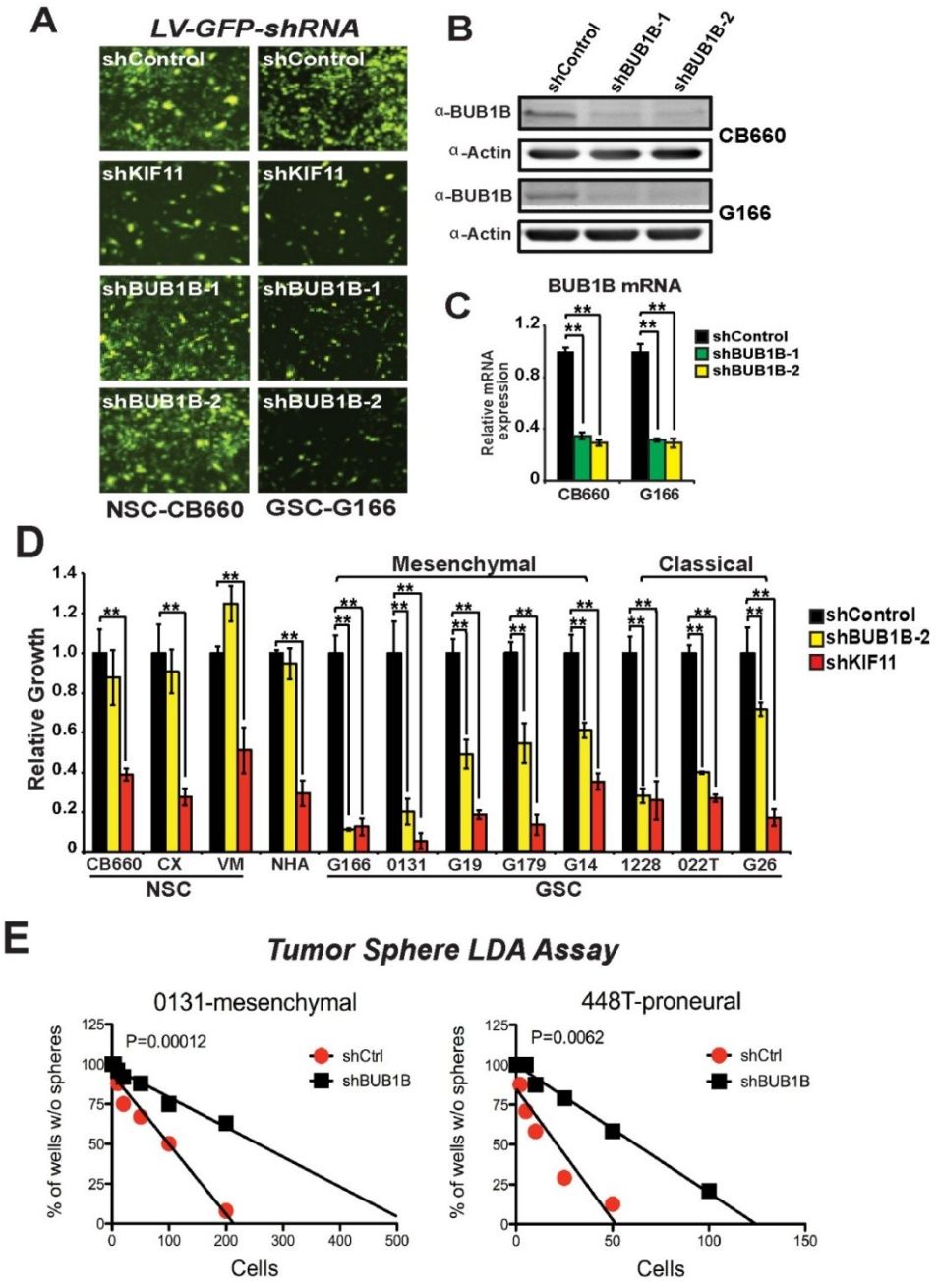

Figure 3.2. BUB1B validates as a candidate GBM-lethal gene *in vitro*

(A) BTIC-specific effects of BUB1B knockdown, visualized using shRNA-GFP+ BTICs and NSCs 6 days after post-transduction with pGIPz-shRNA virus. Knockdown of KIF11/EG5, which encodes a microtubule motor protein critical for bi-polar spindle formation during mitosis (Sawin et al., 1992), was used as a positive control for both RNAi pathway activity and cell proliferation.

(B-C) Examination of BUB1B knockdown by western blot and RT-qPCR analysis in BTIC-G166 and NSC-CB660 cells.

(D) Comparison of the effects of BUB1B knockdown on *in vitro* expansion of multiple BTIC and NSC lines and normal human astrocytes (NHAs). **indicates student's t-test p <.01. BTIC isolates were developmentally subtyped according to (Verhaak et al., 2010).

(E) Limiting dilution assays (LDA) for *in vitro* tumor sphere formation. BTIC-0131 cells and also un-passaged primary GBM tumor cells (448T) were transduced with indicated LV-GFP-shRNAs, diluted and assayed for sphere formation after 14 days. Linear regression analysis was used to evaluate significance. Figure by Yu Ding.

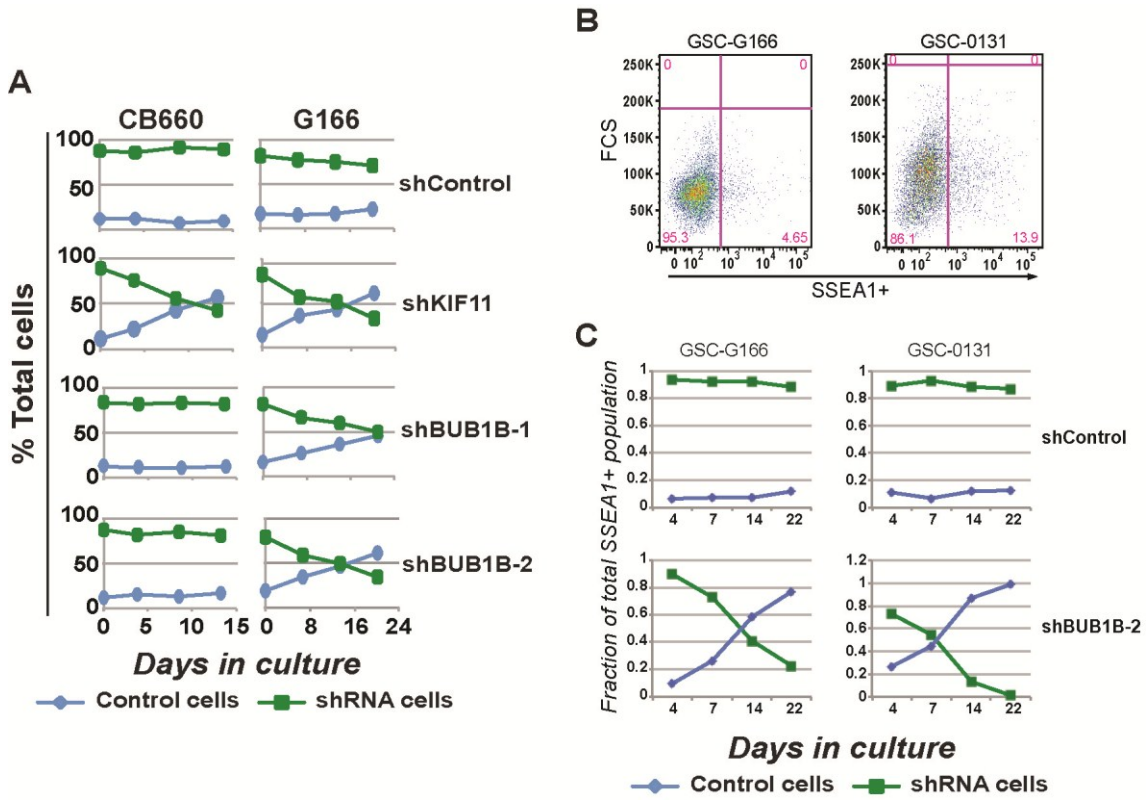

Figure 3.3. BUB1B knockdown prevents longer-term expansion BTICs and SSEA1+ BTIC subpopulations.

(A) ShRNA competition experiments during BTIC and NSC in vitro expansion. Transduced NSC-CB660 and BTIC-G166 cells were mixed in a 9:1 ratio with non-infected cells, and out grown for indicated number of days (n=3). ShKIF11 served as a positive control for growth inhibition.

(B) Assessment of SSEA1+ subpopulations in G166 and 0131 BTICs by FACS. Approximately 5% of G166 and 14% of 0131 cells are SSEA1+ in asynchronously monolayer cultures.

(C) ShRNA competition assay monitoring SSEA1+ BTIC subpopulations. Cells were transduced with shControl or shBUB1B GFP expression vectors, mixed with non-transduced cells at approximate 9:1 ratio at time zero, and expanded *in vitro* in monolayer conditions. Populations were flow analyzed over the course of 22 days during *in vitro* expansion. Similar results to shBUB1B were observed with shKIF11 (data not shown). Linear regression analysis demonstrated significant differences between changes in shBUB1B representation (G166, p-value=0.002333; 0131, p-value=0.01099). Figure by Yu Ding.

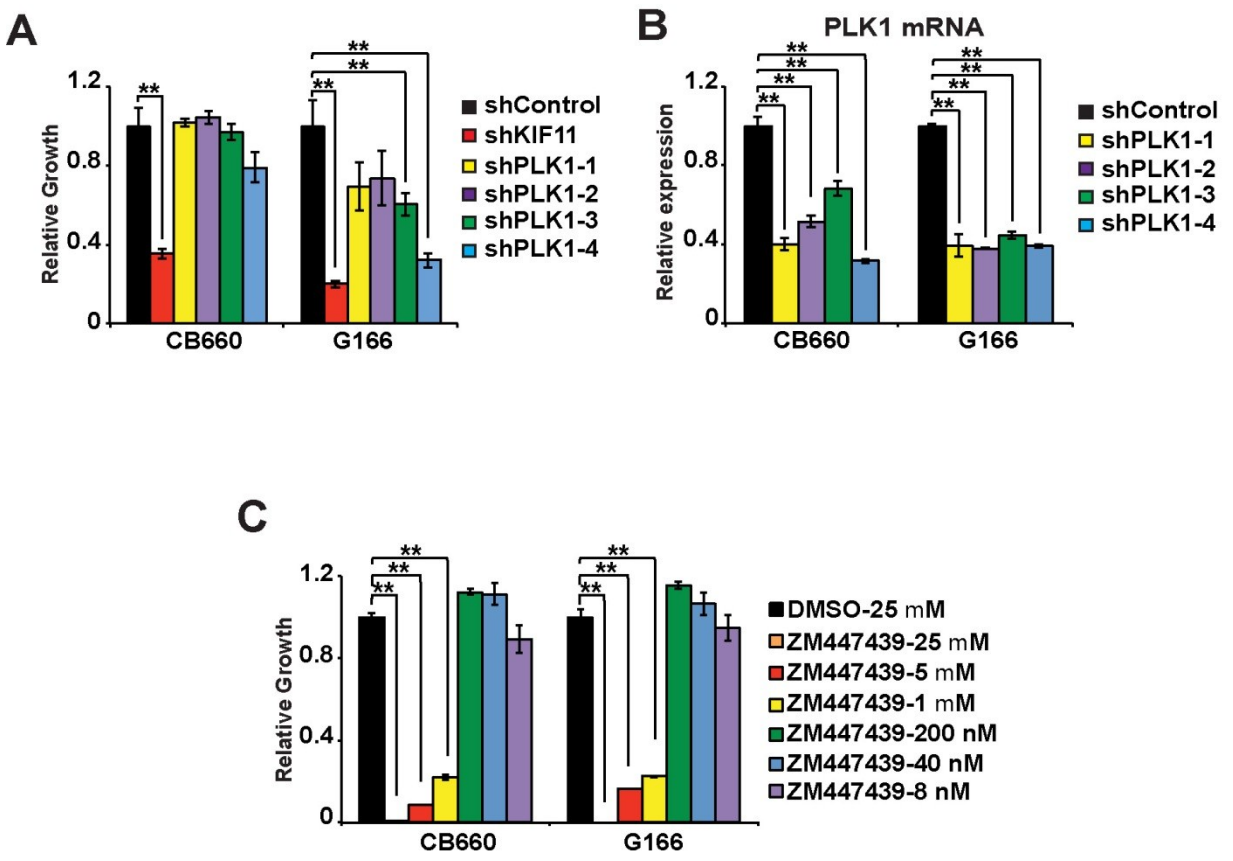

Figure 3.4. BTIC and NSC growth phenotypes resulting from knockdown of PLK1 and pharmacological inhibition of Aurora B kinase.

(A) Knockdown of PLK1 using pGIPz-shRNA lentiviral expression system. Cells were transduced,puromycin selected, seeded in microtiter growth dishes, outgrown for 7 days, and assayed using Alamar blue viable stain (Invitrogen).
(B) PLK1 expression after shRNA knockdown. RNA expression measured by RT-QPCR.
(C) Pharmacological inhibition of AurkB using ZM447439. CB660 and G166 cells were seeded in microtiter grow dishes and treated with various concentrations of ZM447439 in normal culture conditions. After seven days, wells were assayed for cell growth using Alamar blue. Medium was changed every two days with same drug dilutions. Results show that AurkB inhibition impacts BTICs and NSC equally. Similar results were observed in Ras-transformed and non-transformed human fibroblasts (data not shown). **indicates student's t-test $p < .01$. Figure by Yu Ding.

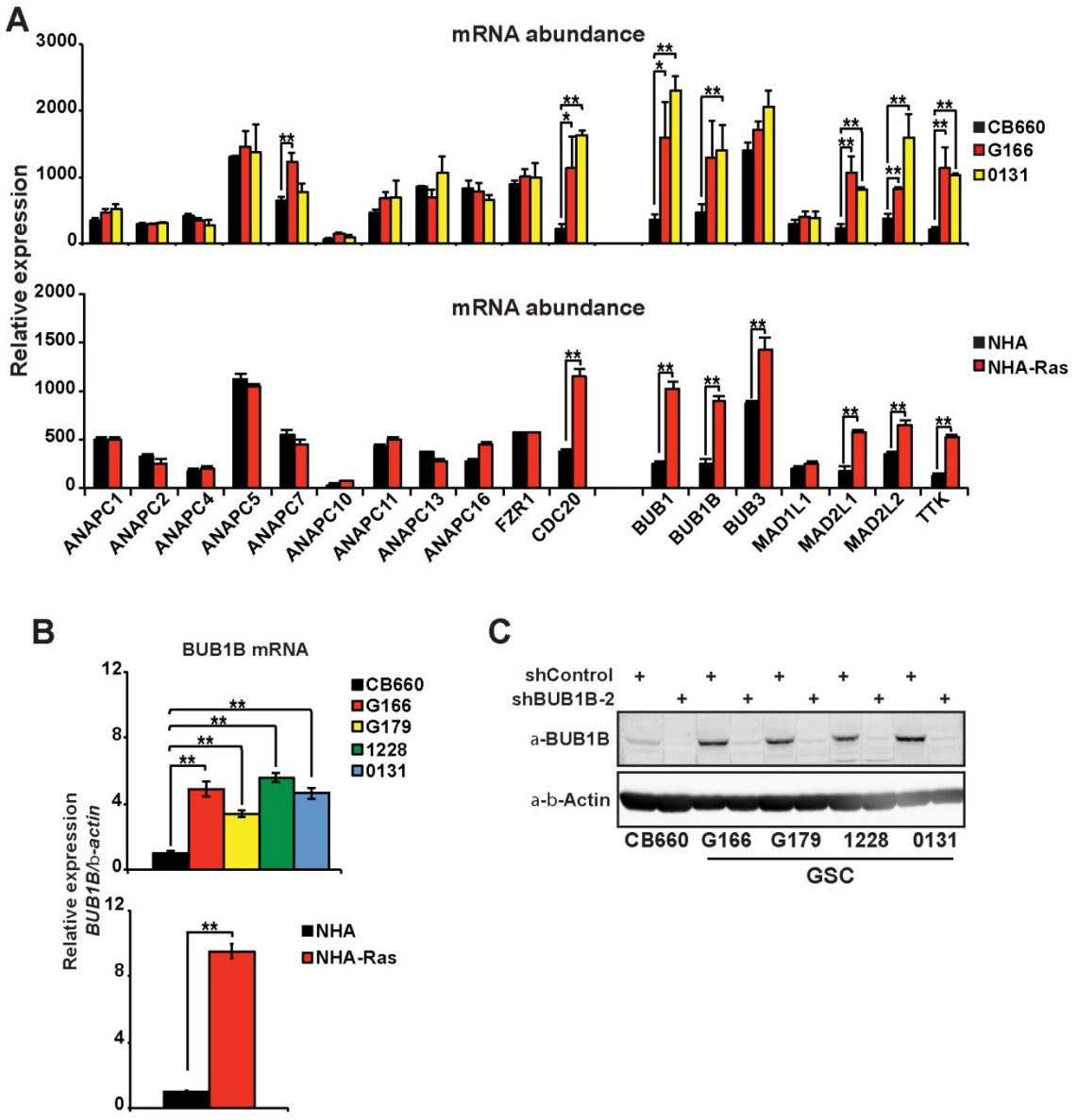

Figure 3.5. BUB1B and other mitotic checkpoint genes are up-regulated in BTIC isolates and Rastransformed astrocytes.

(A) mRNA abundance of mitotic checkpoint genes and components of the anaphase promoting complex (APC) in BTICs, NSCs, Ras-transformed astrocytes, and normal human astrocytes (NHAs). RNAsequencing (n=3) was performed on each cell type (see Supplementary Information for details). After normalization, relative abundance of checkpoint and APC gene RNA was examined. While APC core subunits failed to show a change in expression, several mitotic checkpoint genes, including BUB1B, showed significant up regulation. *indicates student's t-test p <.05, **indicates student's t-test p <.01.
(B) Verification of BUB1B RNA expression differences in BTIC and NHA-Ras cells. RT-qPCR was performed on total RNA extracted from indicated cell type. BUB1B values were normalized to beta-actin expression, showing similar results to those seen in a. **indicates student's t-test p <.01.
(C) Verification of BUB1B protein expression differences in BTICs and NSCs. Figure by Yu Ding.

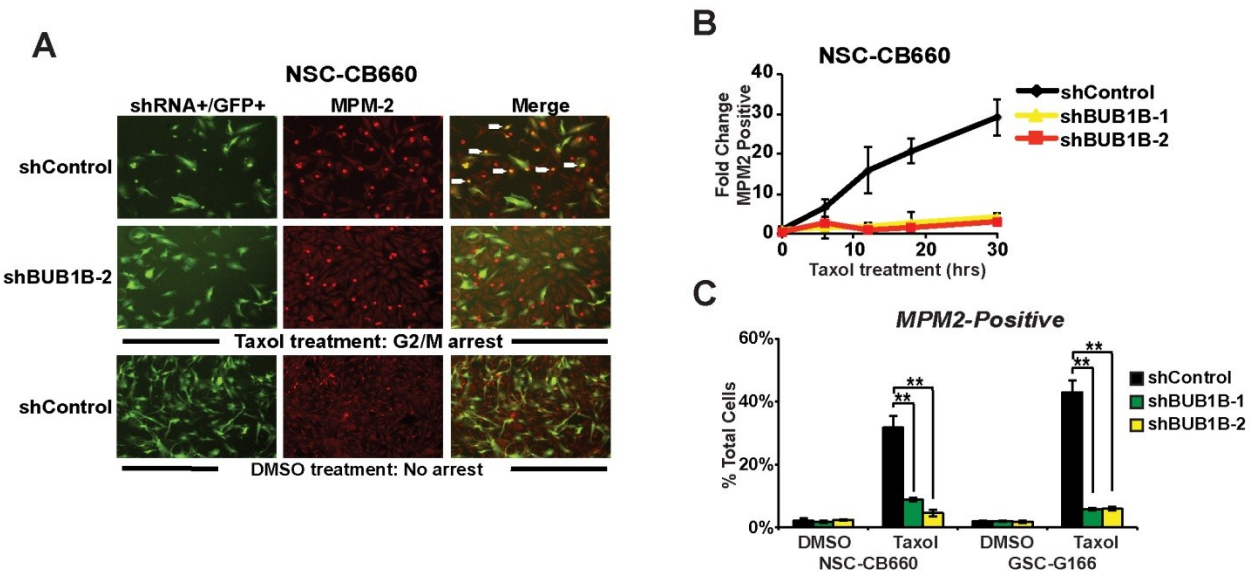

Figure 3.6. Examination of the effects of BUB1B knockdown on mitotic checkpoint activity.
(A) Fluorescent micrographs of checkpoint arrest assay using MPM-2 staining to identify mitotic cells. Fixation and staining was performed in shRNA/GFP transduced NSCs 18hrs post-taxol treatment (10x maginification). Arrows show overlap with GFP+ and MPM-2+ cells in control cells. Low panel shows DMSO treated controls at lower magnification (4x) showing few MPM-2+ cells.
(B) Quantification of Taxol-induced mitotic arrest in NSCs with and without BUB1B knockdown. Cells were infected with shControl and shBUB1B virus at <20% infection efficiency. 72hrs post-infection, cells were treated with taxol for indicated times and stained with the MPM-2 antibody. GFP+ and MPM-2+ cells were counted at various time points (n=3). Fold change reflects the change in GFP+MPM2+ staining
relative to time 0. **indicates t-test pvalue<.01.
(C) Comparison of Taxol-induced arrest in BTICs and NSCs. Cells were infected with indicated hairpins and selected with puromycin (48hrs). After selection, cells were treated with Taxol for 18hrs and stained with MPM-2 antibody and counted (n=3). Results show similar abrogation with BUB1B knockdown. **indicates student's t-test pvalue<.01. Figure by Yu Ding.

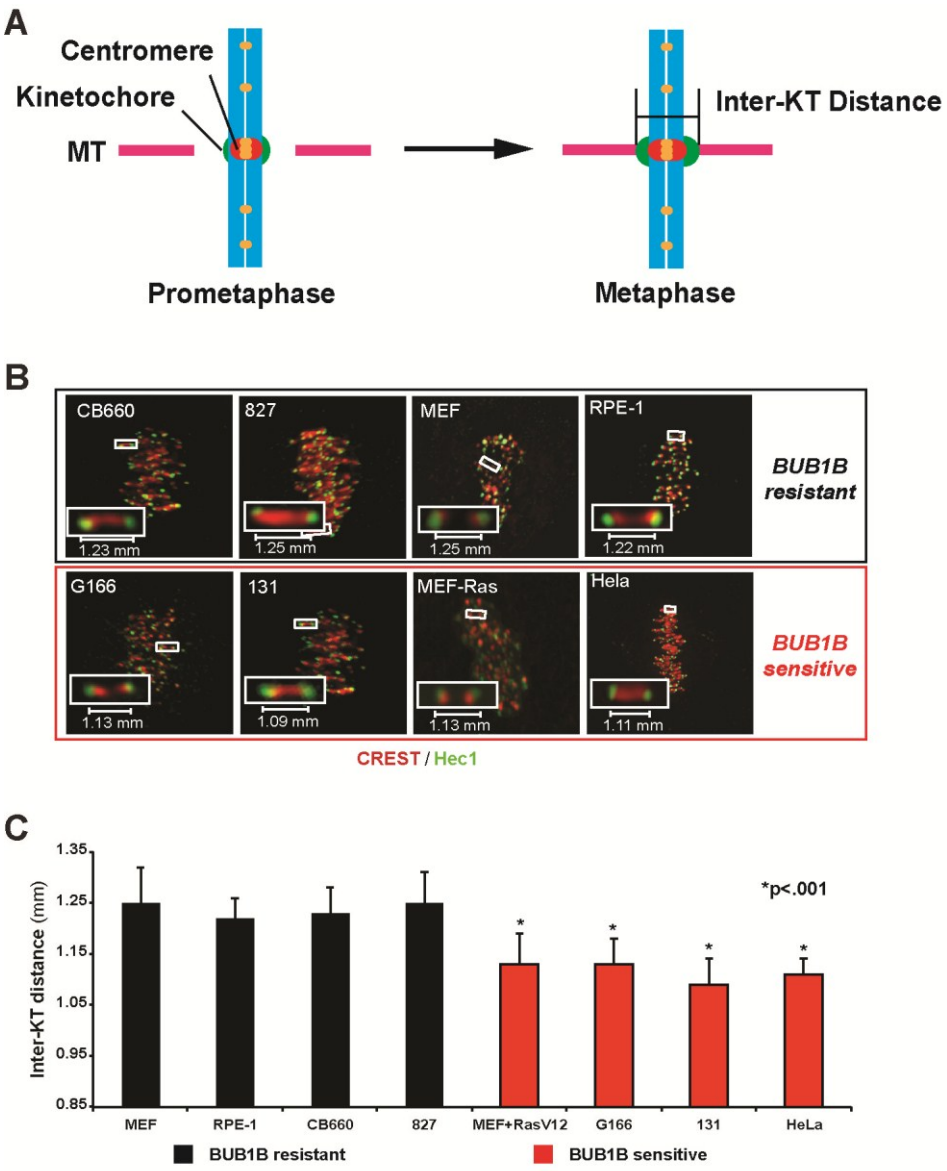

Figure 3.7. Measurement of inter-kinetochore distance (IKD) in BUB1B resistant and sensitive cells

(A) Cartoon showing IKD measurement.

(B) Measurement of IKDs in BTICs, NSCs, MEF, MEF-Ras, RPE and Hela cells using immunofluorescent staining of kinetochores. Constitutive associated centromere network (CCAN/CREST) proteins (red) and outer kinetochore protein, Hec1, (green) were visualized to identify kinetochore pairs. IKDs were measured between Hec1 centroids using AppliedPrecision Softworx software package.

(C-D) Quantification of IKDs from (B). *denotes p<.001 by student's t-test. Figure by Yu Ding.

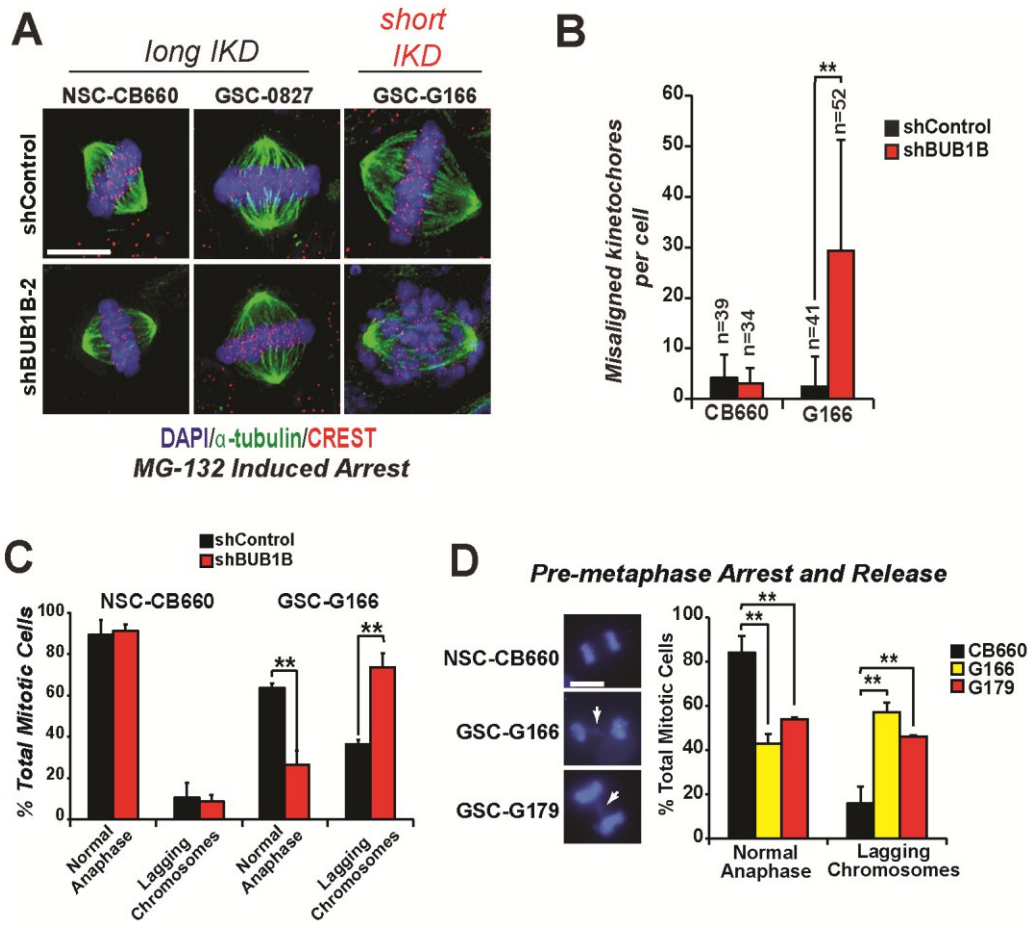

Figure 3.8. BTICs with short inter-kinetchore distances require BUB1B activity to suppress KT-MT attachment defects

(A) Chromosome alignment assays in BTICs and NSCs with BUB1B knockdown. Transduced cells were treated by 10 μM MG-132 for 2 hours to arrest them at metaphase and then fixed, stained as indicated (CREST anti-serum stains human kinetochores) and visualized using deconvolution microscopy. Scale bar indicates 10 microns.

(B) Quantification of misaligned kinetochores ("n" indicates number of metaphase cells counted; ** indicates p<.001 by student's t-test).

(C) Chromosome segregation defects observed in BTICs are exacerbated by BUB1B knockdown. Cells were transduced with LV-GFP-shRNA vectors, selected in puromycin, stained with an MPM-2 antibody, which marks mitotic cells, and DAPI, and examined for the appearance of lagging chromosomes in anaphase/telophase cells (n=3, >40 anaphases scored).

(D) Assays for lagging anaphase chromosomes were performed by overnight arrest with the KIF11 inhibitor monastrol (100μM) followed by release for 2 hours in normal media. Lagging chromosomes were visualized by fluorescence microscopy after fixation and DAPI staining. White arrows in left panels show typical examples of lagging chromosomes scored in BTICs (scale bar = 10 μm). >400 nuclei were counted for each trial (n=5). Figure by Yu Ding.

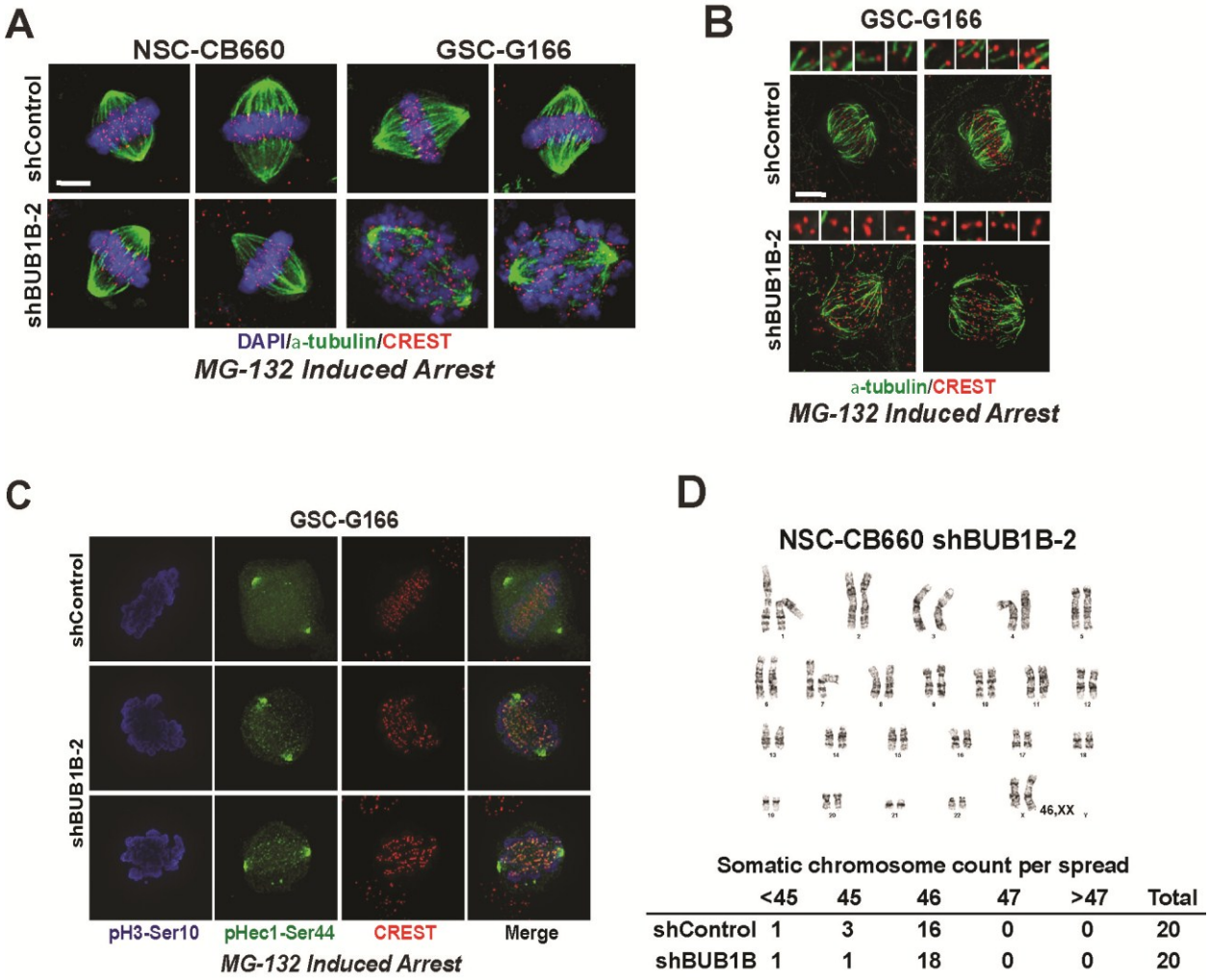

Somatic chromosome count per spread

	<45	45	46	47	>47	Total
shControl	1	3	16	0	0	20
shBUB1B	1	1	18	0	0	20

Figure 3.9. Additional information showing cancer cells have added requirement on BUB1B for chromosome alignment and KT-MT attachment.

(A) Additional examples from chromosome alignment assays used in Figure 3.8A & 3.8B. shRNA transduced cells were treated by 10 μM MG-132 for 2 hours to arrest them at metaphase and then fixed, stained as indicated (CREST anti-serum stains human kinetochores) and visualized using deconvolution microscopy. Scale bar indicates 5.5 microns.

(B) KT-MT attachment assay. shRNA transduced cells were treated by 10 μM MG-132 for 2 hours to arrest them at metaphase. Cell were treated with cold and then fixed, stained as indicated (CREST anti-serum stains human kinetochores). Cold stable microtubules were visualized using deconvolution microscopy. Scale bar indicates 5.5 microns.

(C) BUB1B knockdown in BTICs results in increased Hec1-Ser44 phosphorylation. Mitotic kinetochores that are not stably attached to MTs have increased phosphorylation of Hec1 on Ser44 (see main ref. 23). BTICs transduced with BUB1B shRNAs were treated with 10μM MG-132 to elicit metaphase arrest and stained for histone H3-Ser10-P (to detect mitotic cells), Hec1-Ser44-P, and CREST anti-serum. Typical results are shown, indicating that Hec1-S44-P is detected at kinetochores of BUB1B knockdown BTICs.

(D) Karyotype of NSC-CB660 after two weeks of expansion with BUB1B knockdown. No significant differences were noted from control knockdown cells (n=20 metaphase spreads). Figure by Yu Ding.

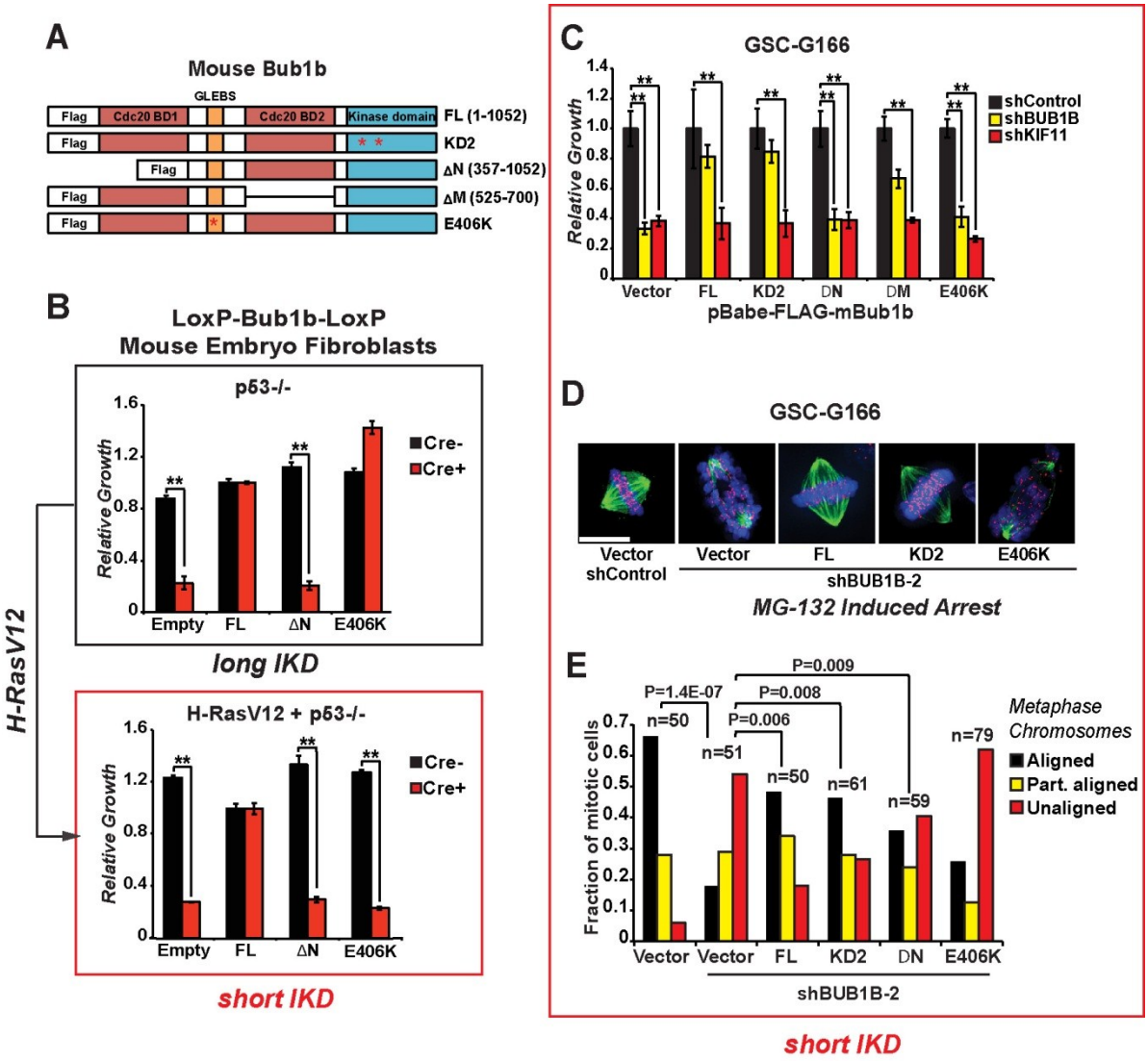

Figure 3.10. Allelic complementation studies with mouse Bub1b mutants in Bub1b-/- MEFs and BTICs

(A) The mouse alleles used in these studies were previously published (Malureanu et al., 2009) and include: full length; KD2, which harbors two point mutations in the kinase domain (K784>R in the ATP binding domain and K802>R in the catalytic domain); ΔN, which lacks the N-terminal Cdc20-binding domain 1; ΔM, which lacks the C-terminal Cdc20-binding domain 2; and E406K, which creates a point mutation in the GLEBS motif that interferes with kinetochore localization and Bub3 binding.
(B) Viability assessment of complementation studies using p53-/- MEFs with floxed alleles of Bub1b with and without transformation via H-RasV12.
Knockdown of BUB1B in Ras-transformed normal human astrocytes (NHAs) phenocopies BUB1B requirement observed in BTICs with respect to viability. MEFs were transduced with MSCV-GFP-mBub1b constructs, sorted for GFP+, outgrown, transduced with pMSCV-Puro-Cre, selected, and seeded into microtiter growth dishes for proliferation assays.
(C) Viability assessment of complementation studies using BTIC-G166 with shBUB1B (or controls) expressing each of five mBub1b alleles from (A). Assays were performed as in Figure 3.1C.
(D) & (E) Chromosome alignment after complementation of BUB1B knockdown with mBub1b alleles, as in Figure 3.8A & 3.8B. Scale bar indicates 10 microns. Figure by Yu Ding.

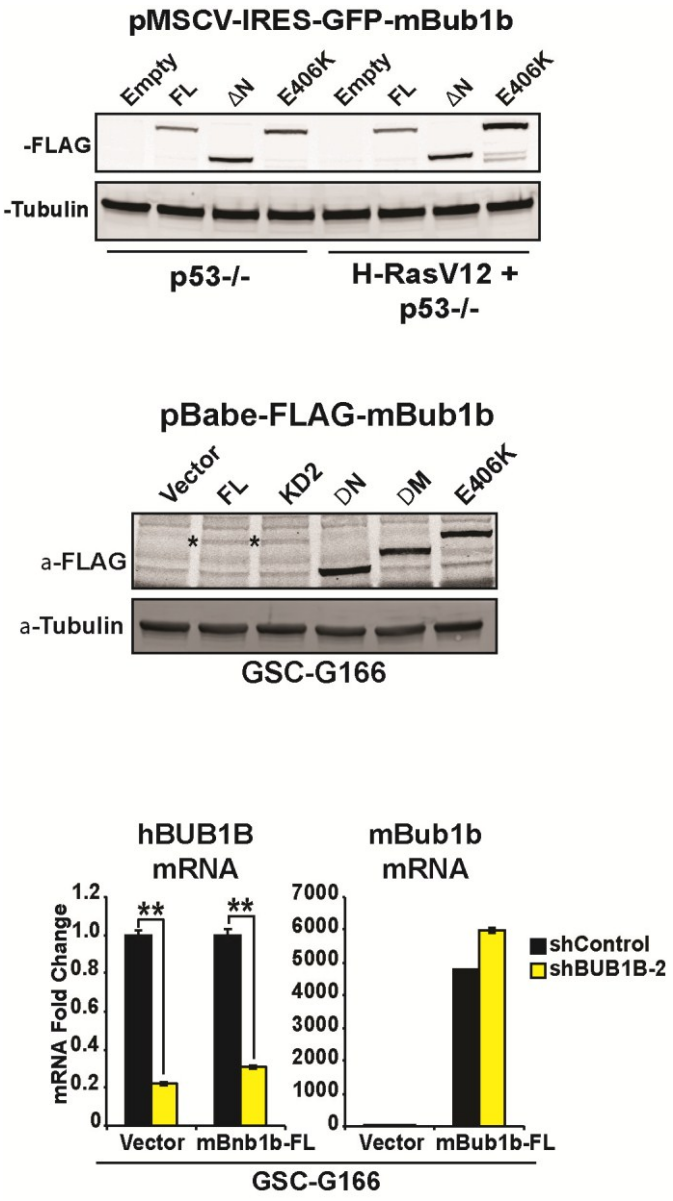

Figure 3.11. Supplemental data for Figure 3.10.
(A) Verification of protein expression of mBUB1B alleles in MEFs from Figure 3.10B & 3.10C.
(B) Verification of protein expression of mBUB1B alleles in BTIC-G166 cells from Figure 3.10C. Bub1b alleles were expressed using pBabe-Neo after viral transduction (MOI=1) and G418 selection. While full length and KD2 expression appears weak, higher levels attained using the MSCV vector system in (A) significantly reduced cell growth (data not shown).
(C) Confirmation of RNA expression of endogenous human BUB1B and ectopically expressed mBub1b with and without hBUB1B knockdown. Importantly, the human shBUB1B only silenced the endogenous BUB1B gene, having no effect on expression of the mBub1b allele; conversely, expression mBub1b did not affect the penetrance of hBUB1B silencing. Figure by Yu Ding.

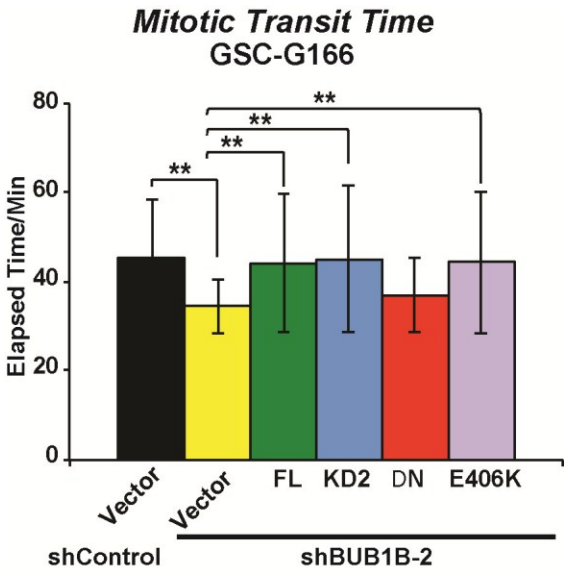

Figure 3.12. Measurement of mitotic transit times BTIC-G166 cells using live microscopy for mBUB1B allelic complementation experiments (from Figure 3.10).
Average mitotic transit times (elapsed time from nuclear envelope break down to cytokinesis) are shown for each complementation trial (n>80 mitotic cells). ** indicates p<.001 by student's t-test. Figure by Yu Ding.

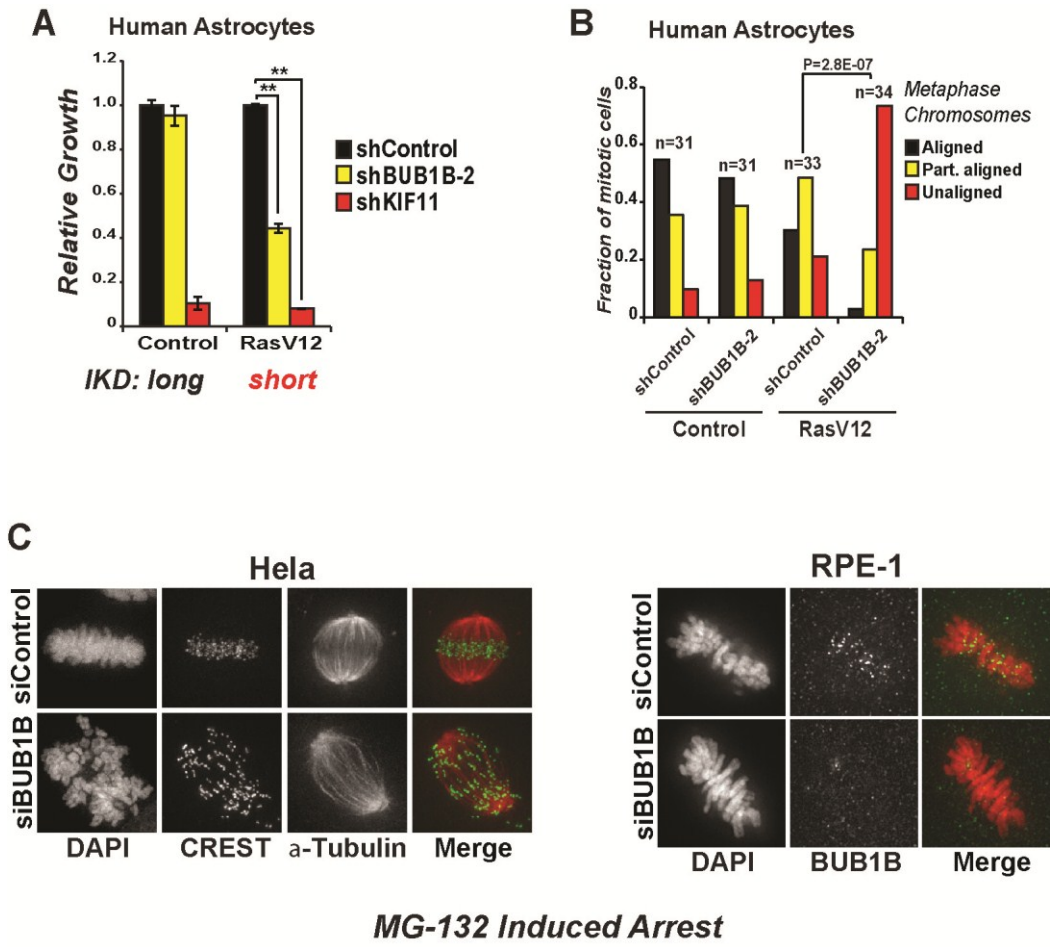

Figure 3.13. Effects of BUB1B knockdown on in human astrocytes, RasV12 transformed astrocytes, Hela cells and RPE-1 cells.

(A) & (B) Knockdown of BUB1B in Ras-transformed human astrocytes phenocopies BUB1B requirement observed in BTICs. (A) BUB1B knockdown results in growth defects in RasV12-astrocytes but not untransformed astrocytes. Assays were performed as in Figure 3.2C. ** indicates p<.001 by student's t-test. .

(B) Chromosome alignment assays in NHAs and Ras-NHAs as performed in Figure 3.10E.

(C) Chromosome alignment assays in Hela cells and RPE-1 cells transfected with siControl or siBUB1B. BUB1B/BUBR1 knockdown results in severe chromosome alignment defects in Hela cells but not in untransformed RPE-1 cells. Cells were transfected with control or BUB1B/BUBR1 siRNA (Dharmacon) and 48hrs later treated with MG-132 for 2hrs to induce mitotic arrest and stained for BubR1, CREST, Tubulin and/or DAPI. 93% of HeLa cells treated with siBUB1B have severe KT-MT attatchment defects (n>100), compared to only 17% for control; while KT-MT attachment was similar regardless of siBUB1B treatment (n>150). Figure by Yu Ding.

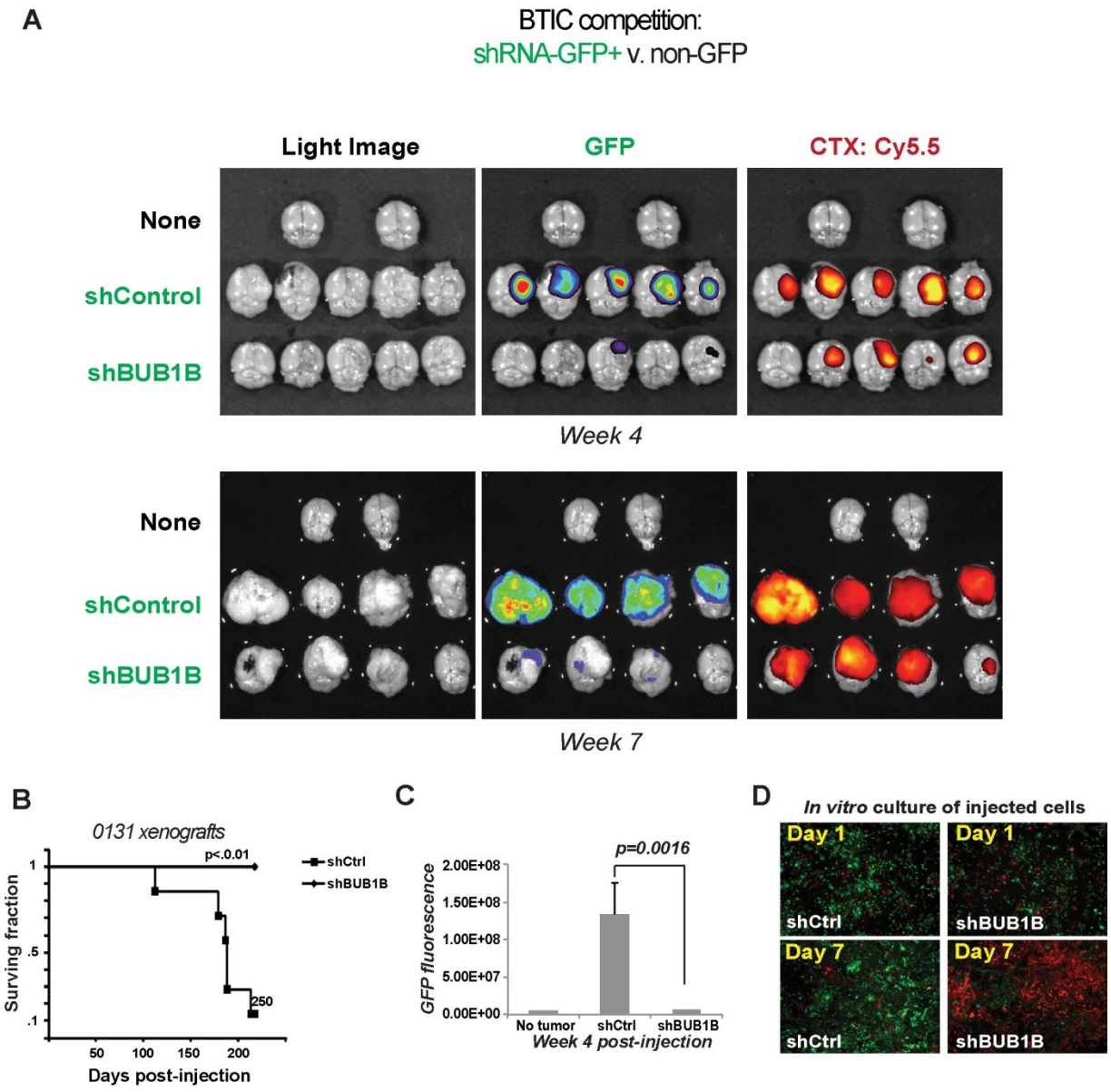

Figure 3.14. BUB1B knockdown inhibits BTIC-dependent tumor growth

(A) Orthotopic xenotransplants of 131 BTIC cells after stable transduction with shControl or shBUB1B. Upper & lower panels: experimental NSG mice 4 and 7 weeks post injection, respectively. Right panels: light images of brains from control Middle panels: GFP+ fluorescence marking shRNA containing cells. Left panels: fluorescent signal from Chlorotoxin:Cy5.5 conjugate marking bulk tumor mass. Results indicate that GFP expressing shBUB1B cells were unable to contribute to formation of orthotopic tumors and yielded tumor masses dominated by wild type control cells with little to no detectible GFP expression. Quantification of GFP fluorescence in tumor 0131 orthotopic xenotransplants is shown in Figure S9.
(B) Survival plots for mice with BTIC-0131 brain xenografts with or without knockdown of BUB1B. (Median survival for shCtrl = 178 days; shCtrl n=7; shBUB1B n=6)
(C) Quantification of GFP fluorescence from part A, 4-week time point.
(D) Fluorescent images of cells from part A cultured in vitro in parallel to in vivo studies. Figure by Yu Ding.

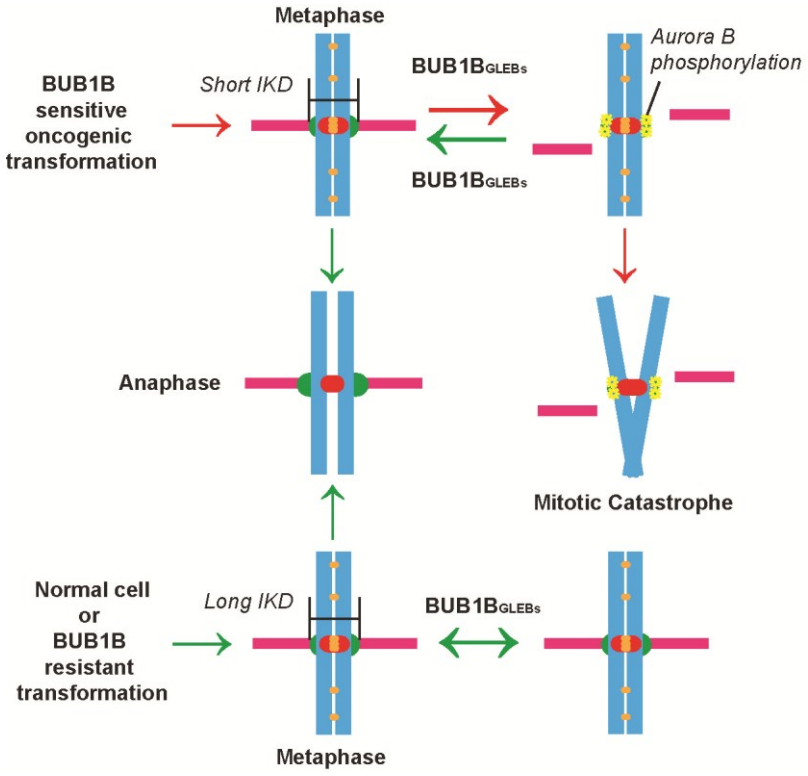

Figure 3.15. A model for BUB1B function in GBM and genetically transformed cells
Figure by Yu Ding.

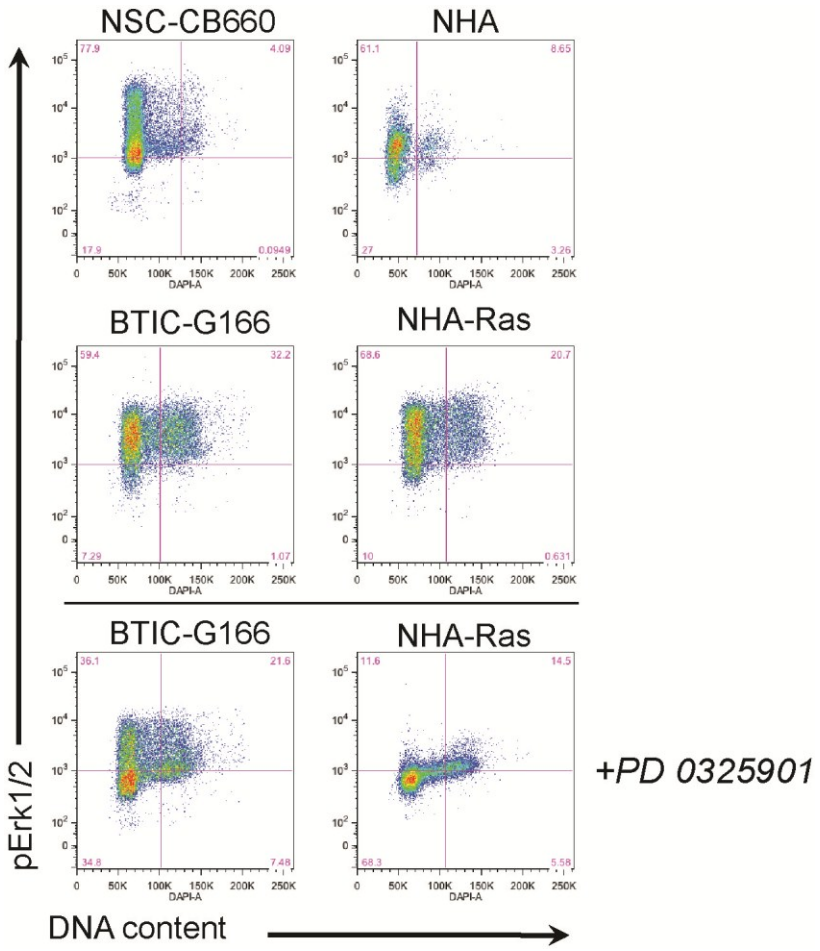

Figure 3.16 Ras-Mapk signaling is inappropriately high BTICs and NHA-Ras cells.
Phosphorylation status of down stream effectors of Ras signaling pathway Erk1/2 was assayed at different phases of the cell cycle. Erk1 and Erk2 are phosphorylated by MEK1/2 at Thr202/Tyr204 and Thr185/Tyr187 as a direct result of Ras/Raf/Mek activity. Using FACS as a read out, we observed significant increases in the intensity of phopho-Erk1/2 staining in G2/M populations of both Ras-transformed NHAs and G166-BTICs as compared to the G2/M populations of NSCs and NHAs. Use of MEK inhibitor PD 0325901 and Ras-NHA versus NHA controls demonstrated that mitotic phosphorylation was specific to the Ras/MAPK pathway. Figure by Yu Ding.

Table 3.1 Genes scoring as significant for reduction of GSC growth compared to NSC growth.

Name	Symbol
SCY1-like 2 (S. cerevisiae)	SCYL2
Calcium/calmodulin-dependent protein kinase IV	CAMK4
Diacylglycerol kinase, iota	DGKI
Adenylate kinase 3	AK3
BUB1 budding uninhibited by benzimidazoles 1 homolog beta (yeast)	BUB1B
NIMA (never in mitosis gene a)-related kinase 1	NEK1
Receptor tyrosine kinase-like orphan receptor 2	ROR2
Ribosomal protein S6 kinase, 90kDa, polypeptide 5	RPS6KA5
Tribbles homolog 1 (Drosophila)	TRIB1
PTK2B protein tyrosine kinase 2 beta	PTK2B
PCTAIRE protein kinase 1	PCTK1
Protein kinase, cAMP-dependent, regulatory, type I, alpha (tissue specific extinguisher 1)	PRKAR1A
Eukaryotic translation initiation factor 2-alpha kinase 1	EIF2AK1
PCTAIRE protein kinase 3	PCTK3
V-erb-b2 erythroblastic leukemia viral oncogene homolog 2, neuro/glioblastoma derived oncogene homolog (avian)	ERBB2
EPH receptor A2	EPHA2
Mitogen-activated protein kinase 1	MAPK1
KIAA0999 protein	KIAA0999
Kinase insert domain receptor (a type III receptor tyrosine kinase)	KDR
Vaccinia related kinase 2	VRK2
Phosphoinositide-3-kinase, regulatory subunit 2 (p85 beta)	PIK3R2
LIM domain kinase 2	LIMK2
Polo-like kinase 1 (Drosophila)	PLK1
Pyruvate kinase, muscle	PKM2
Protein kinase (cAMP-dependent, catalytic) inhibitor beta	PKIB
Protein kinase, cAMP-dependent, catalytic, beta	PRKACB
Platelet-derived growth factor receptor, alpha polypeptide	PDGFRA
PTK2 protein tyrosine kinase 2	PTK2
TYRO3 protein tyrosine kinase	TYRO3
Microtubule associated serine/threonine kinase-like	MASTL
G protein-coupled receptor kinase 4	GRK4
Conserved helix-loop-helix ubiquitous kinase	CHUK
FK506 binding protein 12-rapamycin associated protein 1	FRAP1
PI-3-kinase-related kinase SMG-1	SMG1
FAST kinase domains 3	FASTKD3
Serine/threonine kinase 32B	STK32B
WNK lysine deficient protein kinase 4	WNK4

Table 3.1 (cont.)

Name	Symbol
V-raf-1 murine leukemia viral oncogene homolog 1	RAF1
Cyclin-dependent kinase inhibitor 1A (p21, Cip1)	CDKN1A
Integrin-linked kinase	ILK
C-mer proto-oncogene tyrosine kinase	MERTK
RB1-inducible coiled-coil 1	RB1CC1
Cdc2-related kinase, arginine/serine-rich	CRKRS
Maternal embryonic leucine zipper kinase	MELK
Aurora kinase B	AURKB
Protein kinase, cAMP-dependent, regulatory, type II, beta	PRKAR2B
Adenylate kinase 2	AK2
Non-metastatic cells 5, protein expressed in (nucleoside-diphosphate kinase)	NME5
Doublecortin-like kinase 1	DCLK1
N-acetylglucosamine kinase	NAGK
Activin A receptor, type IIB	ACVR2B
Serine/threonine kinase 32C	STK32C
Dual-specificity tyrosine-(Y)-phosphorylation regulated kinase 1B	DYRK1B

Chapter 4 – Genome-wide RNAi screens in human brain tumor isolates reveal a novel viability requirement for PHF5A

Adapted from an article submitted for publication:

Christopher G. Hubert, Robert K. Bradley, Yu Ding, Chad M. Toledo, Kyobi Skutt-Kakaria, Emily J. Girard, Jerry Davison, Jason Berndt, Philip Corrin, Ryan Basom, Jeffery J. Delrow, Thomas Webb, Steven M. Pollard, Jeongwu Lee, James M. Olson, and Patrick J. Paddison

I. ABSTRACT

PHF5A is a highly conserved PHD-finger domain protein that facilitates interactions between the U2 snRNP complex and ATP-dependent helicases. Here, we report a novel requirement for PHF5A in patient-derived glioblastoma multiforme (GBM) stem cells (GSCs) from genome-wide shRNA screens in multiple GSC isolates versus normal neural stem cells (NSCs). In GSCs, but not untransformed cells, PHF5A inhibition triggered a G2/M cell cycle arrest and loss of viability. PHF5A knockdown in GSCs inhibited splicing of an unusual class of exons with distinctive C-rich 3' splice sites, leading to defects in constitutive and alternative splicing in thousands of essential genes, including many required for cell cycle progression. Notably, pharmacologic inhibition of U2 snRNP activity phenocopied PHF5A knockdown both in GSCs and genetically transformed cells. Furthermore, PHF5A inhibition compromised GSC tumor formation *in vivo* and inhibited growth of established GBM tumors. Our results demonstrate a novel viability requirement for PHF5A to maintain proper exon recognition in GSCs.

II. INTRODUCTION

Malignant glioma is the most common and lethal form of brain cancer. Glioblastoma multiforme (GBM) is the most invasive and aggressive grade of glioma and is notoriously drug- and radiation-resistant. There are currently no highly effective therapies against GBM and with standard of care treatments, including surgery, radiation, and chemotherapy, ~90% of adult patients die within 2 years of diagnosis (Asbury; CBTRUS, 2011), underscoring the need for novel therapeutic targets. The hierarchical organization of adult and pediatric brain tumors suggests a cancer stem cell origin (Galli et al., 2004; Hemmati et al., 2003; Singh et al., 2003; Singh et al., 2004). Consistent with this notion, tumor-initiating GBM stem cells (GSCs) isolated from patients retain the developmental potential and specific genetic alterations found in the original tumor (Hemmati et al., 2003; Lee et al., 2006; Pollard et al., 2009; Singh et al., 2003).

Recently, a new method for deriving and maintaining GSCs was developed that allows adult GSCs to be isolated and grown in serum-free, defined monolayer culture (Lee et al., 2006; Pollard et al., 2009). Through this method GSCs can retain tumor-initiating potential and tumor-specific genetic and epigenetic signatures over extended outgrowth periods as well as recreate tumor cellular hierarchies when implanted into the cortex of immune-compromised mice (Lee et al., 2006; Pollard et al., 2009). GSCs isolated under these conditions also retain expression of neural progenitor molecular networks, which may contribute to the aggressive behavior of GBM tumors through enhancing self-renewal or developmental programs (Gangemi et al., 2009; Mangiola et al., 2007; Stiles and Rowitch, 2008), DNA repair pathways (Bao et al., 2006a), angiogenesis (Bao et al., 2006b), and/or invasiveness (Liu et al., 2009). Here, we took advantage of GSCs to implement both focused and genome-wide shRNA functional genetic screens to identify genes specifically required for *in vitro* GSC expansion. We used human fetal neural stem cells (NSCs) as controls. NSCs share phenotypic features with GSCs, including: identical

isolation and growth in serum-free conditions, similar doubling times, and similar developmental potential (Fael Al-Mayhani et al., 2009; Galli et al., 2004; Sun et al., 2008). These attributes create an ideal screening system for the identification of specific glioblastoma-lethal gene targets (Goidts et al., 2012).

Our screening procedures identified the PHD-finger domain protein PHF5A as being differentially required for growth and viability of GSC isolates. Cell based assays revealed that PHF5A activity is required for G2/M progression in GSCs. Molecular studies demonstrated that GSCs have a novel requirement for PHF5A activity to facilitate recognition of exons with distinctive 3' splice sites. PHF5A knockdown (KD) resulted in splicing defects in thousands of essential genes, a subset of which are predicted to affect mitotic progression (e.g., CDC20). Our results demonstrate an unexpected role for PHF5A in maintaining proper exon recognition in GSCs, which is critical for growth and maintenance of patient-derived tumors.

III. RESULTS

Functional genetic screens identify PHF5A as differentially required for GSC expansion.

To identify genes necessary for the growth and survival of GSCs but likely dispensable to non-cancerous neural cells and tissues, we performed shRNA functional genetic screens targeting 1086 DNA binding factors and most of the human genome (~19,000 genes) in primary GSC tumor isolates and human fetal NSC-CB660 cells. For these screens, we assayed genes required for GSC and NSC *in vitro* expansion in serum-free monolayer culture (Pollard et al., 2009) (Figure 4.1A).

Cells were infected with pools of shRNAs (Luo et al., 2009a; Paddison et al., 2004) in triplicate screening populations and expanded in normal conditions for 21 days. Comparisons of shRNA representation over time in GSCs or NSCs using microarrays or deep sequencing revealed shRNAs that became significantly under- or over-represented during expansion. Candidate GSC-specific lethal genes were defined by those shRNAs significantly underrepresented in GSC cultures relative to NSC control cultures.

Our initial DNA binding factor screen, performed in a single GBM isolate (G166 cells) along with NSC controls, yielded 27 genes as candidate GBM-lethal hits (Figure 4.2A). Retests of each screen hit were performed using multiple single-shRNA viral clones. Validation studies using single clone outgrowth (Figure 4.2A) or mixed *in vitro* competition with FACS analysis (Figures 4.1B, 4.2B) both revealed PHF5A KD as the top hit affecting *in vitro* expansion of GSC-G166 cells. To ensure that the results were applicable to other GBM tumors and that hits would score similarly when comparing the entire genome, we also performed genome-wide shRNA screens in multiple GSC isolates from three different GBM patients representing two developmental subtypes (G166-mesenchymal, 0131-mesenchymal, 0827-proneural), again in triplicate using NSCs as controls. This approach yielded GSC screen hits that were mainly isolate-specific, likely owing to different tumor backgrounds and heterogeneity in cell populations during expansion (Figure 4.1C). However, there were 17 candidate lethal genes shared by each GSC isolate that did not score in NSCs. Among these was PHF5A (Figure 4.1C).

PHF5A is a highly conserved PHD (plant homeo domain)-zinc finger domain protein that facilitates interactions between the U2 snRNP complex and DNA/RNA helicases (Rzymski et al., 2008). PHF5A may also bind to chromatin by virtue of its PHD domain (Trappe et al., 2002), which in other PHD family members can facilitate interactions with specific histone marks in

chromatin-bound nucleosomes (Mellor, 2006; Musselman and Kutateladze, 2009). Consistent with this latter notion, PHF5A protein was found to be an enhancer of estrogen-mediated transcription of the Connexin 43 gene (Oltra et al., 2003). PHF5A has also been characterized as a member of the SF3b component of the U2 snRNP splicing complex (Will et al., 2002). Since PHF5A was a highly reproducible GSC-specific screen hit and nothing is known about a cancer-specific role for PHF5A, we further pursued it as a GBM-lethal target.

PHF5A is differentially required for GSC *in vitro* expansion and its knockdown triggers G2/M cell cycle arrest in GSCs but not NSCs.

To further confirm differential effects of PHF5A KD, we performed short-term outgrowth assays in five primary GSC cultures using multiple shRNAs. In each case, PHF5A KD showed a strong GSC-specific loss of viability (Fig 4.3A). Next, we examined effects on SSEA1+ GSC subpopulations, which are enriched for tumor initiating cell activity (Son et al., 2009). In three different GSC isolates examined, PHF5A KD compromised outgrowth of SSEA1+ populations over the course of several weeks (Figure 4.4A). This indicates that PHF5A suppression blocks gross expansion of GSC isolates and GSC subpopulations with tumor-initiating capability.

GSCs and NSCs express PHF5A at relatively similar levels and KD is equivalently effective in each cell type at both the RNA and protein level (Figures 4.3B, 4.5), indicating that the lack of phenotype in NSCs is not due to inefficient knockdown or major differences in expression. Moreover, PHF5A expression levels were similar in GSCs, NSCs, and in other tissues, indicating that GSCs do not abnormally overexpress the gene (Figure 4.4B). We further performed a complementation assay in which a validated shPHF5A sequence targeting the PHF5A endogenous 3'UTR was co-expressed with the PHF5A open reading frame (ORF)

lacking its endogenous 3'UTR. Expression of the PHF5A ORF rescued the growth defect observed by PHF5A KD (Figure 4.3C, 4.4C), indicating that the phenotypic effects are PHF5A-specific.

A striking feature of PHF5A depletion in GSCs was that, preceding widespread GSC cell death, PHF5A KD triggered a dramatic cell cycle arrest that resembled the rounded-up phenotype of kinesin motor protein KIF11 KD (Sawin et al., 1992), our non-specific cell-lethal control (Figure 4.3D). MPM-2 staining, indicative of CyclinB/CDK activity, dramatically increased in shPHF5A GSCs confirming mitotic arrest (Figure 4.3D inset, 4.3E). Moreover, FACS analysis showed a striking increase in the percent of G2/M cells in GSCs, but not NSCs or normal fibroblasts, with PHF5A KD (Figure 4.3F).

Further examination of mitotic spindle formation indicated that shPHF5A in GSCs, but not NSCs, showed condensed chromatin but primarily formed monopolar or multipolar spindles with few metaphase or anaphase cells (Fig 4.3G). These results suggest that in GSCs, but not NSCs, PHF5A activity is required for progression through mitosis.

PHF5A binding partners involved in RNA splicing are also differentially required by GSCs.

Since PHF5A has been characterized as both a splicing factor (Rzymski et al., 2008; Will et al., 2002) and a transcriptional regulator (Oltra et al., 2003), we next wished to define which of these activities is most relevant for GBM cell survival. To this end we analyzed KD of two PHF5A binding partners in the spliceosome, U2AF1 and DDX1, which interact with PHF5A C- and N-terminal domains, respectively (Rzymski et al., 2008). U2AF1 is a key member of the U2 snRNP required for RNA branch point recognition (Jurica and Moore, 2003; Kramer, 1996) and

DDX1 is an ATP-dependent DEAD-Box RNA helicase (Fang et al., 2005). Knockdown of either U2AF1 or DDX1 phenocopied PHF5A KD in GSCs (Figure 4.6A). Moreover, comprehensive examination of multiple shRNAs against PHF5A and U2AF1 in short-term growth assays showed the same strong trend of requirement in GSCs versus NSCs (Figure 4.6B). These results suggest that the PHF5A function most relevant for GSC-specific viability is associated with its role in splicing and the U2 snRNP complex. Supporting this notion, examination of PHF5A interacting proteins by co-IP mass spectrometry yielded strong enrichment (GO:0008380 RNA splicing $p = 10^{-14}$) for candidate interacting proteins involved in splicing and the U2 snRNP complex, including U2AF1, U2AF2 and multiple DDX/DHX helicase family members (Table S1).

To further substantiate these results, we examined the effects of two candidate small molecule inhibitors of the U2 snRNP complex, Spliceostatin A (SSA) and Sudemycin C1 (SudC1). SSA binds to and inhibits the U2 snRNP subunit SF3b, which contains PHF5A, resulting in a reduction in the fidelity of branch point recognition and a downregulation of genes important for cell division. (Corrionero et al., 2011; Kaida et al., 2007). SudC1 shares the consensus pharmacophore of SSA and pladienolide (Kotake et al., 2007) and has also been shown to modulate RNA splicing (Fan et al., 2011; Lagisetti et al., 2009; Lagisetti et al., 2008). We reasoned that if the most relevant GSC-specific function of PHF5A is its function in the U2 snRNP splicing activity, then these drugs should show a similar pattern of viability effects on GSCs and NSCs. This was indeed the case. Treatment of GSCs with SSA or SudC1 resulted in greater dose-dependent viability loss in GSCs relative to NSCs (Figure 4.6C, 4.5) and also resulted in the characteristic cell cycle arrest in GSCs but not NSCs at doses within this efficacy window (Figure 4.6D).

To better characterize GSC-specific SudC1/SSA G2/M arrest, we treated H2B-GFP expressing GSCs with the proteasome inhibitor MG132, which arrests mitotic cells as they enter metaphase. After overnight SudC1 or SSA treatment, cells were treated with MG132 for 2 hours. Control cells displayed proper metaphase arrest, with chromosomes aligned along the metaphase plate (Figure 4.6E). However, SSA- or SudC1-treated cells accumulated in mitosis without properly aligned chromosomes (Figure 4.6E). Live cell imaging further demonstrated this pre-metaphase cell cycle arrest from SudC1 or SSA treatment without the need for MG132 (Supplemental videos 1-3). We also observed that the viability loss in drug-treated GSC cultures comes from the death of previously arrested mitotic cells and not interphase GSCs. A fraction of arrested GSCs were able to survive by aborting mitosis after arresting, but these cells displayed disorganized multi-lobed nuclei and were not observed to successfully divide again (Supplemental videos 2-3).

Taken together, the above results establish that PHF5A and U2 snRNP complex activity are differentially required for GSC viability compared to NSCs, and their activity is necessary for GSC but not NSC transit through pre-metaphase mitosis. Moreover, since treatment of GSCs with SSA or SudC1 did not affect the timing of mitoses for several hours after drug treatment (Supplemental videos 2-3), it is unlikely that PHF5A and U2 snRNP activity are directly required for mitotic progression.

PHF5A is specifically required for normal exon recognition in GSCs but not NSCs.

We next sought to identify glioblastoma-specific defects in cellular function induced by PHF5A KD that could cause the observed mitotic arrest phenotype. Recently, Paulsen et al. found that KD of multiple spliceosomal genes in HeLa cells resulted in double-strand DNA

breaks and H2AX phosphorylation (Paulsen et al., 2009). We therefore hypothesized that PHF5A KD might similarly give rise to DNA damage in GSCs, thereby triggering arrest. However, upon PHF5A KD in GSCs, we did not see an increase in pH2AX levels or phosphorylation of the DNA damage signaling proteins CHK1 and CHK2 (Figure 4.7A). These results suggest that the shPHF5A phenotype does not simply arise from a DNA damage response. Furthermore, BUB1B is not phosphorylated following PHF5A KD in GSCs (Figure 4.7A), suggesting that the spindle assembly checkpoint is also not being triggered.

We next considered the possibility that PHF5A KD might specifically inhibit RNA splicing in GSCs but not NSCs, thereby indirectly giving rise to glioblastoma-specific mitotic arrest. Motivated by a previous study in yeast, where defective splicing of α-tubulin caused cell cycle arrest in the *cef1-13* mutant (Burns et al., 2002), we hypothesized that PHF5A KD might induce GSC-specific aberrant splicing of genes required for cell cycle progression. To test this, we performed deep RNA-seq in control NSCs (CB660 cells) and GSCs (G166 and 0827 cells) treated with control or PHF5A-targeting shRNAs. Consistent with our hypothesis, we observed severe RNA processing defects in many genes important for cell cycle progression, including CDC16, CDC20, CDC25C, CDC37, CDC45, and RCC2, in GSCs (G166 and 0827 cells) but not NSCs (CB660). For example, following PHF5A KD, the 3'-most constitutive exons of CDC20 were frequently skipped in G166 cells (Figure 4.8A), and many constitutive exons in RCC2 were skipped in 0827 cells (Figure 4.7B). If translated, these aberrant mRNAs would produce C terminal-truncated proteins that are unlikely to function normally in cell cycle progression. This severe dysregulation of cell cycle genes in GSCs, but not NSCs, suggests that aberrant splicing in GSCs following PHF5A KD may give rise to the observed mitotic arrest and inviability.

We next asked whether splicing was globally dysregulated following PHF5A KD in GSCs. We quantified changes in isoform ratios following PHF5A KD in NSCs and GSCs using only reads crossing splice sites, an approach that treats all splicing events with equivalent statistical power (Bradley et al., 2012). Classifying alternative splicing events as competing 5' and 3' splice sites, mutually exclusive exons, and cassette exons, we found that PHF5A KD induced a global trend towards skipping of cassette exons—but few other splicing changes—in GSCs, but not NSCs (Figure 4.8B-I). Most of the resulting splicing changes introduced in-frame stop codons into the mRNAs, strongly suggesting that the splicing changes are aberrant, rather than functionally relevant, splicing. Genes expressing higher levels of isoforms with in-frame stop codons introduced by PHF5A had lower average expression (Figure 4.8J), consistent with degradation of the aberrant mRNAs by the nonsense-mediated decay (NMD) pathway.

These data suggested that PHF5A primarily functions to facilitate exon recognition, rather than to regulate alternative splicing, which is consistent with its characterization as a core component of the spliceosome (Will et al., 2002). Analyzing all annotated constitutive splice junctions in the human genome, we found that PHF5A KD caused a broad shift towards alternative splicing of constitutive junctions (Figure 4.8K) and retention of constitutive introns (Figure 4.8L). Importantly, most such alternative splicing of constitutive junctions and almost all retention of constitutive introns will introduce in-frame stop codons, again resulting in non-functional mRNAs encoding truncated proteins.

Only a relatively small subset of splice junctions were affected by PHF5A depletion in GSCs, indicating that the requirement for PHF5A is not universal across exons. To gain mechanistic insight into the origins of the observed splicing dysregulation, we identified specific features characteristic of 3' splice sites susceptible to KD in GSCs. 3' splice sites associated with

abnormal splicing of constitutive junctions had slightly shorter, but otherwise normal, polypyrimidine tracts relative to unaffected 3' splice sites; in contrast, 3' splice sites associated with retained constitutive introns had unusual, C-rich tracts (Figure 4.9A). Retained constitutive introns were short (Figure 4.9B) and had unusually proximal branch points (Figure 4.9C). While PHF5A is known as a core component of the spliceosome, it appears to be most important for recognition of an unusual class of exons with distinctive 3' splice sites.

Taken together, these results indicate that PHF5A is important for proper recognition of a specific, relatively small class of exons in GSCs. KD of PHF5A causes defective RNA processing of thousands of essential genes, a subset of which are required for mitotic progression. Given the broad splicing dysregulation that we observed, there are likely other cellular defects induced by PHF5A KD that contribute to the observed GSC inviability; mitotic arrest may simply be the most obvious phenotype. This model is consistent with our observation that multiple methods of inhibiting U2 snRNP activity—including KD of other spliceosomal genes, as well as SSA and SudC1 treatment—mimic the effects of PHF5A KD, even though these distinct perturbations are unlikely to lead to identical defects in RNA processing.

RasV12 can trigger susceptibility to U2 snRNP inhibition.

We next wished to determine the possible mechanism by which GSCs become differentially sensitive to inhibition of PHF5A and U2 snRNP activity. One possibility was that the process of oncogenic transformation itself resulted in mis-regulation of splicing. Increased RTK/Ras signaling activity is a near-universal feature of GBM tumors and other cancers (Parsons et al., 2008; TCGA, 2008), and there are possible links between RTK/Ras signaling and regulation of RNA splicing (see discussion). To investigate this possibility, we utilized several

different cellular models of Ras-induced transformation in combination with SSA or SudC1 (which we used interchangeably, depending on their availability). Attempts to bypass RasV12-induced senescence in control NSCs used above proved unsuccessful. Therefore, we used IMR90 embryonic lung fibroblasts (Mason et al., 2006; Nichols et al., 1977), mouse embryonic fibroblasts (MEFs)(Furic et al., 2010), and normal human astrocytes (NHAs) (Sonoda et al., 2001).

In each case, cells expressing RasV12 were more sensitive to SSA and/or SudC1 than unmodified controls. The most dramatic sensitivities occurred in IMR90-Tert fibroblasts partially transformed with RasV12 and E1A, which are p53 positive. In these cells, PHF5A KD (Figure 4.10A) or drug treatments (Figure 4.10B) resulted in massive cells death, even with short drug exposure (Figure 4.10C). $p53^{-/-}$ RasV12 MEFs and RasV12 E6/E7 human astrocytes showed characteristic cell cycle arrest accompanied by cell death observed in GSCs (Figure 4.10D, 4.11). Thus, in all three systems, RasV12 activity evoked sensitivity to PHF5A and/or U2snRNP inhibition.

Taken together, these results suggest that oncogenic Ras activity can give rise to an added requirement for PHF5A and U2 snRNP activity. However, will these results translate to cancers other than GBM? In support of this notion, we found that PHF5A and U2AF1 were both uncharacterized screen hits in an RNAi screen for RasV12-specific lethal genes (Luo et al., 2009a). In this screen, RasV12 was overexpressed in a colorectal cancer cell line and screened for shRNAs that differentially inhibit RasV12 over-expressing populations (Luo et al., 2009a). Both PHF5A and U2AF1 specifically scored as RasV12-lethals. This further suggests that oncogenic activity of Ras in other cancers, whether arising through RTK stimulation or Ras

mutation, will trigger RNA splicing deficiencies sensitive to PHF5A and/or U2snRNP inhibition and also SSA and SudC1 analogues (with clinically relevant pharmacokinetic properties).

Suppression of PHF5A expression compromises GBM tumor formation and maintenance in vivo.

Finally, we wished to test whether PHF5A expression would be required for GBM tumor formation and maintenance *in vivo*. To examine tumor formation, we devised an *in vivo* competition experiment to directly test the proliferative effects of PHF5A suppression in an orthotopic xenograft model of glioblastoma. GSCs were infected with GFP-expressing shPHF5A or shCtrl virus and then mixed with 10% ChFP-expressing control cells. This cell mixture was then either grown in adherent culture or xenografted into the cortex of immunocompromised mice (Figure 4.12A). Whereas shCtrl cells were able to proliferate and maintain their representation in culture, shPHF5A cells began to exhibit characteristic cell cycle arrest within 2 days of xenograft and were almost completely replaced by ChFP+ control cells within 2 weeks (Figure 4.12B). Likewise, orthotopically xenografted GFP+ shCtrl GSC cells were able to proliferate *in vivo* whereas GFP+ shPHF5A GSCs were unable to proliferate and meaningfully contribute to *in vivo* tumor growth (Figure 4.12C). The small fraction of coinjected ChFP+ control GSCs were able to engraft and give rise to tumors in every case, and ChFP expression mirrored bulk tumor mass as marked by the Chlorotoxin:Cy5.5 conjugate Tumor Paint (Veiseh et al., 2007). This underscores the fact that expression of PHF5A shRNA was the key determinant in whether GSCs could contribute to tumor growth.

We next wished to examine whether PHF5A inhibition after tumor formation would compromise tumor maintenance, a key metric in evaluating potential therapeutic avenues. To this end, we generated xenograft mice bearing GSC tumors with Dox-inducible PHF5A shRNA

(Figure 4.3C, 4.4C) or Ctrl shRNAs. Tumors were allowed to grow to approximately 75mm^3 in size prior to continuous Dox treatment. Whereas control shRNA tumors showed no measurable difference in growth rate upon Dox treatment (Figure 4.12E), shPHF5A tumor growth arrested upon Dox administration and tumors diminished until they were nearly undetectable (Figure 4.12F). PHF5A inhibition therefore compromises both GBM tumor formation and maintenance, suggesting that U2 snRNP inhibition may be an effective therapy for GBM.

IV. DISCUSSION

Here, we performed parallel shRNA screens during *in vitro* expansion of human GSCs and NSCs to identify novel gene activities required for growth and viability of patient-derived GSCs but not normal NSCs. Despite observing a high degree of GSC isolate-specific variation in the screening results, we identified PHF5A as differentially required for expansion of all GSCs examined. PHF5A is a highly conserved PHD-zinc finger domain protein that facilitates interactions between the U2 snRNP complex and ATP-dependent helicases (Rzymski et al., 2008). *In vitro* assays established that PHF5A activity was required for G2/M progression in GSCs but not NSCs. Consistent with a role in GSC-specific splicing phenomena, KD of other U2 snRNP complex members or pharmacological inhibition of U2 snRNP activity both phenocopied PHF5A KD. Further, PHF5A KD triggered defective splicing of thousands of essential genes, including many important for mitotic progression (e.g., CDC20). Examination of affected splice sites revealed a specific requirement for PHF5A in recognition of 3' splice sites with C-rich polypyrimidine tracts in GSCs. Moreover, modeling experiments in Ras-transformed cells suggested that oncogenic signaling gives rise to the added requirement for PHF5A and U2

snRNP activity. Finally, *in vivo* tumor experiments suggested that PHF5A is required for generation and, more importantly, maintenance of GBM tumors. Taken together, our results support a model whereby oncogenic signaling through the Ras pathway leads to an enhanced reliance on PHF5A, without which transformed cells are unable to properly recognize a subclass of 3' splice sites within thousands of essential genes.

Our results provide new insight into cancer-specific RNA splicing phenomena. Oncogene-associated activities, e.g., c-myc, Akt, and Ras, can alter splicing of select genes, including pyruvate kinase (Clower et al., 2010; David et al., 2010), caspases (Shultz et al., 2010), and CD44 (Weg-Remers et al., 2001), to promote tumor formation or growth. Our results provide two important contrasts to these findings. First, while previous examples of cancer-associated splicing events can be largely explained by the activity of canonical splicing regulators on individual substrates, our results indicate that fundamental aspects of 3' splice site recognition are modulated by transformation. In particular, the GSC-specific reliance on PHF5A suggests that basal spliceosome composition may differ between normal and transformed cells. Therefore, many cancer-associated changes in splicing may be inherently global, rather than specific, phenomena. Second, the many reports of cancer-promoting protein isoforms suggest that splicing can confer tumor robustness. However, our findings suggest a different model, wherein splicing is a source of tumor vulnerability due to “fragile” recognition of specific subclasses of exons.

Future studies are required to define just how this vulnerability might arise in GBM and other transformed cells. One possibility is that oncogenic signaling leads to direct perturbation of U2 snRNP activity by affecting complex assembly, activity, turnover, nuclear localization and/or coordination with transcription (reviewed in (Heyd and Lynch, 2011). As many splicing factors

have complementary or compensatory activity, and also participate in feedback loops to maintain cellular homeostasis, one attractive model is that transformation disrupts expression of spliceosomal proteins that normally complement PHF5A's role. Consistent with this model, oncogene activity is known to affect the expression levels of select splicing factors (Das et al., 2012; David et al., 2010). Transformation could also leave total expression levels unchanged while indirectly modulating spliceosomal protein activity or accessibility. For example, hnRNP A1 is sequestered in the cytoplasm after osmotic shock via phosphorylation by MNK1/2 kinases (van der Houven van Oordt et al., 2000). These kinases are also part of the RTK/Ras/Raf signaling cascade and are necessary for Ras-dependent transformation (Wendel et al., 2007).

Another key question arising from our studies is whether PHF5A and U2 snRNP represent reasonable therapeutic targets for GBM. One notable benefit of targeting their activity is that partial inhibition simultaneously affects the splicing of thousands of essential genes. For the vast majority of affected genes, the resulting isoforms contain in-frame stop codons, resulting in either degradation by nonsense-mediated decay or translation of aberrant truncated proteins. Therefore, targeting PHF5A or U2 snRNP leads to partial or complete loss of function for many essential genes, collectively causing loss of viability. For example, the observed arrest phenotype is likely due to simultaneous dysregulation of many genes required for cell cycle progression (CDC16, CDC20, CDC25C, CDC37, CDC45, RCC2, etc.), rather than abrogation of a single "target" gene's activity. In contrast to the yeast *cef1-13* example—where the arrest phenotype was rescued by removal of a single mis-spliced intron in α-tubulin (Burns et al., 2002)—mutations affecting just one of the thousands of dysregulated splice sites are highly unlikely to rescue GSCs. As a result, targeting PHF5A/U2 snRNP may have an advantage over current targeted therapeutic strategies focused on inhibiting activities of single oncogenic drivers (e.g.,

EGFR, RAF, AKT, etc.), which cancer cells can circumvent through mutation or upregulation of parallel or downstream pathway components. Moreover, classes of synthetic and natural compounds already exist which inhibit U2 snRNP activity (e.g., SudC1 and SSA). The natural product splicing modulators were originally identified on the basis of anti-cancer activity *in vitro* and *in vivo* (Kaida et al., 2007; Kotake et al., 2007; Mizui et al., 2004; Nakajima et al., 1996), and at least one derivative has entered clinical trials for solid tumors (NCT00499499). Our results suggest that further investigation of this family of compounds may be beneficial for GBM as well as other cancers.

In summary, this work establishes that patient-derived GSCs are vulnerable to perturbation in recognition of a subclass of 3' splice sites, which results in a reduction in GSC viability and loss of GBM tumor maintenance. Since standard of care therapies are ineffective against GBM, we proffer that targeting PHF5A and/or U2 snRNP activity may offer a new therapeutic in-road for this cancer.

V. METHODS

Pooled shRNA bar-code screens and analysis

For both the focused and genome-wide RNAi screens, GSC or NSC cells were infected with pooled GIPZ lentivirus (Open Biosystems) at and MOI < 1 and selected with puromycin (Sigma) to remove uninfected cells. Cells were propagated in culture for an additional 21 days during which time a minimal representation of 1000 fold per replicate was maintained. For each corresponding sample, shRNA barcodes (for microarray or ½ hairpin for deep shRNA sequencing) were PCR-recovered from genomic DNA samples. The change in the relative

abundance of each shRNA in the library over time was measured using the normalized Cy3/Cy5 ratio of its probe signal or sequence counts. Barcode probes depleted in the GSC samples were considered candidate screen hits. Hits from the genome wide screens were further filtered based on cellular expression as measured by RNA sequencing.

Cell Culture

GSC and NSC lines were grown in N2B27 neural basal media (StemCell Technologies) supplemented with EGF and FGF-2 (20 ng/ml each) (Peprotech) on laminin (Sigma) coated polystyrene plates according and passaged according to Pollard(Pollard et al., 2009) IMR90 and IMR90-Ras cells were grown in 10% FBS/DMEM (Invitrogen) on standard tissue culture plates. NHA and NHA-Ras cells were grown in astrocyte growth medium (Clonetics) according to the manufacturer's instructions and published protocols (Sonoda et al., 2001).

RNAi and lentiviral production

ShRNAs were obtained from the RNAi Shared Resource (FHCRC) or Open Biosystems (Huntsville, AL) in the pGIPZ lentiviral vector. For virus production pGIPZ-shRNA plasmids were transfected into 293T cells along with psPAX and pMD2.G packaging plasmid to produce lentivirus. ~24 hours after transfection, neural stem cell expansion medium was added to replace original growth medium. Virus was harvested 24 hours after medium change and stored at -80°C. GSCs and NSCs were infected at MOI<1 and selected with 1-4 μg puromycin for 2-4 days, depending on the target cell type.

Genome wide shRNA screens and shRNA-seq analysis

Human shRNA library including ~54,000 hairpins (~15,000 genes) was used to identify genes that are lethal to GSCs but not NSCs when knocked down. Three GSC cell isolates (G166, 0131, 0827) and one NSC cell isolate (CB660) were infected with lentiviral shRNA pool at a representation of ~1000 fold and a multiplicity of infection (MOI) of ~1 in parallel. Cells were then selected by puromycin to remove uninfected population and divided into 3 replicates. Cells were kept in for three weeks, encompassing approximately 10 cell doublings. Afterwards, DNA was harvested and viral inserts containing unique target sequence were PCR amplified. The PCR product went through a column purification procedure to remove primers and genomic DNA and then subjected to Illumina high-throughput sequencing. In this analysis, shRNAs lost in the GSC population represent candidate gene targets that may be required by tumor outgrowth. The shRNA screen and Bar-code array analysis will be performed as previously described (Luo et al., 2009a; Paddison et al., 2004; Silva et al., 2005). Cells will be infected with pools of lentiviral shRNAs and analyzed after 21 days of outgrowth for alterations in shRNA representation (n=3). For each population shRNAs will be amplified using a half-shRNA PCR strategy from genomic DNA representing ~5 million cells (~33 μg). Illumina sequencing adaptors will be ligated onto purified shRNA PCR products (Illumina kit) and used on an Illumina HiSeq 2000 sequencer (Genomics facility, FHCRC). The resulting will be mapped onto a reference library containing library shRNA sequences and filtered (phred score= 37). Mapped reads were tallied and compared using two R/Bioconductor packages, edgeR, developed for RNA-seq analysis, and limma, developed for microarray analysis (Smyth et al., 2005). Both comparisons subtract control from experimental replicates to calculate logFC and use the Benjamini-Hochberg FDR calculation to adjust p-values for multiple comparisons.

Growth Assays

For single clone validation assays, lentivirus was produced in 96-well format (Klinghoffer et al., 2008) and used to transduce G166-GSCs or CB660-NSCs (MOI ~ 1). Following selection with puromycin, cells were released from their plates (Accutase, Millipore) and plated in 96-well plates. Cell viability was quantified at day 0 and day 7 (in triplicate sister plates, CellTiter-Glo, Promega). For invitro competition validation experiments, G166 and CB660 cells were infected with single shRNA clones targeting potential screen hits were mixed uninfected control cells and plated in 96-well format. The percent of GFP+ (shRNA expressing) cells present in each well was quantified by FACS analysis (BD LSR2 flow cytometer; FHCRC Shared Resources) at day 0 and day 10 and ranked by Z-score for each cell line. For short-term outgrowth assays, post-selection, shRNA transduced GSC or NSC cells were harvested, counted (Nucelocounter, NBS), and plated onto a 96-well plate. After 7 days under standard growth conditions, cell proliferative rate was measured using Alamar blue reagent (Invitrogen).

Long-term SSEA1+ outgrowth assays

Cells were infected with shPHF5A, shKIF11, or shCtrl virus for 48 hours followed by selection with puromycin for 72 hours (Day 0). Cells were detached from their respective plate, counted with a nucleocounter, and mixed with untreated cells. After mixing, cells were either seeded to a 6-well tissue culture dish for further growth or washed with cold PBS containing 0.5% bovine serum albumin (BSA) for flow analysis. Cells used for flow analysis were then blocked with cold PBS containing 0.5% BSA for 15 minutes at 4˚C, followed by an 1h incubation with APC mouse anti-human CD15 (SSEA1, BD Pharmingen) at 4˚C on a shaker. Following two washes with cold PBS containing 0.5% BSA, cells were suspended with PBS and analyzed using a FACS Canto flow cytometer (Becton Dickinson). Cells were analyzed at days 0, 4, 7, 14, and 22.

Time-lapse imaging

0827-GSCs were infected with virus expressing GFP-tagged Histone 2B. Immediately after addition of SudC1 (2μM) or SSA (0.2ng/ml) cells were placed in a 37°C humidified chamber and imaged for GFP or light once every 10 minutes for 48 hours (Nikon Ti, 10X objective, FHCRC shared resources). Images were merged and compiled using ImageJ.

Western blotting

Cells were treated with Cisplatin (20 μM, 24 hour), nocodazole (100 ng/mL, 24 hour), or shRNA virus (2 day infection, 4 day selection with puromycin). After treatment, western blots were carried out using standard laboratory practices (www.cshprotocols.org), except that a modified RIPA buffer was used for protein extraction (150 mM NaCl, 50 mM Tris, 2 mM $MgCl_2$, 0.1% SDS, 0.4% DOC, 0.4% Triton-X 100, 2 mM DTT, and complete protease inhibitors (Roche) followed by a 15 min digestion with 125 U of Benzonase (Merck) at RT. Cell lysates were quantified using Pierce 660 nm protein assay reagent and identical amounts of proteins were loaded onto SDS-PAGE for western blot. Antibodies against BUB1B (Sigma), pCHK1 (Cell Signaling), pCHK2 (Cell Signaling), beta-Tubulin (Sigma), or PHF5A (PTGlab, 15554) were used for these experiments. Either chemiluminescent detection (ECL, Amersham) and X-ray film (Kodak), or an Odyssey infrared imaging system (Li-cor) was used to visualize blots following manufacturer instructions.

Inducible PHF5A KD and PHF5A ORF Rescue

A validated shRNA hairpin targeting the 3' UTR of PHF5A was cloned from a GIPZ vector backbone (Open Biosystems) into a TRIPZ doxycycline-inducible backbone using company procedures (Open Biosystems). TRIPZ-shPHF5A virus (or shControl virus) was used to infect

GSC-0131 cells prior to puromycin selection and cloning by limiting dilution. An effective silencing clone was infected with lentivirus constitutively expressing the full length PHF5A open reading frame (ORF) lacking the endogenous 3'UTR (Yang et al., 2011a) and selected with blasticidin.

Immunofluorescence

For image based assessment of mitotic index, cells were fixed with 2% paraformaldehyde for 30 minutes, permeabilized with 0.25% Triton X-100, and blocked in PBS containing 3% BSA and 5% goat serum. After 3 washes with PBS, cells were stained with MPM-2 (1:300, Millipore) at room temperature for 1 hour. Next, cells were washed and incubated with Alexaflour-568 secondary antibody (Invitrogen) and DAPI for 1 hour in dark. Staining was visualized by Nikon eclipse Ti microscope. Approximately one third of MPM-2 positive cells in asynchronous cultures where in anaphase/telophase, while the other two thirds where in prometaphase or metaphase.

Cell Cycle FACS

For FACS-based assessment, cells were then collected and fixed in 70% ethanol for 1 hour at 4°C, then rinsed with ice-cold PBS+2% FCS and stained with DAPI (1 μg/ml). Cells were washed, re-suspended in PBS and filtered. DNA content was measured by BD LSR2 flow cytometer (FHCRC Shared Resources).

Affinity purification mass spectrometry and bioinformatics

A2058 melanoma or G166 glioma cells grown in 15 cm plates were rinsed twice in cold phosphate buffer saline and lysed in 50 mM Tris pH=8.0, 1% Triton-X 100, 0.2% sodium

deoxycholate, 150 mM sodium chloride and 2 mM EDTA with protease and phosphatase inhibitors (Roche, 05 892 791 001 and 04 906 845 001). Approximately 5 mg of protein lysate per immunoprecipitation reaction was cleared with 50 uL magnetic protein-G beads (Pierce, 21349) for 3hours at 4°C. 5 ug of antibody (PHF5A, PTGlab, 15554; U2AF1, Bethyl labs, A302-80A) was pre-bound to 50 µL beads and then added to the cleared lysate and incubated overnight at 4°C. Protein-bead complexes were rinsed three times in lysis buffer and twice with 50 mM ammonium bicarbonate pH=8.0. Proteins were reduced and alkylated, then trypsinized overnight at 37°C (Promega, v5113). The resultant peptides were desalted with Sep-pak columns (Waters, WAT054955), dehydrated, and re-suspended in 0.1% formic acid. Samples were subjected to separation by reverse phase nano-HPLC (Eksigent) on a 20 cm column (Michrom Bioresources, MagicC18AQ 100A-5U) and eluted directly into a LTQ-XL mass spectrometer (Thermo-Fisher Scientific). Resultant spectra were searched using Sequest and the Transproteomic Pipeline on a Sorcerer2 (Sage N Research, Milpitas, CA). Proteins represented in both samples by at least three unique peptides are represented in Supplemental Table S2. In addition, the filtered protein list was submitted to the STRING database in order to curate known interactions (von Mering et al., 2003) and evaluated for enrichment of functional gene sets by gene ontology analysis (GO-miner).

Xenotransplantation

0131 GSC cells were infected with pGIPZ-shRNA virus and selected for 4 days in puromycin (2µg/mL). Control 0131 GSC cells were infected with mChFP lentivirus (FHCRC Shared Resources) and FACS sorted for ChFP+ cells (BD FACS Aria, FHCRC Shared Resources). Cells were harvested using Accutase (Sigma), counted, resuspended in an appropriate volume of culture media, mixed 90% GIPZ plus 10% mChFP, and kept on ice prior to immediate

transplantation. NOD-scid IL2Rgammanull mice (Jackson Labs #005557) were anesthetized by IP injection of 0.2ml/10 grams 1.25% Avertin Solution and kept at 37°C. A small bore hole was made in the skull using a hand drill with a Meisinger #009 steel burr bit (Hager & Meisinger GmbH). 2x10^5 cells were slowly injected by pipet into the right frontal cortex approximately 2mm rostral to Bregma, 2mm lateral and 3mm deep through a 0.2-10 µl disposable sterile aerosol barrier tip (Fisher Scientific #02-707-30). The burr hole was closed using SURGIFOAM (Johnson & Johnson) and the skin rejoined using TISSUMEND II (Veterinary Product Laboratories, Phoenix AZ). Residual cells were counted and plated into cell culture on laminin coated plates. Five weeks after initial transplantation, mice were injected intravenously with 50µl of 40µM Chlorotoxin:Cy5.5 conjugate (Veiseh et al., 2007) 4 hours prior to sacrifice by carbon dioxide inhalation. The brain and tumor were removed from the skull and imaged for Cy5.5, ChFP, and GFP fluorescence using the Xenogen IVIS Spectrum imaging system (Caliper Life Sciences).

For inducible xenografts, 0131 GSC TRIPZ shCtrl or shPHF5A cell clones were implanted subcutaneously into the flanks of nude mice (Harlan). Tumors were monitored by caliper measurement and allowed to grow to ~75 mm^3 before commencing treatment. Mice were randomized into cages and given 2 mg/ml Doxycycline (hyclate salt, Sigma) plus 5% sucrose in their drinking water (or control water). Tumor size was measured by caliper.

RNA-seq library preparation

We prepared poly (A)-selected single-end RNA-seq libraries using the Illumina TruSeq protocol and sequenced all libraries on the HiSeq 2000 instrument with a read length of 99 bp.

Gene expression analysis

We used the RSEM software version 1.1.20 (Li and Dewey, 2011) to quantify expression levels of all genes in our previously computed set of non-redundant gene annotations (Bradley et al., 2012), representing a merge of Ensembl (Flicek et al., 2011) and UCSC (Fujita et al., 2010). We used the TMM normalization procedure (Robinson and Oshlack, 2010) to normalize our RNA-seq data for all gene expression estimates.

Splicing analysis

We used previously published annotations of competing 3' and 5' splice sites, mutually exclusive exons, and skipped exons (Wang et al., 2008). For each splicing event, we assigned it to its most likely parent isoform and assessed whether it was likely to induce nonsense-mediated decay (if it introduced an in-frame stop codon at least 50 bp upstream of a splice junction). We furthermore enumerated all constitutive junctions, where a constitutive junction was defined as a splice junction for which neither the 5' nor 3' splice site was annotated as possibly spliced to another 3' or 5' (respectively) splice site in either Ensembl or UCSC. We mapped the raw FASTQ files using Bowtie version 0.12.8 (Langmead et al., 2009) and TopHat version 1.3.3 (Trapnell et al., 2009). We mapped to the genome, all splice junctions in the annotations described above, and all possible splice junctions that could result from skipping of exons in our gene annotations. To reduce the false positive rate of mapping, we did not allow novel junction discovery and furthermore required at least 6 bp of overhang on either side of splice sites.

For Fig. 4.8B-I,K,L, in order to detect changes in all classes of splicing events with equal statistical power, we used only reads crossing the minimal identifying splice junctions for each event and tested for changes in splicing following PHF5A KD using the binomial proportion test, which is appropriate for RNA-seq data, where the number of reads is variable. We described this

approach previously (Bradley et al., 2012). To fairly assess retention of constitutive introns, we treated reads crossing the 5' splice site (the 3' end of the upstream exon) with at least 6 bp of overhang in both the exon and intron as identifying reads. We required p-value < 0.01 and a change of at least 10% in isoform ratio.

For Fig. 4.8J and Fig. 4.9A-C, we sought to obtain the most comprehensive set of splicing events affected by PHF5A. We therefore took the union of the events detected using the approach described above with events identified with a binomial proportion test on the reads assigned to each isoform by MISO version 0.4.4 (Katz et al., 2010), which uses a Bayesian approach to assign non-identifying reads.

ACKNOWLEDGEMENTS

We thank: Stephen Tapscott, Bruce Clurman, and Valeri Vasioukhin for critical reading of this manuscript; Minoru Yoshida, Howard Fine, Russell Pieper, and Austin Smith for providing cell lines and/or reagents; Stacey Hansen, Kyle Pedro, and Sally Ditzler for technical help; Pam Lindberg and Laima Abele for administrative support; members of the Paddison and Olson labs for helpful discussions. This work was supported by FHCRC institutional funds (PP & RKB) and grants from: the PEW scholar program (PP), the Accelerate Brain Cancer Cure foundation (PP), NCI / NIH P30 CA15704 (PP), NCI/NIH R01CA155360 (JO), NCI/NIH R01 CA135491 (JO), NCI/NIH 5R01 CA114567 (JO), a UK-US Stem Cell Collaboration Development Award program (SP/PP), NCI / NIH P30 CA15704 (PP), Phi Beta Psi Sorority cancer grant program (PP), the DoD young investigator award program (PP), Damon Runyon Cancer Research

Foundation DFS 04-12 (RKB), Association of American Cancer Institutes (YD), and NIH Interdisciplinary Training in Cancer Research Program #T32CA080416 (CH).

VI. FIGURES

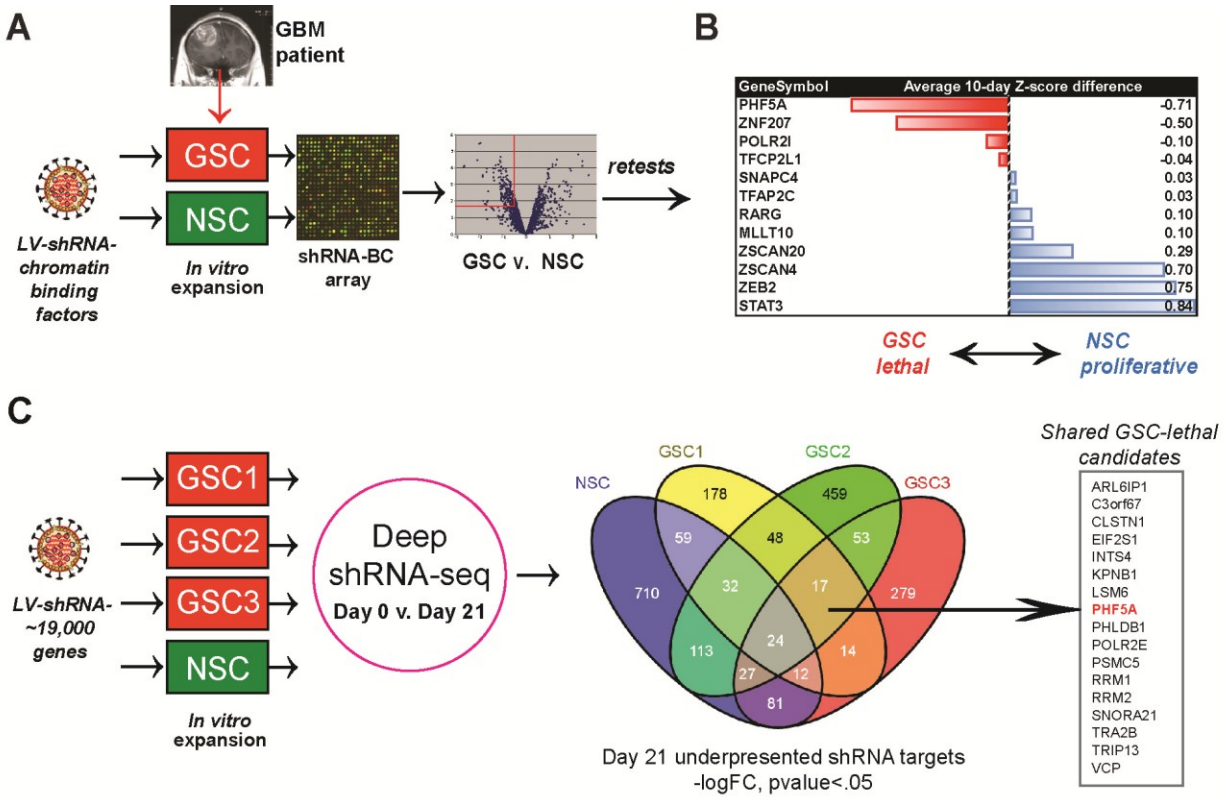

Figure 4.1. Functional genetic screens identify PHF5A as differentially required for GSC expansion.

(A) The shRNA screening approach used to initially identify PHF5A as differentially required for GSC expansion. Pooled viruses targeting DNA binding factors were used in outgrowth screens in human GSC-G166 and NSC-CB660 cells. Candidate genes differentially required for GSC expansion over 21-days of outgrowth were identified through hybridization of viral DNA barcodes to custom microarrays. (B) Average differential between GSC and NSC for shRNA clones targeting candidate screen hits by *in vitro* competition assay. Cells infected with single shRNA clones (GFP+) were mixed with uninfected cells and outgrown for 10 days, and the change in GFP+ cells in each culture was quantified by FACS analysis. (C) Our genome-wide shRNA screening strategy used in NSC-CB660 and three primary GSC isolates. Viral shRNA pools targeting ~19,000 human genes were infected into cells prior to 21-day outgrowth *in vitro*. The change in viral shRNA representation in each cell population was quantified by sequencing. Gene targets statistically underrepresented at the end of the culture period are shown. See also Figure 4.2.

A Single clone viability analysis

Gene Symbol	Avg. Norm. Growth Ratio	p-Value	Total Clones
PHF5A	0.52	0.001	12
POLR2I	0.71	0.027	8
ZNF207	0.80	0.091	12
ZSCAN20	0.84	0.336	3
GATA4	0.88	0.241	5
NANOG/NANOGP8	0.90	0.354	3
RARG	0.91	0.596	6
MYEF2	0.93	0.485	16
NR1H3	0.93	0.599	7
TFAP2C	0.95	0.665	9
SNAPC4	0.95	0.718	6
ZSCAN4	0.98	0.888	5
MLLT10	0.99	0.988	4
MAX	1.00	0.951	4
TFCP2L1	1.01	0.909	9
OTP	1.02	0.827	3
HOXA5	1.04	0.561	6
E2F3	1.06	0.493	3
EGR3	1.07	0.346	4
FOSL2	1.13	0.540	12
STAT3	1.20	0.236	8
VSX2	1.26	0.109	4
GABPA	1.29	0.152	8
NR2C2	1.31	0.113	12
CITED1	1.41	0.026	6
HSFY1/2	1.42	0.060	6
ZEB2	1.43	0.001	4

B Single clone GFP FACS analysis

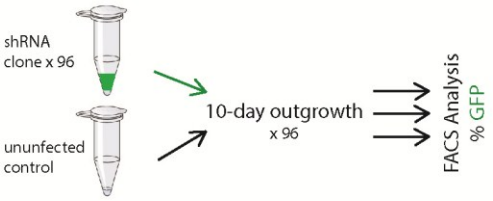

Gene Symbol	Average 10-day %GFP Z-score difference
PHF5A	-0.71
ZNF207	-0.50
POLR2I	-0.10
TFCP2L1	-0.04
SNAPC4	0.03
TFAP2C	0.03
RARG	0.10
MLLT10	0.10
ZSCAN20	0.29
ZSCAN4	0.70
ZEB2	0.75
STAT3	0.84

GSC lethal ⟷ *NSC proliferative*

Figure 4.2. Validation of primary DNA binding factor screen hits.

(a) G166 and CB660 cells infected with single shRNA clones targeting potential screen hits were plated in 96-well format. Cell viability was quantified at day 0 and day 7 to measure growth and measurements were normalized to control shRNA wells for each cell line. The average ratio of normalized G166/CB660 growth for all clones targeting each gene is presented. (b) As an orthogonal validation approach, we performed *in vitro* competition assays testing a subset of putative screen hits in G166 and CB660 cells. Cells were infected with single shRNA clones targeting potential screen hits were mixed uninfected control cells and plated in 96-well format. The percent of GFP+ (shRNA expressing) cells present in each well was quantified by FACS analysis at day 0 and day 10 and ranked by Z-score to allow comparisons between each cell line. The average difference in Z-score between G166 and CB660 for all clones targeting each gene is presented.

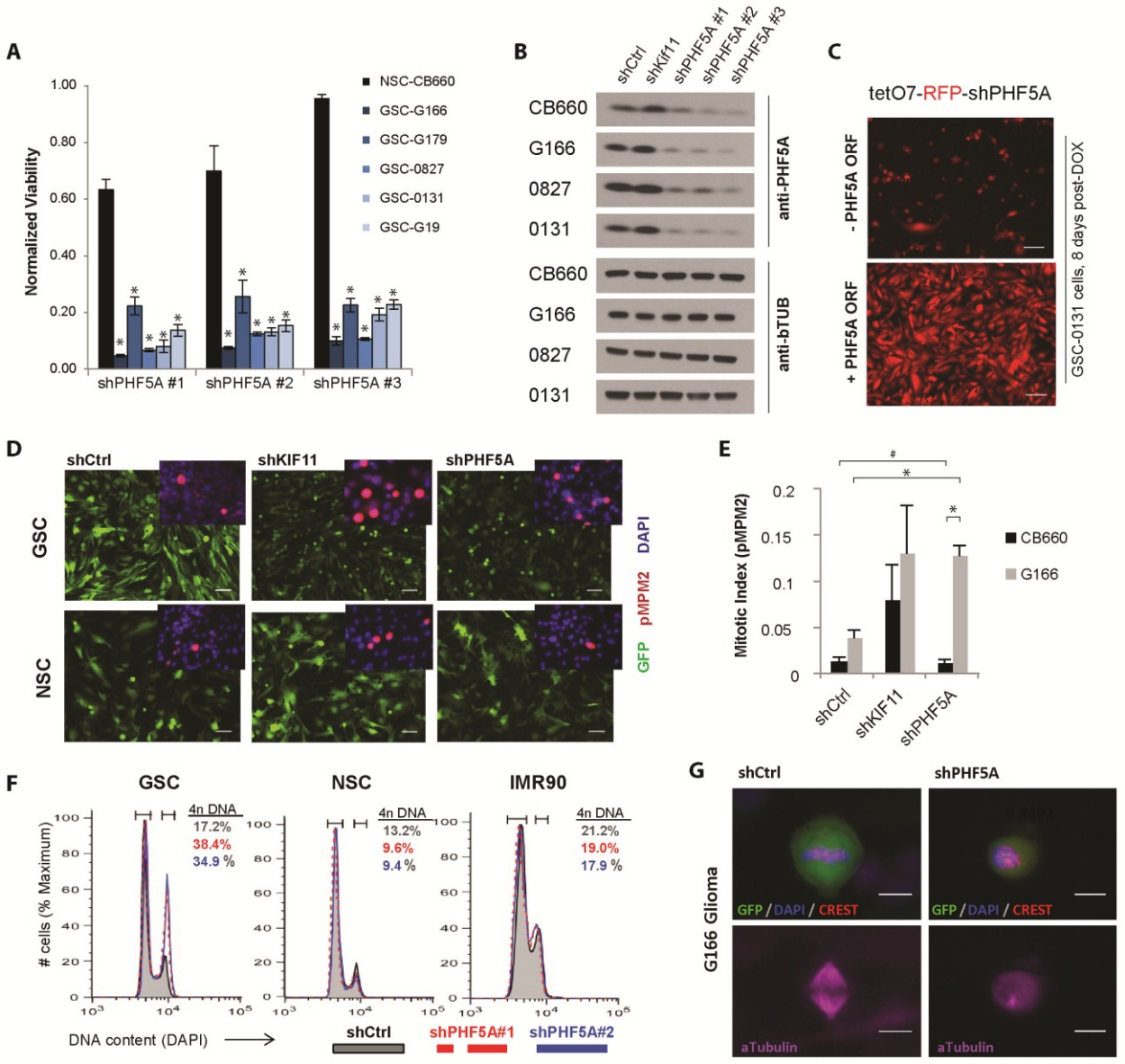

Figure 4.3. PHF5A is differentially required for GSC expansion and its knockdown triggers G2/M cell cycle arrest in GSCs but not NSCs.

(A) Viability of NSC and five GSC cell isolates infected with three independent shRNA viral clones targeting PHF5A. (* denotes p-value <0.002 vs. CB660) (B) Western blot analysis of PHF5A protein expression in NSC and GSC cells after PHF5A KD. (C) Images of GSC-0131 cell clones expressing an inducible shRNA construct targeting the endogenous 3'UTR of PHF5A, with or without rescue by exogenous expression of full length PHF5A. Scale bar = 50µm. (D) Fluorescence microscopy images of GSCs or NSCs expressing constitutive GFP and PHF5A KD or control constructs. Inset immunofluorescent images of phospho-MPM2, indicative of mitotic activity, in GSCs and NSCs depleted for PHF5A. Scale bar = 100µm. (E) Quantification of phospho-MPM2 staining in GSCs and NSCs infected with control or shPHF5A virus. (* denotes p-value < 0.001; # denotes insignificant p-value = 0.5) (F) Cellular DNA content as measured by DAPI staining and FACS analysis in GSC, NSC, and IMR90 normal fibroblast cultures with or without PHF5A KD. The percentage of cells in each sample with 4n DNA content is shown, indicative of cells that have completed DNA replication in S-phase. (G) Immunofluorescent images of DNA (DAPI), kinetochore location (CREST) and spindle formation (alpha-tubulin) in mitotic GSCs with or without PHF5A KD. Scale bar = 10µm. See also Figure 4.4.

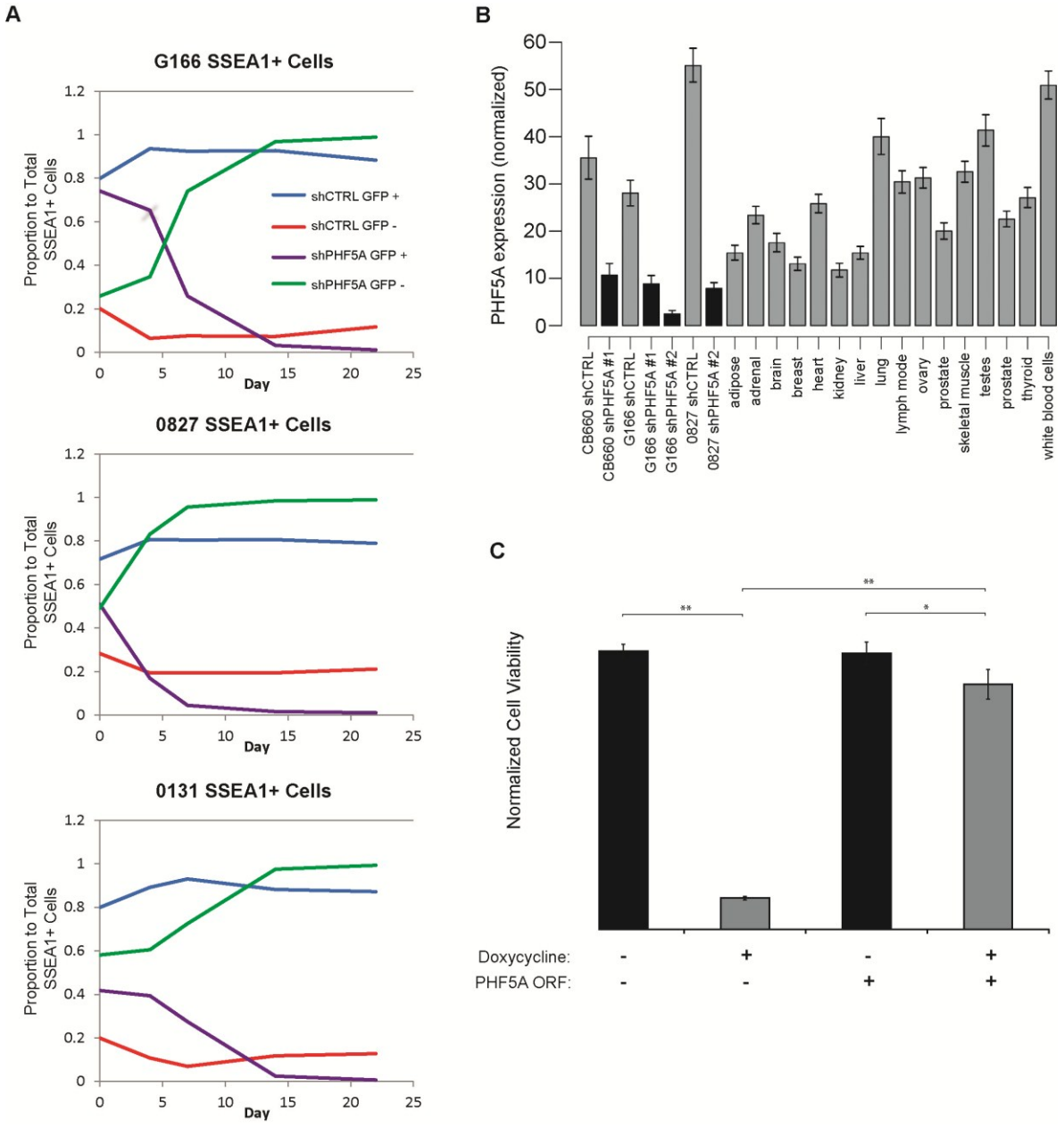

Figure 4.4. PHF5A is required for GSC *in vitro* expansion. (a) *In vitro* competition assay of SSEA1 cell population. GSCs infected with shPHF5A or shCtrl lentivirus (GFP+) were mixed with a smaller fraction of uninfected control cells (GFP-). Cells were analyzed at days 0, 4, 7, 14, and 22 for SSEA1 and GFP expression by FACS analysis. The proportion of SSEA1+ cells expressing or not expressing GFP is shown for both shRNA competition cultures for each GSC isolate. PHF5A depleted SSEA1+ GSCs drop out of culture and are replaces by GFP- control cells, whereas shCtrl cells maintain their representation in culture over time. (b) Normalized PHF5A expression (from RNA-seq data) in CB660, G166, and 0827 cells with or without PHF5a KD. PHF5A expression in a panel of normal human cell types is also shown for comparison. (c) Cell viability data from a doxycycline inducible shPHF5a 0131 GSC cell clone targeting the endogenous PHF5a 3' UTR. Cells were with or without exogenous PHF5A ORF expression were treated with or without doxycycline for 11 days before being assayed for cell viability by AlamarBlue assay (Invitrogen). (* denotes p-value < 10^{-6}; ** denotes p-value < 10^{-23}.)

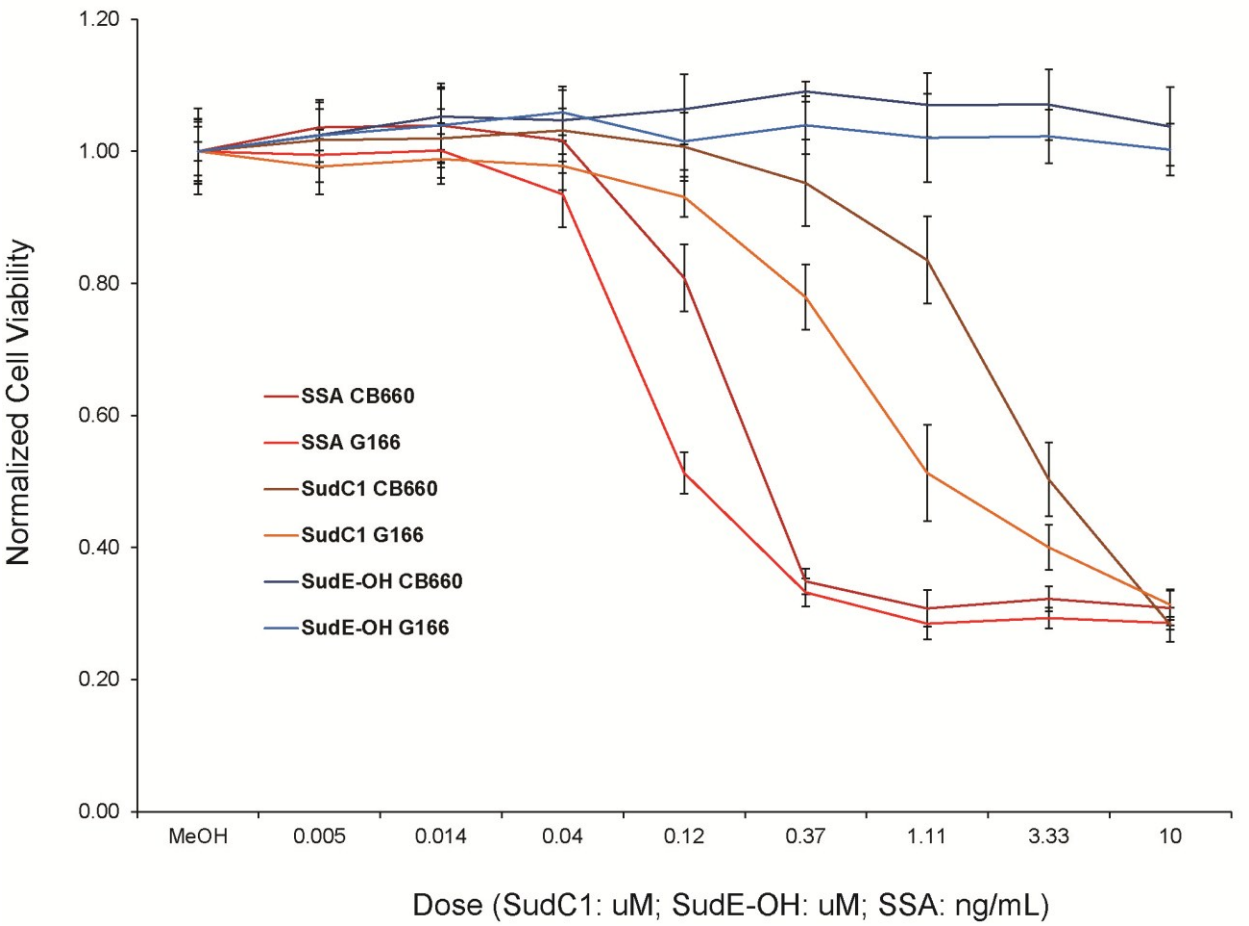

Figure 4.5. GSCs have increased sensitivity to splicing inhibition compared to NSCs.
G166 or CB660 cells were exposed to a dilution series of SSA, SudC1, or SudE-OH (inactive alcohol form of Sudemycin) for 24 hours then assayed for cell viability by AlamarBlue assay (Invitrogen) at 72 hours after exposure.

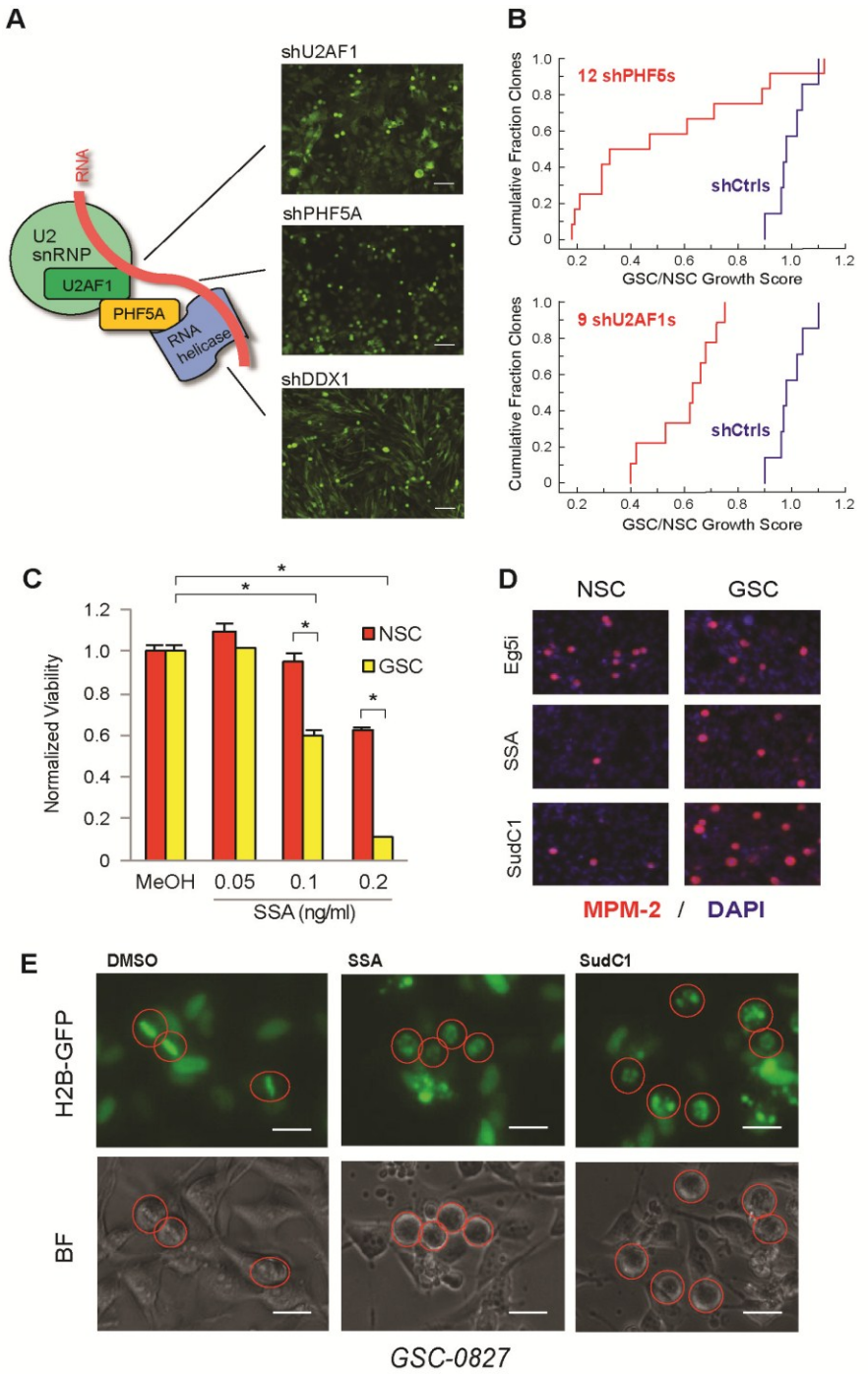

Figure 4.6. PHF5A binding partners involved in RNA splicing and U2snRNP activity are differentially required by GSCs for mitotic progression.

(A) A model of PHF5A splicing interactions based on previous research. Knockdown of known PHF5A binding partners in the spliceosome recapitulates the PHF5A KD phenotype, shown. Scale bar = 50µm. (B) Cumulative probability plot of multiple shRNAs scoring as cell lethal versus their GSC to NSC viability ratio. (C) Viability of GSC or NSC cells treated with increasing doses of SSA. (* denotes *p*-value < 0.0003) (D) Immunofluorescent images of phospho-MPM2 in GSCs and NSCs treated with SSA or SudC1. (E) Fluorescent and light images of GSCs expressing Histone 2B-GFP fusion protein which marks DNA. Cells were pretreated with SSA or SudC1 for 22hrs before addition of MG132 for an additional 2 hours to arrest dividing cells in metaphase. Circles mark the same cell in corresponding images. See also Figure 4.5.

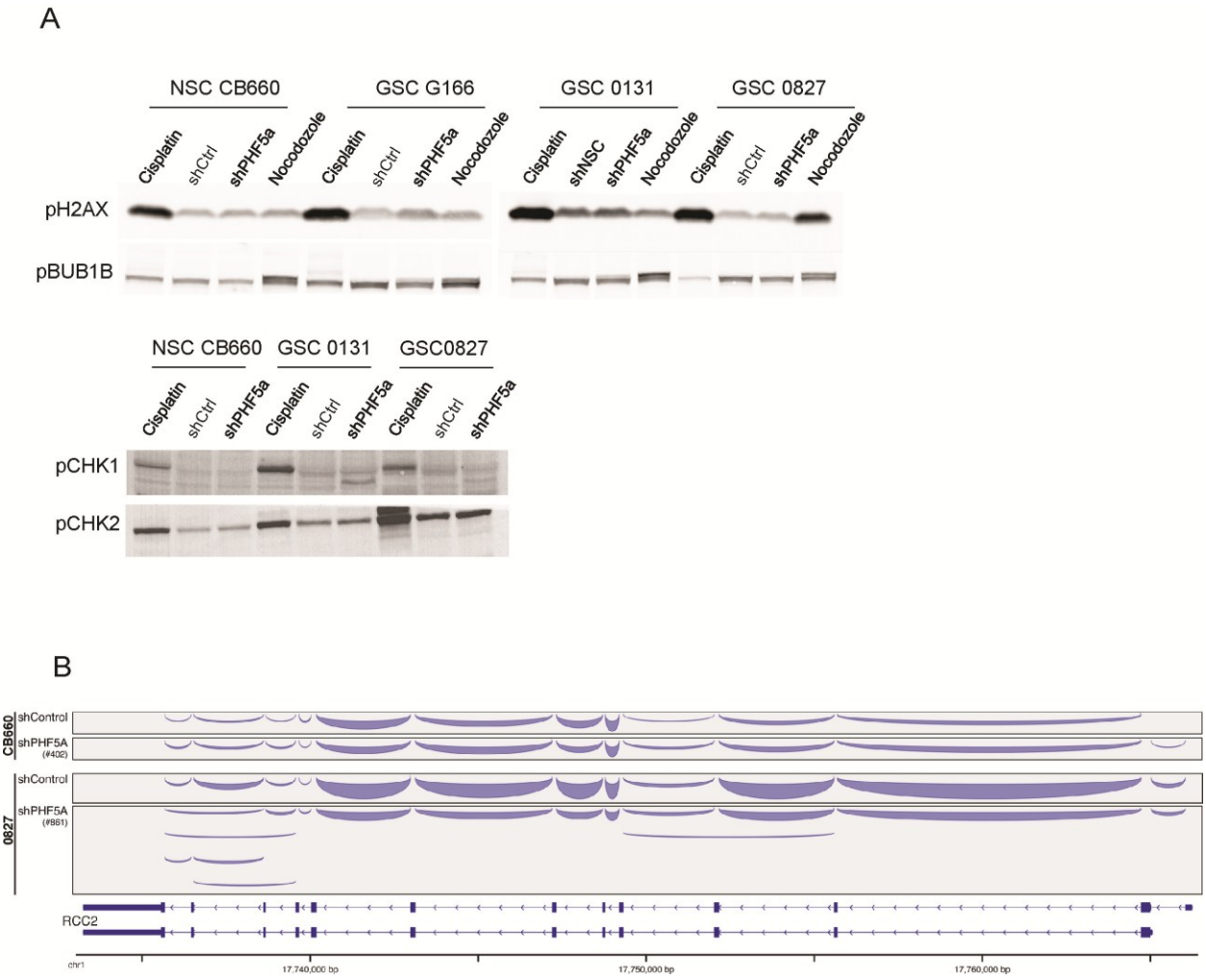

Figure 4.7. Depletion of PHF5A does not trigger the DNA damage response, but does cause splicing defects in GSCs.

(a) NSC or GSC cultures were infected with shCtrl or shPHF5A virus then selected with puromycin. Positive control cultures were treated with Cisplatin or Nocodozole for 24hours. Equal cell lysates were run as western blots and incubated with the indicated phospho-specific antibodies. (b) Plot illustrates the density of RNA-seq reads crossing splice junctions and was created with IGV (Robinson et al., 2011). Aberrant isoforms of RCC2 lacking constitutive exons appear following PHF5A KD.

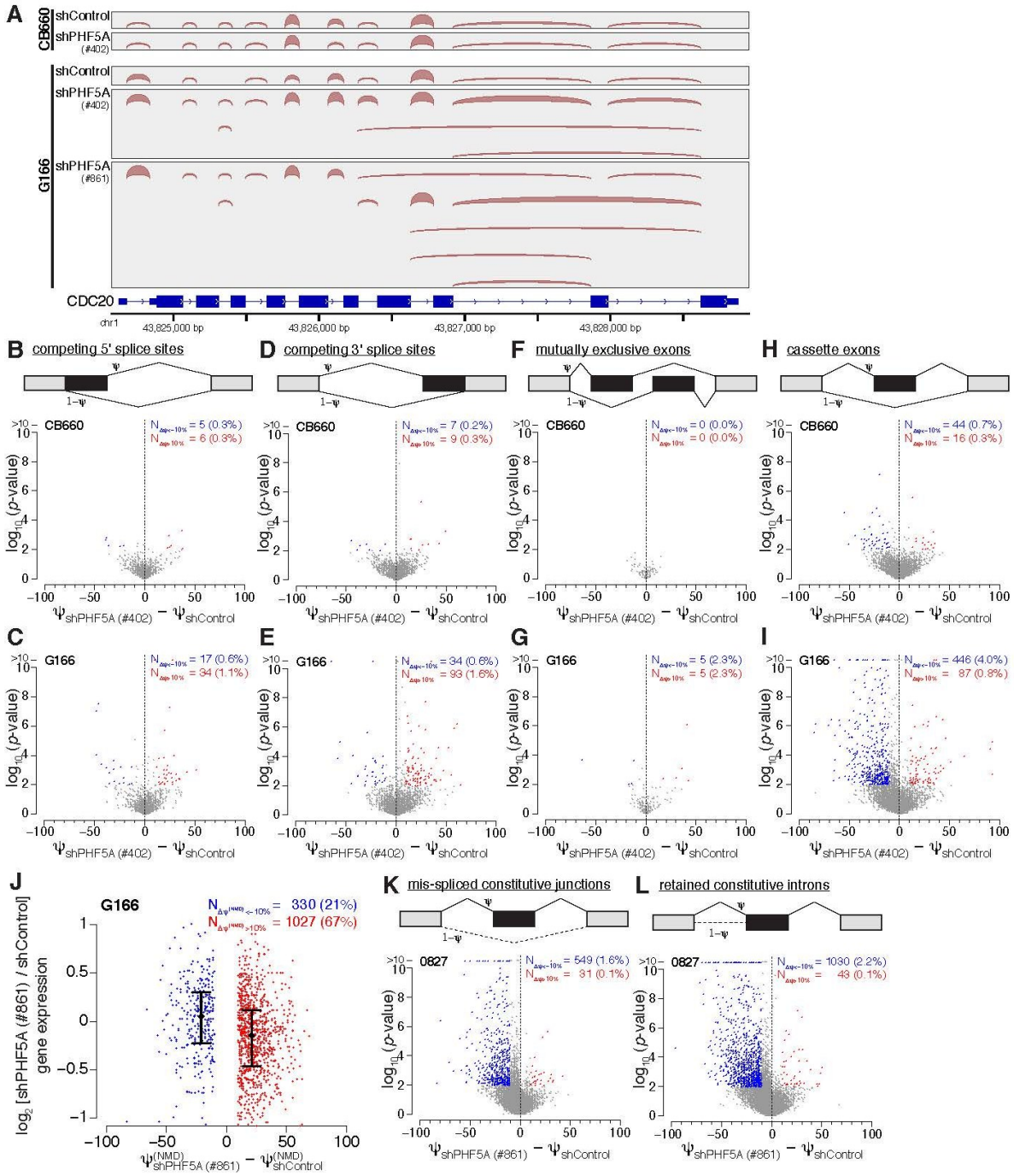

Figure 4.8. Loss of PHF5A results in global splicing defects in GSCs, but not NSCs.
(A) Select genes important for cell cycle progression, such as CDC20, display broad splicing defects following PHF5A KD. Plot illustrates the density of RNA-seq reads crossing splice junctions and was created with IGV (Robinson et al., 2011). Aberrant isoforms lacking constitutive exons appear following KD of PHF5A with two distinct shRNAs. (B-C) KD of PHF5A results in few changes in usage of competing 5' splice sites, (D-E) competing 3' splice sites, or (F-G) mutually exclusive exons in either NSCs or GSCs. (H-I) However, PHF5A KD causes a broad increase in skipping of cassette exons in GSCs, but not NSCs. (J) Many of the splicing changes induced by PHF5A KD in GSCs introduce in-frame stop codons, suggesting that the resulting transcripts will be degraded by NMD. Gene expression values were computed with RSEM (Li and Dewey, 2011) and normalized with the TMM method (Robinson and Oshlack, 2010). Confidence intervals indicate the 1st and 3rd quartiles of expression. (K) PHF5A KD causes a dramatic increase in mis-splicing of constitutive junctions, (L) as well as retention of constitutive introns. See also Figure 4.7b. Figure by Rob Bradley.

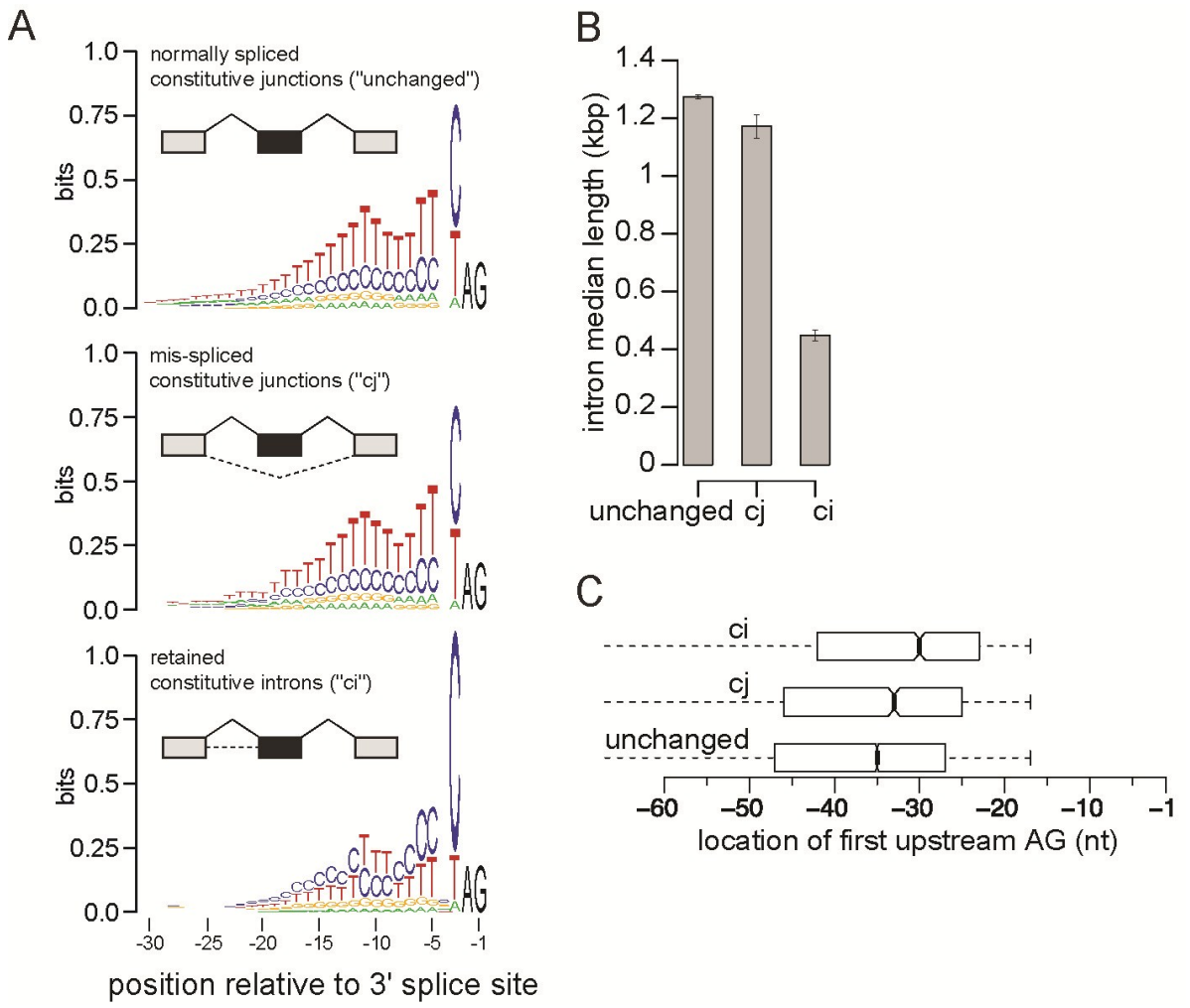

Figure 4.9. PHF5A is required for proper recognition of an unusual class of exons.
(A) Constitutive junctions that are mis-spliced following PHF5A KD in GSCs (center) have slightly shorter polypyrimidine tracts than do unaffected constitutive junctions (top); in contrast, retained constitutive introns (bottom) have unusually C-rich polypyrimidine tracts. (B) Retained constitutive introns are much shorter. Plot illustrates the median intron length, and error bars indicate the standard error estimated by bootstrapping. (C) Retained constitutive introns have branch points that are unusually proximal to the 3' splice site. Box plots indicate 1st and 3rd quartiles of the first upstream AG, a proxy for the branch point location (Gooding et al., 2006). Figure by Rob Bradley.

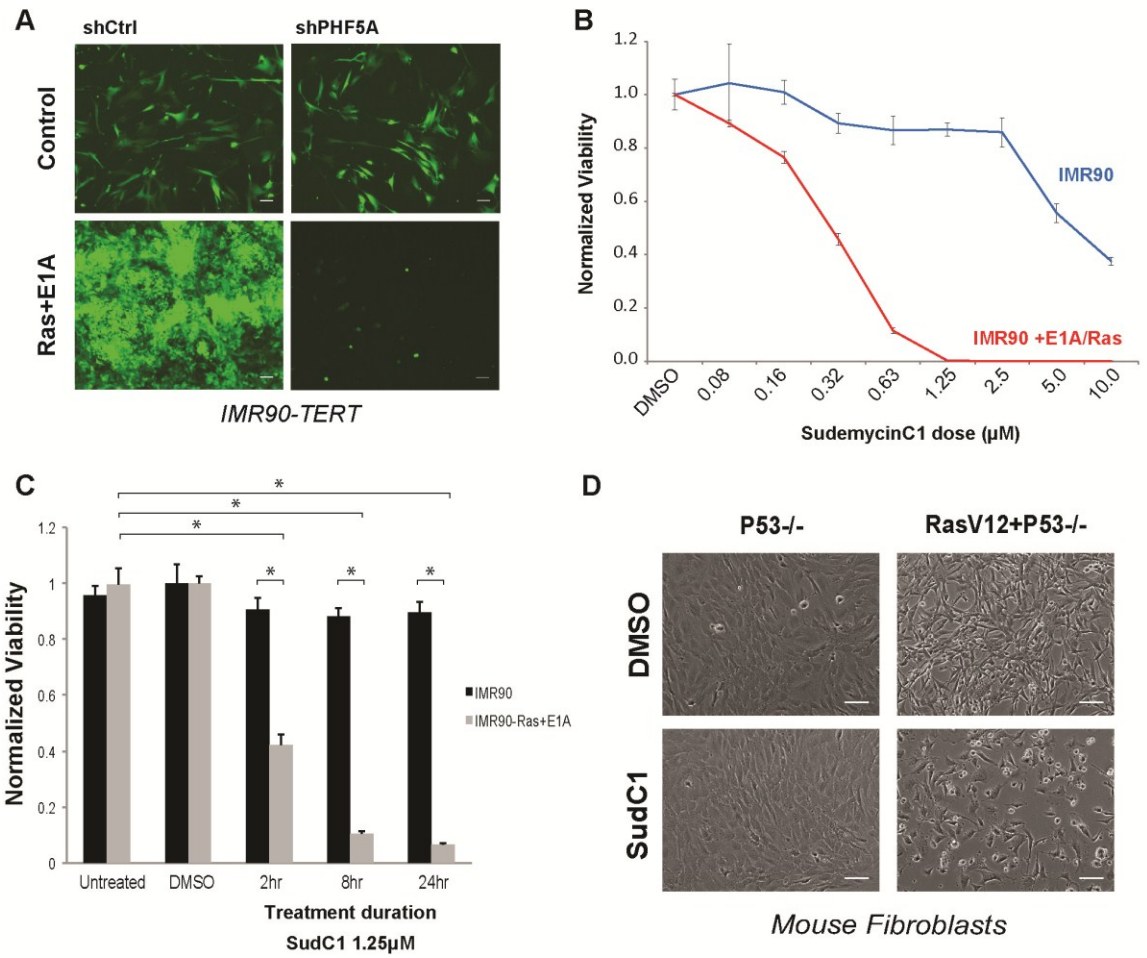

Figure 4.10. Partial oncogenic transformation triggers an added requirement for U2snRNP activity. (A) Fluorescent microscopy images IMR90 fibroblasts with or without expression of RasV12 after knockdown of PHF5A. Scale bar = 100μm. (B) Cellular viability of IMR90 fibroblasts with or without expression of the RasV12 oncogene after treatment with increasing doses of SudC1. (C) Viability of IMR90 cells with or without RasV12 expression after different exposure times to SudC1. (* denotes p-value < $2x10^{-6}$) (D) Light microscopy images of $p53^{-/-}$ MEFs with or without RasV12 expression treated with SudC1. Scale bar = 100μm. See also Figure 4.11.

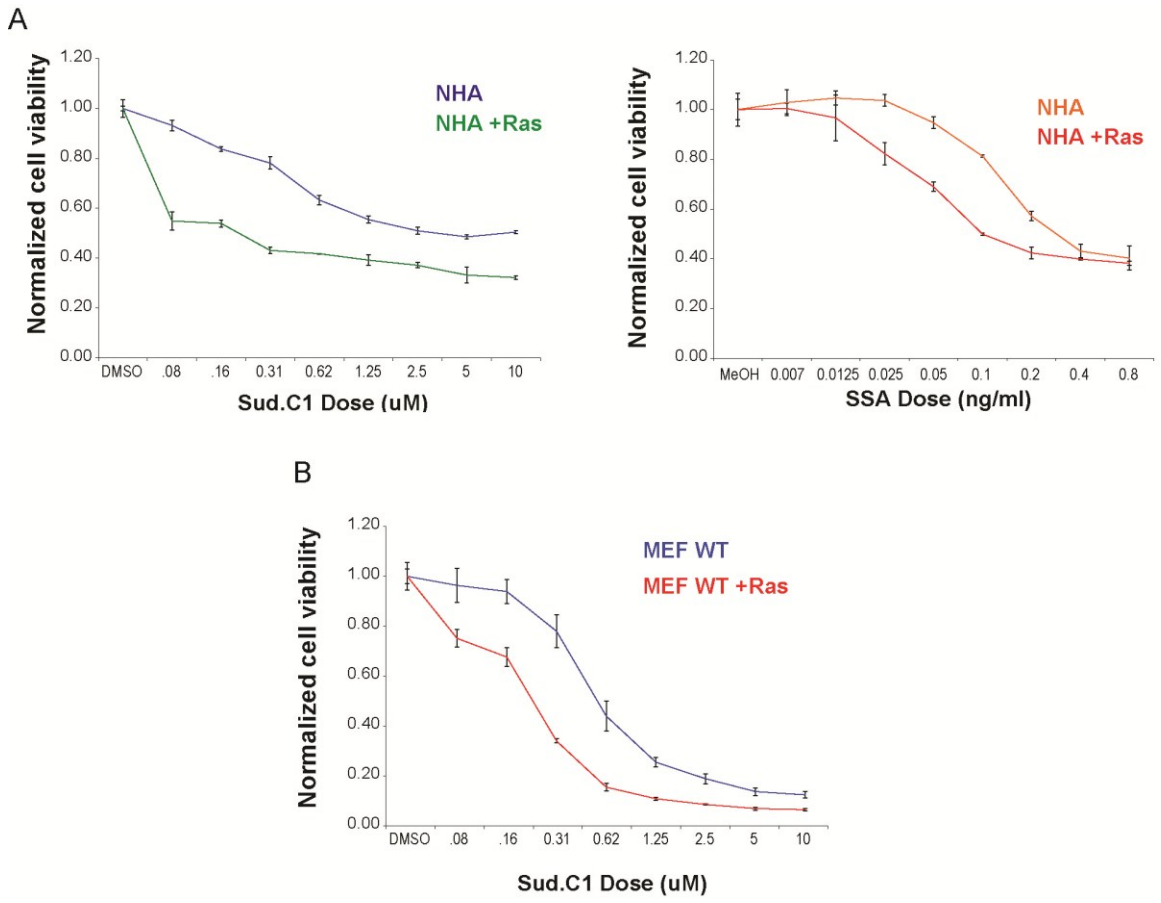

Figure 4.11. Oncogenic transformation triggers an added requirement for U2 snRNP activity. Cellular viability of normal human astrocytes (NHA) or mouse fibroblasts (MEF) with or without expression of the RasV12 oncogene after treatment with increasing doses of SSA or SudC1.

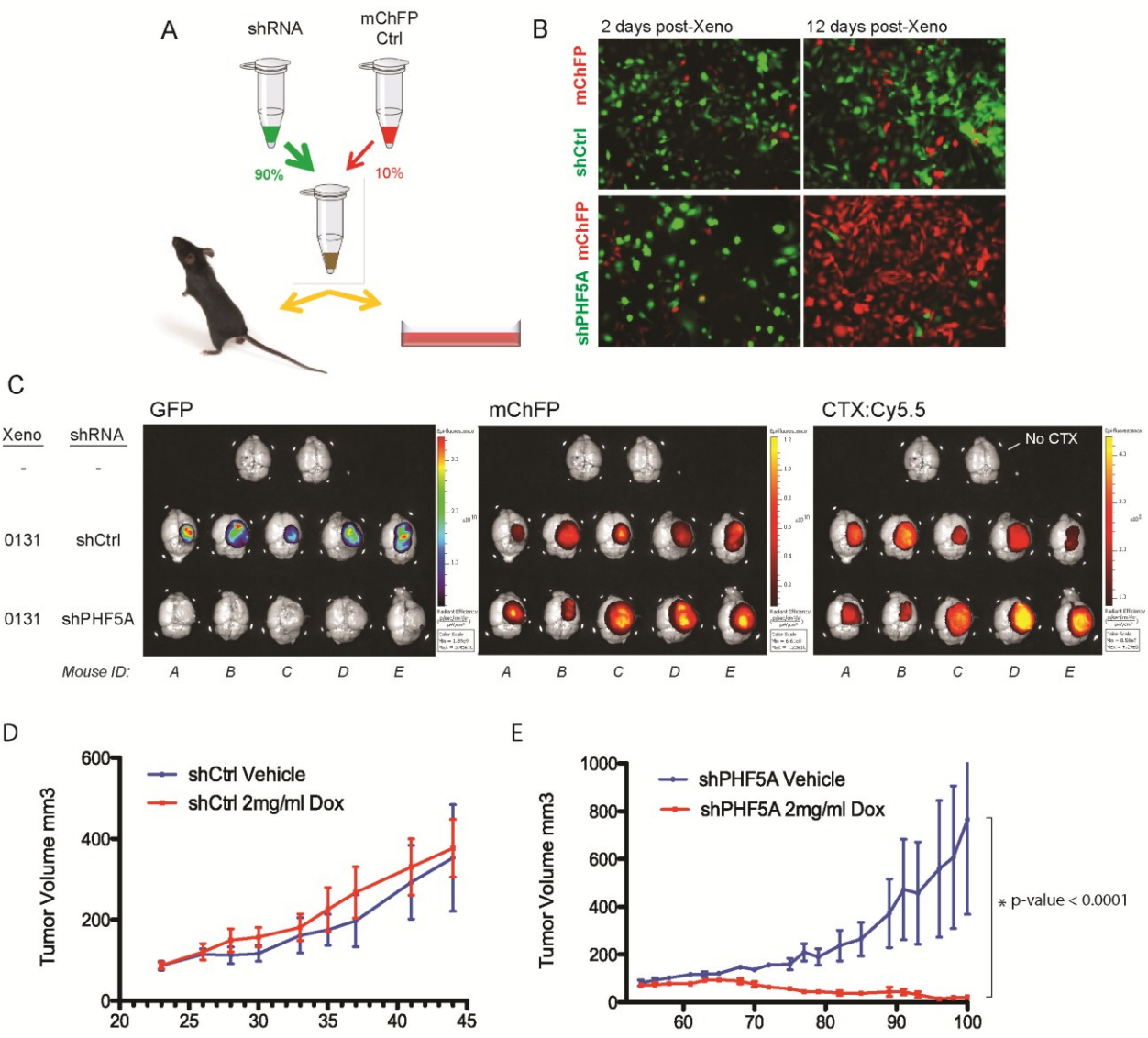

Figure 4.12. Suppression of PHF5A expression compromises GBM tumor formation and maintenance *in vivo.*

(A) Schematic diagram of the *in vivo* competition experiment. GSCs expressing GFP and either control of PHF5A shRNA were mixed in a 90:10 ratio with mChFP-expressing control cells. This cell mix was then either propagated in culture or xenografted into the right cortical hemisphere of mice. (B) Fluorescent microscopy images of the 90:10 GSC mix grown in culture for 2 or 10 days. (C) Fluorescence overlay images of *in vivo* competition mouse brains 5 weeks after xenograft. In addition to GFP and ChFP signal, CTX:Cy5.5 (Tumor Paint) was used to mark total tumor mass. (D-E) Flank xenograft volume over time of GSC-0131 clones expressing doxycycline-inducible PHF5A shRNA or Ctrl shRNA. Tumors were allowed to progress in absence of Dox until the tumor volume of each cohort averaged approximately 75mm^3. Mice were then randomized onto continuous doxycycline or vehicle treatment and tumor volume was monitored over time.

Table 4.1. PHF5A candidate binding partners identified by IP-MS.
Protein complexes in GSC-G166 or A2058 cells were purified by immunoprecipitation and analyzed by mass spectroscopy. Proteins represented in both samples by at least three unique peptides are shown.

PHF5A IP-MS results		
ABCF1	GNL3	RPL17
AP3D1	GPATCH1	RPL18
ARGLU1	HNRNPH1	RPL27A
BUD13	HSPA8	RPL32
C1orf35	HSPA9	RPL35
C9orf114	KRT1	RPS23
C9orf86	KRT10	RPS3
CCDC49	KRT16	RPS4X
CCDC55	KRT2	RPS8
CCNL1	KRT9	SAP30BP
CPSF1	LTV1	SART1
CPSF2	LUC7L2	SFRS11
CPSF3	LYAR	SFRS12
CPSF6	MED19	SFRS17A
CRKRS	MORG1	SNRNP200
CROP	NKAP	SNRNP40
CWF19L2	NOL10	SON
DDX17	NOP56	SRPK1
DDX18	NOP58	SRRM1
DDX27	NUDT21	SRRM2
DDX3X	PARP1	TAF2
DDX41	PHF5A	TAF3
DDX46	PPIB	TAF4
DDX5	PPIL4	TAF5
DHX15	PRDX1	TAF6
DHX35	PRPF38B	TAF9
DHX8	PRPF40A	TCOF1
EEF1A1	PRPF4B	TINP1
EFTUD2	PRPF8	TOP1
EIF5B	PUF60	TRIM21
ENO1	RBBP6	TUBB2C
FAM133B	RBM25	TWISTNB
FAU	RBMX2	U2AF1
FIP1L1	RCC2	U2AF2
FRG1	RP9	WDR33
		ZCCHC17

Chapter 5 – Discussion

Most eukaryotic genes contain intervening sequences (introns) that interrupt the protein coding sequences (exons). For a protein to be properly translated from an unspliced precursor mRNA (pre-mRNA), these introns must first be removed through the process of RNA splicing (Chen and Manley, 2009). Splicing events can be constitutive (always performed in the maturation of an RNA isoform), or alternative (conditionally performed in one of several ways). Alternative splicing of a single gene can generate multiple different protein isoforms each with distinct and sometimes opposing functions (David and Manley, 2010). RNA splicing therefore plays an important role in generating the diverse protein products that govern cell growth, behavior, and death.

The process of RNA splicing is carried out by the spliceosome, a complex macromolecular machine comprised of hundreds of individual proteins and RNA molecules. The massive structure of the spliceosome is mainly composed of five small nuclear ribonucleoprotein particles (snRNPs) and a large number of accessory proteins that direct snRNPs to splice sites or catalyze steps of the splicing reaction (Chen and Manley, 2009). Splicing begins on a pre-mRNA by recognition of the 5' splice site by the U1 snRNP, the RNA branch point by SF1, and the 3' splice site and polypyrimidine tract by U2AF1, forming the E complex and committing the RNA to splicing. With the recruitment of the protein subcomplexes called splicing factor 3a and splicing factor 3b (SF3a and SF3b), the U2 snRNP forms and replaces SF1 at the RNA branch point near the 3' splice site, completing the transition to the 'pre splicing' A complex. Further recruitment of the U4/U6–U5 tri-snRNP complex leads to the formation of the 'early splicing' B complex. This is converted into to the catalytically active 'late splicing' C complex which

completes the splicing reaction. The 5' splice site of the preceding exon is thus joined to the 3' splice site of the following exon, the lariat of intervening RNA is discarded, and the spliceosomal proteins are released to perform subsequent rounds of splicing (reviewed in (Kramer, 1996)).

Formation of the A complex above relies on proper assembly of the U2 snRNP. This subcomponent of the spliceosome is formed by sequential interactions of SF3a and SF3b with a number of accessory proteins including U2AF1 (Kramer et al., 1999). The SF3b complex plays an important role in the recruitment and tethering of the U2 snRNP to the intronic branch site (Champion-Arnaud and Reed, 1994) and thus is important in 3' splice site usage. This complex consists of approximately 7 protein members including SAP14b, also known as PHF5A.

Although RNA splicing is an essential process required by all eukaryotic cells (Chen and Manley, 2009; Kramer, 1996), the functions of many individual spliceosomal proteins are poorly understood. Here I have demonstrated that the largely uncharacterized SF3b complex member PHF5A is differentially required for the proliferation and survival of glioblastoma cells but not normal neural stem cells. PHF5A is a 12.4kd PHD (plant homeo domain)-zinc finger domain protein that is highly conserved from yeast to man (Trappe et al., 2002). Other PHD protein family members can facilitate interactions with specific histone marks in chromatin-bound nucleosomes (Mellor, 2006; Musselman and Kutateladze, 2009, 2011). As such, PHF5A has been shown to bind to the promoter of Connexin43 in human cells where it enhances Connexin43 gene transcription by the Estrogen Recepter-alpha transcriptinon factor (Oltra et al., 2003). PHF5A also co-purifies with components of the 17S U2 snRNP complex of the spliceosome (Behzadnia et al., 2007). This is consistent with the role of the PHF5A homolog RDS3p in *s. cereviscae* as a member of the yeast SF3b complex (Dziembowski et al., 2004;

Wang et al., 2005) A temperature sensitive mutation of RDS3p inhibits proper mRNA splicing in yeast at non-permissive temperatures due to a lack of U2 snRNP recruitment necessesary for splicing complex maturation (Wang and Rymond, 2003). The structure of RDS3p is that of a triquetra knot and its surface properties suggest that it functions as a platform for protein assembly within the multiprotein SF3b complex of U2 snRNP (van Roon et al., 2008). PHF5A's broad conservation and high homology to RDS3p, and the ability of human PHF5A to rescue deletion of the PHF5A homolog in the fission yeast *s. pombe* INI1, suggests that human PHF5A may play a similar role in facilitating SF3b assembly.

I have demonstrated a requirement for PHF5A in GBM tumor formation and maintenance in vivo and shown that in vitro knockdown triggers G2/M arrest in GSCs but not untransformed cells. This result is consistent with previous studies of INI1 in yeast where deletion mutants exhibit an elongated cell phenotype and 2C DNA content indicative of a G2 cell cycle arrest (Oltra et al., 2004). These results also echo several studies exploring the alteration of RNA splicing in mammalian cells. Loss of splicing factor ASF/SF2 is known to induces genomic instability (Li and Manley, 2005), resulting in G2 cell cycle arrest and apoptosis (Li et al., 2005). Human cells treated with small molecule inhibitors of SF3b accumulate 4n DNA content (Corrionero et al., 2011; Fan et al., 2011; Kaida et al., 2007), also indicating an arrest in the G2/M phase of the cell cycle. Furthermore, inhibition of splicing factors or aurora kinase activity resulted in a shift to proapoptotic isoforms of BCLx, MCL1, and caspase 9 prior to cell cycle arrest, elucidating an alternative splicing network in HeLa cells that controls G2/M cell cycle arrest and apoptosis (Moore et al., 2010).

PHF5A is a bridge protein which plays a key role in the tethering of U2 snRNP associated proteins, especially U2AF1, to RNA helicases associated with the spliceosome,

notably DDX1 (Rzymski et al., 2008). I have shown that knockdown of either of PHF5A's binding partners U2AF1 or DDX1 reproduces to a lesser degree the cancer-specific arrest observed upon PHF5A depletion. This demonstrates that the PHF5A knockdown phenotype is specific to its function in the spliceosome, as opposed to any other roles it may play in the cell. This could further suggest that the PHF5A bridging interaction may be a molecular 'hot spot' within the spliceosome whose disruption may be able to exert a maximal cancer-lethal effect.

Pre-mRNA splicing is well characterized as an essential process required for all eukaryotic cells, but the spliceosome consists of over two hundred proteins forming a highly complex and dynamic system (Kramer, 1996). The repression of PHF5A expression or inhibition of its subcomplex does not cause a complete loss of cellular splicing ability but rather results in repeatable shifts of many specific mature RNA spliceforms within the cell (Figure 4.6), implying true biological functions rather than random mis-splicing underlying these molecular changes. This suggests that, rather than PHF5A being essential in and of itself, normal cellular splicing is plastic enough that other members of the splicing machinery are able to imperfectly complement PHF5A loss and carry out the majority of necessary splicing events. However, upon loss of PHF5A expression within GNS cells, we have uncovered a global bias towards mis-splicing of many specific gene transcripts (Figure 4.6). Further studies are required to determine which of these cancer-specific alterations, either alone, in combination, or *en masse*, contribute to the cancer-lethal cell cycle arrest observed upon PHF5A knockdown.

In our analysis, only a relatively small subset of splice junctions were affected by PHF5A depletion in GSCs, indicating that the requirement for PHF5A is not universal across exons. 3' splice sites associated with abnormal splicing of constitutive junctions had slightly shorter, but otherwise normal, polypyrimidine tracts relative to unaffected 3'splice sites; in contrast, 3' splice

sites associated with retained constitutive introns had highly atypical C-rich tracts (Figure 4.9A). While PHF5A is known as a core component of the spliceosome, it appears to be most important for recognition of an unusual class of exons with distinctive 3' splice sites.

Potential mechanisms for the cancer specificity of PHF5A inhibition

An important question raised by these studies is why the molecular splicing alterations seen in the GNS cells are *not* seen in normal NSCs. Our partial transformation experiments have ruled out the possibility of an unknown and unique resistance mechanism on the part of NSCs. This leaves a number of potential mechanisms through which this splicing related non-oncogene addiction may be conferred.

Many tumors have high rates of chromosome mis-segregation resulting in chromosome instability, chromosome disruption, and rapid genetic evolution (Komarova et al., 2002). This phenotype may result from the state of aneuploidy exhibited by most tumor cells and the added burden placed on the mitotic machinery needed to properly segregate these supernumerary chromosomes (Ganem et al., 2007). Since normal mitotic cells are rarely if ever aneuploid, mitotic stress derived from extra chromosomes may represent a unique vulnerability in cancer cells (Luo et al., 2009b; Solimini et al., 2007). Since we see in increased requirement in normal diploid cells after RasV12 transformation, it is unlikely that mitotic stress from aneuploidy plays a role in a cancer-specific requirement for PHF5A. We do know, however, that mitotic stress and chromosome instability may result indirectly from mutation of oncogenes such as Ras through the induction of double-stranded DNA breaks and chromosome instability (Halazonetis et al., 2008). However we were unable to find any evidence of double-stranded DNA breakage (as evidenced by γ-H2AX phosphorylation) or DNA damage response after PHF5A inhibition.

(Figure 4.7A) Furthermore, we did not observe mitotic checkpoint activation after PHF5A KD suggesting that the lethality is not related to chromeosome alignment and subsequent mis-segregation defects. (Figure 4.7A) This is perhaps to be expected since the arresting cells do not progress through mitosis to the point of mitotic plate formation. (Figure 4.6E) Although the precise cause of mitotic stress is not known for the vast majority of tumors (Luo et al., 2009b) it is unlikely that cancer-specific PHF5A-medited arrest and cell death functions through the known mechanisms of mitotic stress.

In addition to stress on mitotic machinery, it is possible that transformation confers increased dependence upon certain spliceosome components by forcing the transformed cells to adopt an unusual splicing complex stoichiometry. As many splicing factors have complementary or compensatory activity, and also participate in feedback loops to maintain cellular homeostasis, one attractive model is that transformation alters the expression of spliceosomal proteins that normally complement PHF5A's role. Consistent with this model, oncogene activity is known to affect the expression levels of select splicing factors (Das et al., 2012; David et al., 2010). For instance, we have observed consistently decreased expression of the core SF3b complex component, PHF5A interactor, and splicing inhibitor target SF3B1 in multiple patient derived glioblastoma tumor isolates (unpublished data). Although the reasons for this deficiency are unknown, it is not unreasonable to hypothesize that a paucity of one key complex member may place an increased importance of the expression of other members (ie. PHF5A) to maintain functionality. Transformation could also leave total expression levels unchanged while indirectly modulating spliceosomal protein activity or accessibility. For example, hnRNP A1 is sequestered in the cytoplasm after osmotic shock via phosphorylation by MNK1/2 kinases (van der Houven van Oordt et al., 2000). These kinases are also part of the RTK/Ras/Raf signaling cascade –

known to be upregulated in our cells and in clinical GBM – and are necessary for Ras-dependent transformation (Wendel et al., 2007).

RNA splicing is known to be executed cotranscriptionally (de la Mata and Kornblihtt, 2006; Kornblihtt et al., 2004) and altered RNA polymerase transcriptional rate (de la Mata et al., 2003; de la Mata et al., 2010; de la Mata et al., 2011) has been shown to induce exon skipping similar to what we observe after PHF5A knockdown. Ras-mediated transformation causes global chromatin changes (He et al., 2008; Shaw and Cantley, 2006) which could theoretically alter polymerase transcription rates. Future experiments are needed to test whether transformed cells indeed transcribe DNA at a higher processive rate, and the subsequent hypothesis that constitutively increased transcription rates in transformed cells confer an asymetric dependence on splicing complex members such as PHF5A to maximize 3' splice site recognition efficiency.

In addition to transcriptional rate, cotranscriptional splicing is also directly affected by epigenetic modifications (Allo et al., 2010; Luco et al., 2010). For instance, MRG15, which recognizes histone 3 when tri-methylated on lysine 36 (H3K36me3), forms a complex the splicing repressor PTB, which recognizes target RNA sequences and inhibits their alternative splicing. The action of this chromatin-splicing adapter complex is to promote skipping of exons whose splice sites reside near H3K36me3 motifs (Luco et al., 2010). Other chromatin-splicing adapters such as Gcn5 or CHD1 serve to increase exon inclusion by recruiting the U2 snRNP to splice sites nearK4me3 or acetylated H3 chromatin marks, respectively (Gunderson and Johnson, 2009; Sims et al., 2007). Loss of such factors or the chromatin marks they recognize could cause exon skipping effects similar to the cancer specific splicing defects we observe upon PHF5A KD (Figure 4.6). PHF5A is known to bind chromatin and affect transcription (Oltra et al., 2003) but any role in specific chromatin mark recognition is currently unknown. However, chromatin mark

recognition is the canonical role of PHD finger domains (Mellor, 2006; Musselman and Kutateladze, 2011). This raises the mechanistic possibility that PHF5A may normally read chromatin marks through its PHD finger domain and enhance the recruitment and recognition of these sites by its binding partners within the U2 snRNP, promoting proper intron inclusion and constitutive splicing. Conversely, disruption of splicing through treatment with the splicing inhibitor Spliceostatin A, whose phenotypic effect is similar to PHF5A loss, caused widespread redistribution of H3K36me3 marks (Kim et al., 2011), suggesting a feedback loop where epigenetic modifications and splicing function mutually affect each other. This is also partially supported by our findings that SF3b splicing inhibition elicits a response in transformed cells that persists days or weeks after even transient exposure to the drug. (Figures 4.5, 4.6C, 4.10C) We know that cellular transformation, including transformation through the activation of Ras and its associated changes in polycomb group proteins, is known to cause global alterations to chromatin structure and cellular epigenetic profiles (He et al., 2008; Pylayeva-Gupta et al., 2011; Shaw and Cantley, 2006). This raises the hypothesis that chromatin changes resulting from transformation place an increased burden on certain chromatin-splicing adapters, possibly but not necessarily PHF5A, whose function is needed to maintain efficient splicing in the transformed epigenetic state.

Cancer cells are well characterized to have higher growth rates and higher levels of transcription and translation compared to normal cells (Blagden and Willis, 2011 and refrences therein). Myc-mediated transformation, for instance, functions as a general transcriptional amplifier increasing the number of transcripts of actively transcribed genes in each cell (Lin et al., 2012). This higher average transcriptional profile may place an increased burden upon the splicing machinery within a cancer cell resulting in conditions of “splicing stress” which would

reduce the cell's ability to cope with perturbations in spliceosome function. Under this hypothesis, normal cells would have a buffer of available splicing components ready to recognize a nascent RNA strand. In the transformed cells, an increased ratio of newly-synthesized RNA to available splicing proteins would place an increased reliance on the presence and efficiency of each splicing component compared to normal cells, creating unique point of vulnerability in the transformed cells. Our findings that inhibition of multiple components of the spliceosome either through knockdown or pharmacologic inhibition suggest that transformation-induced splicing stress may be a plausible hypothesis and viable target for cancer therapy.

Proper RNA splicing is important for all eukaryotic cells to generate mature gene products that can be translated into functional proteins, as well as generating a greater diversity of proteins and functions from single gene transcripts. Misregulation of RNA splicing, however, can contribute to a number of diseases including cancer. In addition to contributing to the oncogenic state of cells, we have demonstrated that RNA splicing is also a weakness in cancer cells arising from their transformed state. Although the complete mechanisms of this weakness will take many years to elucidate, it is clear that compared to normal cells, cancer cells including glioblastoma have a greatly decreased ability to maintain proper splicing fidelity after perturbations in spliceosome function. This results in the translation of potentially thousands of mis-spliced mRNAs into proteins with likely aberrant or non-existent functions, resulting in disastrous consequences for the cancer cell. Our work clearly demonstrates the utility of and need for modulators of RNA splicing in cancer therapeutics, and highlights the deadly and nearly incurable brain cancer glioblastoma as a disease likely to benefit from splicing therapeutics.

References

Al-Hajj, M., Wicha, M.S., Benito-Hernandez, A., Morrison, S.J., and Clarke, M.F. (2003). Prospective identification of tumorigenic breast cancer cells. Proceedings of the National Academy of Sciences of the United States of America *100*, 3983-3988.

Alcantara Llaguno, S., Chen, J., Kwon, C.H., Jackson, E.L., Li, Y., Burns, D.K., Alvarez-Buylla, A., and Parada, L.F. (2009). Malignant astrocytomas originate from neural stem/progenitor cells in a somatic tumor suppressor mouse model. Cancer cell *15*, 45-56.

Allo, M., Schor, I.E., Munoz, M.J., de la Mata, M., Agirre, E., Valcarcel, J., Eyras, E., and Kornblihtt, A.R. (2010). Chromatin and alternative splicing. Cold Spring Harbor symposia on quantitative biology *75*, 103-111.

American Cancer Society American Cancer Society: Cancer Facts and Figures 2010.

Anders, S. (2010). HTSeq: Analysing high-throughput sequencing data with Python.

Asbury, A., McKhann, McDonald, Goadsby, McArthur, ed.Diseases of the Nervous System: Clinical Neuroscience and Theraputic Principals, Third Edition edn (Cambridge University Press).

Bachoo, R.M., Maher, E.A., Ligon, K.L., Sharpless, N.E., Chan, S.S., You, M.J., Tang, Y., DeFrances, J., Stover, E., Weissleder, R.*, et al.* (2002). Epidermal growth factor receptor and Ink4a/Arf: convergent mechanisms governing terminal differentiation and transformation along the neural stem cell to astrocyte axis. Cancer cell *1*, 269-277.

Bao, S., Wu, Q., McLendon, R.E., Hao, Y., Shi, Q., Hjelmeland, A.B., Dewhirst, M.W., Bigner, D.D., and Rich, J.N. (2006a). Glioma stem cells promote radioresistance by preferential activation of the DNA damage response. Nature *444*, 756-760.

Bao, S., Wu, Q., Sathornsumetee, S., Hao, Y., Li, Z., Hjelmeland, A.B., Shi, Q., McLendon, R.E., Bigner, D.D., and Rich, J.N. (2006b). Stem cell-like glioma cells promote tumor angiogenesis through vascular endothelial growth factor. Cancer Res *66*, 7843-7848.

Barbie, D.A., Tamayo, P., Boehm, J.S., Kim, S.Y., Moody, S.E., Dunn, I.F., Schinzel, A.C., Sandy, P., Meylan, E., Scholl, C.*, et al.* (2009). Systematic RNA interference reveals that oncogenic KRAS-driven cancers require TBK1. Nature *462*, 108-112.

Behzadnia, N., Golas, M.M., Hartmuth, K., Sander, B., Kastner, B., Deckert, J., Dube, P., Will, C.L., Urlaub, H., Stark, H.*, et al.* (2007). Composition and three-dimensional EM structure of double affinity-purified, human prespliceosomal A complexes. The EMBO journal *26*, 1737-1748.

Bie, L., Zhao, G., Cheng, P., Rondeau, G., Porwollik, S., Ju, Y., Xia, X.Q., and McClelland, M. (2011). The accuracy of survival time prediction for patients with glioma is improved by measuring mitotic spindle checkpoint gene expression. PLoS One *6*, e25631.

Blagden, S.P., and Willis, A.E. (2011). The biological and therapeutic relevance of mRNA translation in cancer. Nature reviews Clinical oncology *8*, 280-291.

Bradley, R.K., Merkin, J., Lambert, N.J., and Burge, C.B. (2012). Alternative splicing of RNA triplets is often regulated and accelerates proteome evolution. PLoS biology *10*, e1001229.

Brough, R., Frankum, J.R., Sims, D., Mackay, A., Mendes-Pereira, A.M., Bajrami, I., Costa-Cabral, S., Rafiq, R., Ahmad, A.S., Cerone, M.A.*, et al.* (2011). Functional viability profiles of breast cancer. Cancer discovery *1*, 260-273.

Bryant, H.E., Schultz, N., Thomas, H.D., Parker, K.M., Flower, D., Lopez, E., Kyle, S., Meuth, M., Curtin, N.J., and Helleday, T. (2005). Specific killing of BRCA2-deficient tumours with inhibitors of poly(ADP-ribose) polymerase. Nature *434*, 913-917.

Burns, C.G., Ohi, R., Mehta, S., O'Toole, E.T., Winey, M., Clark, T.A., Sugnet, C.W., Ares, M., Jr., and Gould, K.L. (2002). Removal of a single alpha-tubulin gene intron suppresses cell cycle arrest phenotypes of splicing factor mutations in Saccharomyces cerevisiae. Molecular and cellular biology *22*, 801-815.

Cahill, D.P., Lengauer, C., Yu, J., Riggins, G.J., Willson, J.K., Markowitz, S.D., Kinzler, K.W., and Vogelstein, B. (1998). Mutations of mitotic checkpoint genes in human cancers. Nature *392*, 300-303.
Cancer Genome Atlas Research Network (2008). Comprehensive genomic characterization defines human glioblastoma genes and core pathways. Nature *455*, 1061-1068.
CBTRUS (2011). Central Brain Tumor Registry of the United States (www.cbtrus.org).
Champion-Arnaud, P., and Reed, R. (1994). The prespliceosome components SAP 49 and SAP 145 interact in a complex implicated in tethering U2 snRNP to the branch site. Genes & development *8*, 1974-1983.
Chen, M., and Manley, J.L. (2009). Mechanisms of alternative splicing regulation: insights from molecular and genomics approaches. Nature reviews Molecular cell biology *10*, 741-754.
Cheung, H.W., Cowley, G.S., Weir, B.A., Boehm, J.S., Rusin, S., Scott, J.A., East, A., Ali, L.D., Lizotte, P.H., Wong, T.C.*, et al.* (2011). Systematic investigation of genetic vulnerabilities across cancer cell lines reveals lineage-specific dependencies in ovarian cancer. Proceedings of the National Academy of Sciences of the United States of America *108*, 12372-12377.
ClinicalTrials.gov (2009). www.clinicaltrials.gov (U.S. National Institutes of Health).
Cloughesy, T.F., Yoshimoto, K., Nghiemphu, P., Brown, K., Dang, J., Zhu, S., Hsueh, T., Chen, Y., Wang, W., Youngkin, D.*, et al.* (2008). Antitumor activity of rapamycin in a Phase I trial for patients with recurrent PTEN-deficient glioblastoma. PLoS medicine *5*, e8.
Clower, C.V., Chatterjee, D., Wang, Z., Cantley, L.C., Vander Heiden, M.G., and Krainer, A.R. (2010). The alternative splicing repressors hnRNP A1/A2 and PTB influence pyruvate kinase isoform expression and cell metabolism. Proceedings of the National Academy of Sciences of the United States of America *107*, 1894-1899.
Corrionero, A., Minana, B., and Valcarcel, J. (2011). Reduced fidelity of branch point recognition and alternative splicing induced by the anti-tumor drug spliceostatin A. Genes & development *25*, 445-459.
Das, S., Anczukow, O., Akerman, M., and Krainer, A.R. (2012). Oncogenic Splicing Factor Srsf1 Is a Critical Transcriptional Target of Myc. Cell Rep *1*, 110-117.
Davenport, J., Harris, L.D., and Goorha, R. (2006). Spindle checkpoint function requires Mad2-dependent Cdc20 binding to the Mad3 homology domain of BubR1. Exp Cell Res *312*, 1831-1842.
David, C.J., Chen, M., Assanah, M., Canoll, P., and Manley, J.L. (2010). HnRNP proteins controlled by c-Myc deregulate pyruvate kinase mRNA splicing in cancer. Nature *463*, 364-368.
David, C.J., and Manley, J.L. (2010). Alternative pre-mRNA splicing regulation in cancer: pathways and programs unhinged. Genes & development *24*, 2343-2364.
de la Mata, M., Alonso, C.R., Kadener, S., Fededa, J.P., Blaustein, M., Pelisch, F., Cramer, P., Bentley, D., and Kornblihtt, A.R. (2003). A slow RNA polymerase II affects alternative splicing in vivo. Molecular cell *12*, 525-532.
de la Mata, M., and Kornblihtt, A.R. (2006). RNA polymerase II C-terminal domain mediates regulation of alternative splicing by SRp20. Nature structural & molecular biology *13*, 973-980.
de la Mata, M., Lafaille, C., and Kornblihtt, A.R. (2010). First come, first served revisited: factors affecting the same alternative splicing event have different effects on the relative rates of intron removal. Rna *16*, 904-912.
de la Mata, M., Munoz, M.J., Allo, M., Fededa, J.P., Schor, I.E., and Kornblihtt, A.R. (2011). RNA Polymerase II Elongation at the Crossroads of Transcription and Alternative Splicing. Genetics research international *2011*, 309865.
DeLuca, J.G., Gall, W.E., Ciferri, C., Cimini, D., Musacchio, A., and Salmon, E.D. (2006). Kinetochore microtubule dynamics and attachment stability are regulated by Hec1. Cell *127*, 969-982.
DeLuca, J.G., Moree, B., Hickey, J.M., Kilmartin, J.V., and Salmon, E.D. (2002). hNuf2 inhibition blocks stable kinetochore-microtubule attachment and induces mitotic cell death in HeLa cells. J Cell Biol *159*, 549-555.

DeLuca, K.F., Lens, S.M., and DeLuca, J.G. (2011). Temporal changes in Hec1 phosphorylation control kinetochore-microtubule attachment stability during mitosis. J Cell Sci *124*, 622-634.
Dietrich, J., Imitola, J., and Kesari, S. (2008). Mechanisms of Disease: the role of stem cells in the biology and treatment of gliomas. Nature clinical practice *5*, 393-404.
Ding, Y., Hubert, C.G., Herman, J., Corrin, P., Toledo, C.M., Skutt-Kakaria, K., Vazquez, J., Basom, R., Zhang, B., Risler, J.K.*, et al.* (2012). Cancer-specific requirement for BUB1B/BubR1 in human brain tumor isolates and genetically transformed cells. Cancer discovery.
Dirks, P.B. (2008). Brain tumor stem cells: bringing order to the chaos of brain cancer. J Clin Oncol *26*, 2916-2924.
Dziembowski, A., Ventura, A.P., Rutz, B., Caspary, F., Faux, C., Halgand, F., Laprevote, O., and Seraphin, B. (2004). Proteomic analysis identifies a new complex required for nuclear pre-mRNA retention and splicing. The EMBO journal *23*, 4847-4856.
Elowe, S., Dulla, K., Uldschmid, A., Li, X., Dou, Z., and Nigg, E.A. (2010). Uncoupling of the spindle-checkpoint and chromosome-congression functions of BubR1. J Cell Sci *123*, 84-94.
Erlich, Y., Chang, K., Gordon, A., Ronen, R., Navon, O., Rooks, M., and Hannon, G.J. (2009). DNA Sudoku--harnessing high-throughput sequencing for multiplexed specimen analysis. Genome research *19*, 1243-1253.
Fael Al-Mayhani, T.M., Ball, S.L., Zhao, J.W., Fawcett, J., Ichimura, K., Collins, P.V., and Watts, C. (2009). An efficient method for derivation and propagation of glioblastoma cell lines that conserves the molecular profile of their original tumours. Journal of neuroscience methods *176*, 192-199.
Fan, L., Lagisetti, C., Edwards, C.C., Webb, T.R., and Potter, P.M. (2011). Sudemycins, novel small molecule analogues of FR901464, induce alternative gene splicing. ACS chemical biology *6*, 582-589.
Fan, Q.W., Cheng, C.K., Nicolaides, T.P., Hackett, C.S., Knight, Z.A., Shokat, K.M., and Weiss, W.A. (2007). A dual phosphoinositide-3-kinase alpha/mTOR inhibitor cooperates with blockade of epidermal growth factor receptor in PTEN-mutant glioma. Cancer research *67*, 7960-7965.
Fan, Q.W., Knight, Z.A., Goldenberg, D.D., Yu, W., Mostov, K.E., Stokoe, D., Shokat, K.M., and Weiss, W.A. (2006). A dual PI3 kinase/mTOR inhibitor reveals emergent efficacy in glioma. Cancer cell *9*, 341-349.
Fan, Q.W., and Weiss, W.A. (2006). Isoform specific inhibitors of PI3 kinase in glioma. Cell cycle (Georgetown, Tex *5*, 2301-2305.
Fang, J., Acheampong, E., Dave, R., Wang, F., Mukhtar, M., and Pomerantz, R.J. (2005). The RNA helicase DDX1 is involved in restricted HIV-1 Rev function in human astrocytes. Virology *336*, 299-307.
Flicek, P., Amode, M.R., Barrell, D., Beal, K., Brent, S., Chen, Y., Clapham, P., Coates, G., Fairley, S., Fitzgerald, S.*, et al.* (2011). Ensembl 2011. Nucleic Acids Res *39*, D800-806.
Fomchenko, E.I., and Holland, E.C. (2006). Mouse models of brain tumors and their applications in preclinical trials. Clin Cancer Res *12*, 5288-5297.
Fujita, P.A., Rhead, B., Zweig, A.S., Hinrichs, A.S., Karolchik, D., Cline, M.S., Goldman, M., Barber, G.P., Clawson, H., Coelho, A.*, et al.* (2010). The UCSC Genome Browser database: update 2011. Nucleic Acids Res *39*, D876-D882.
Furic, L., Rong, L., Larsson, O., Koumakpayi, I.H., Yoshida, K., Brueschke, A., Petroulakis, E., Robichaud, N., Pollak, M., Gaboury, L.A.*, et al.* (2010). eIF4E phosphorylation promotes tumorigenesis and is associated with prostate cancer progression. Proceedings of the National Academy of Sciences of the United States of America *107*, 14134-14139.
Gage, F.H., Ray, J., and Fisher, L.J. (1995). Isolation, characterization, and use of stem cells from the CNS. Annual review of neuroscience *18*, 159-192.
Galli, R., Binda, E., Orfanelli, U., Cipelletti, B., Gritti, A., De Vitis, S., Fiocco, R., Foroni, C., Dimeco, F., and Vescovi, A. (2004). Isolation and characterization of tumorigenic, stem-like neural precursors from human glioblastoma. Cancer research *64*, 7011-7021.

Ganem, N.J., Storchova, Z., and Pellman, D. (2007). Tetraploidy, aneuploidy and cancer. Current opinion in genetics & development *17*, 157-162.
Gangemi, R.M., Griffero, F., Marubbi, D., Perera, M., Capra, M.C., Malatesta, P., Ravetti, G.L., Zona, G.L., Daga, A., and Corte, G. (2009). SOX2 silencing in glioblastoma tumor-initiating cells causes stop of proliferation and loss of tumorigenicity. Stem cells (Dayton, Ohio) *27*, 40-48.
Goidts, V., Bageritz, J., Puccio, L., Nakata, S., Zapatka, M., Barbus, S., Toedt, G., Campos, B., Korshunov, A., Momma, S*., et al.* (2012). RNAi screening in glioma stem-like cells identifies PFKFB4 as a key molecule important for cancer cell survival. Oncogene *31*, 3235-3243.
Gooding, C., Clark, F., Wollerton, M.C., Grellscheid, S.N., Groom, H., and Smith, C.W. (2006). A class of human exons with predicted distant branch points revealed by analysis of AG dinucleotide exclusion zones. Genome biology *7*, R1.
Groszer, M., Erickson, R., Scripture-Adams, D.D., Lesche, R., Trumpp, A., Zack, J.A., Kornblum, H.I., Liu, X., and Wu, H. (2001). Negative regulation of neural stem/progenitor cell proliferation by the Pten tumor suppressor gene in vivo. Science (New York, NY *294*, 2186-2189.
Gunderson, F.Q., and Johnson, T.L. (2009). Acetylation by the transcriptional coactivator Gcn5 plays a novel role in co-transcriptional spliceosome assembly. PLoS genetics *5*, e1000682.
Halazonetis, T.D., Gorgoulis, V.G., and Bartek, J. (2008). An oncogene-induced DNA damage model for cancer development. Science (New York, NY *319*, 1352-1355.
Harris, L., Davenport, J., Neale, G., and Goorha, R. (2005). The mitotic checkpoint gene BubR1 has two distinct functions in mitosis. Exp Cell Res *308*, 85-100.
Hartwell, L.H., Szankasi, P., Roberts, C.J., Murray, A.W., and Friend, S.H. (1997). Integrating genetic approaches into the discovery of anticancer drugs. Science *278*, 1064-1068.
He, S., Dunn, K.L., Espino, P.S., Drobic, B., Li, L., Yu, J., Sun, J.M., Chen, H.Y., Pritchard, S., and Davie, J.R. (2008). Chromatin organization and nuclear microenvironments in cancer cells. Journal of cellular biochemistry *104*, 2004-2015.
Hemmati, H.D., Nakano, I., Lazareff, J.A., Masterman-Smith, M., Geschwind, D.H., Bronner-Fraser, M., and Kornblum, H.I. (2003). Cancerous stem cells can arise from pediatric brain tumors. Proc Natl Acad Sci U S A *100*, 15178-15183.
Heyd, F., and Lynch, K.W. (2011). Degrade, move, regroup: signaling control of splicing proteins. Trends in biochemical sciences *36*, 397-404.
Holland, E.C. (2001). Gliomagenesis: genetic alterations and mouse models. Nat Rev Genet *2*, 120-129.
Huntly, B.J., and Gilliland, D.G. (2005). Leukaemia stem cells and the evolution of cancer-stem-cell research. Nature reviews *5*, 311-321.
Jurica, M.S., and Moore, M.J. (2003). Pre-mRNA splicing: awash in a sea of proteins. Molecular cell *12*, 5-14.
Kaelin, W.G., Jr. (2005). The concept of synthetic lethality in the context of anticancer therapy. Nature reviews *5*, 689-698.
Kaida, D., Motoyoshi, H., Tashiro, E., Nojima, T., Hagiwara, M., Ishigami, K., Watanabe, H., Kitahara, T., Yoshida, T., Nakajima, H*., et al.* (2007). Spliceostatin A targets SF3b and inhibits both splicing and nuclear retention of pre-mRNA. Nature chemical biology *3*, 576-583.
Karaman, M.W., Herrgard, S., Treiber, D.K., Gallant, P., Atteridge, C.E., Campbell, B.T., Chan, K.W., Ciceri, P., Davis, M.I., Edeen, P.T*., et al.* (2008). A quantitative analysis of kinase inhibitor selectivity. Nature biotechnology *26*, 127-132.
Katz, Y., Wang, E.T., Airoldi, E.M., and Burge, C.B. (2010). Analysis and design of RNA sequencing experiments for identifying isoform regulation. Nat Methods *7*, 1009-1015.
Kelly, P.N., Dakic, A., Adams, J.M., Nutt, S.L., and Strasser, A. (2007). Tumor growth need not be driven by rare cancer stem cells. Science (New York, NY *317*, 337.

Kim, S., Kim, H., Fong, N., Erickson, B., and Bentley, D.L. (2011). Pre-mRNA splicing is a determinant of histone H3K36 methylation. Proceedings of the National Academy of Sciences of the United States of America *108*, 13564-13569.
Klinghoffer, R.A., Roberts, B., Annis, J., Frazier, J., Lewis, P., Linsley, P.S., and Cleary, M.A. (2008). An optimized lentivirus-mediated RNAi screen reveals kinase modulators of kinesin-5 inhibitor sensitivity. Assay and drug development technologies *6*, 105-119.
Komarova, N.L., Lengauer, C., Vogelstein, B., and Nowak, M.A. (2002). Dynamics of genetic instability in sporadic and familial colorectal cancer. Cancer biology & therapy *1*, 685-692.
Kornblihtt, A.R., de la Mata, M., Fededa, J.P., Munoz, M.J., and Nogues, G. (2004). Multiple links between transcription and splicing. Rna *10*, 1489-1498.
Kotake, Y., Sagane, K., Owa, T., Mimori-Kiyosue, Y., Shimizu, H., Uesugi, M., Ishihama, Y., Iwata, M., and Mizui, Y. (2007). Splicing factor SF3b as a target of the antitumor natural product pladienolide. Nature chemical biology *3*, 570-575.
Kramer, A. (1996). The structure and function of proteins involved in mammalian pre-mRNA splicing. Annual review of biochemistry *65*, 367-409.
Kramer, A., Gruter, P., Groning, K., and Kastner, B. (1999). Combined biochemical and electron microscopic analyses reveal the architecture of the mammalian U2 snRNP. The Journal of cell biology *145*, 1355-1368.
Kwon, C.H., Zhao, D., Chen, J., Alcantara, S., Li, Y., Burns, D.K., Mason, R.P., Lee, E.Y., Wu, H., and Parada, L.F. (2008). Pten haploinsufficiency accelerates formation of high-grade astrocytomas. Cancer research *68*, 3286-3294.
Lagisetti, C., Pourpak, A., Goronga, T., Jiang, Q., Cui, X., Hyle, J., Lahti, J.M., Morris, S.W., and Webb, T.R. (2009). Synthetic mRNA splicing modulator compounds with in vivo antitumor activity. Journal of medicinal chemistry *52*, 6979-6990.
Lagisetti, C., Pourpak, A., Jiang, Q., Cui, X., Goronga, T., Morris, S.W., and Webb, T.R. (2008). Antitumor compounds based on a natural product consensus pharmacophore. Journal of medicinal chemistry *51*, 6220-6224.
Lampson, M.A., and Kapoor, T.M. (2005). The human mitotic checkpoint protein BubR1 regulates chromosome-spindle attachments. Nature cell biology *7*, 93-98.
Langmead, B., Trapnell, C., Pop, M., and Salzberg, S.L. (2009). Ultrafast and memory-efficient alignment of short DNA sequences to the human genome. Genome Biol *10*, R25.
Lapidot, T., Sirard, C., Vormoor, J., Murdoch, B., Hoang, T., Caceres-Cortes, J., Minden, M., Paterson, B., Caligiuri, M.A., and Dick, J.E. (1994). A cell initiating human acute myeloid leukaemia after transplantation into SCID mice. Nature *367*, 645-648.
Lee, J., Kotliarova, S., Kotliarov, Y., Li, A., Su, Q., Donin, N.M., Pastorino, S., Purow, B.W., Christopher, N., Zhang, W*., et al.* (2006). Tumor stem cells derived from glioblastomas cultured in bFGF and EGF more closely mirror the phenotype and genotype of primary tumors than do serum-cultured cell lines. Cancer cell *9*, 391-403.
Lens, S.M., Voest, E.E., and Medema, R.H. (2010). Shared and separate functions of polo-like kinases and aurora kinases in cancer. Nat Rev Cancer *10*, 825-841.
Li, A., Walling, J., Kotliarov, Y., Center, A., Steed, M.E., Ahn, S.J., Rosenblum, M., Mikkelsen, T., Zenklusen, J.C., and Fine, H.A. (2008). Genomic changes and gene expression profiles reveal that established glioma cell lines are poorly representative of primary human gliomas. Mol Cancer Res *6*, 21-30.
Li, B., and Dewey, C.N. (2011). RSEM: accurate transcript quantification from RNA-Seq data with or without a reference genome. BMC bioinformatics *12*, 323.
Li, C., Heidt, D.G., Dalerba, P., Burant, C.F., Zhang, L., Adsay, V., Wicha, M., Clarke, M.F., and Simeone, D.M. (2007). Identification of pancreatic cancer stem cells. Cancer research *67*, 1030-1037.

Li, X., and Manley, J.L. (2005). Inactivation of the SR protein splicing factor ASF/SF2 results in genomic instability. Cell *122*, 365-378.
Li, X., Wang, J., and Manley, J.L. (2005). Loss of splicing factor ASF/SF2 induces G2 cell cycle arrest and apoptosis, but inhibits internucleosomal DNA fragmentation. Genes & development *19*, 2705-2714.
Liao, H., Li, G., and Yen, T.J. (1994). Mitotic regulation of microtubule cross-linking activity of CENP-E kinetochore protein. Science *265*, 394-398.
Lin, C.Y., Loven, J., Rahl, P.B., Paranal, R.M., Burge, C.B., Bradner, J.E., Lee, T.I., and Young, R.A. (2012). Transcriptional Amplification in Tumor Cells with Elevated c-Myc. Cell *151*, 56-67.
Liu, Q., Nguyen, D.H., Dong, Q., Shitaku, P., Chung, K., Liu, O.Y., Tso, J.L., Liu, J.Y., Konkankit, V., Cloughesy, T.F*., et al.* (2009). Molecular properties of CD133+ glioblastoma stem cells derived from treatment-refractory recurrent brain tumors. J Neurooncol *94*, 1-19.
Llaguno, S.A., Chen, J., Kwon, C.H., and Parada, L.F. (2008). Neural and cancer stem cells in tumor suppressor mouse models of malignant astrocytoma. Cold Spring Harbor symposia on quantitative biology *73*, 421-426.
Luco, R.F., Pan, Q., Tominaga, K., Blencowe, B.J., Pereira-Smith, O.M., and Misteli, T. (2010). Regulation of alternative splicing by histone modifications. Science (New York, NY *327*, 996-1000.
Luo, J., Emanuele, M.J., Li, D., Creighton, C.J., Schlabach, M.R., Westbrook, T.F., Wong, K.K., and Elledge, S.J. (2009a). A genome-wide RNAi screen identifies multiple synthetic lethal interactions with the Ras oncogene. Cell *137*, 835-848.
Luo, J., Solimini, N.L., and Elledge, S.J. (2009b). Principles of cancer therapy: oncogene and non-oncogene addiction. Cell *136*, 823-837.
Madigan, D., and York, J. (1995). Bayesian Graphical Models for Discrete Data. International Statistical Review *63*, 215-232.
Malureanu, L.A., Jeganathan, K.B., Hamada, M., Wasilewski, L., Davenport, J., and van Deursen, J.M. (2009). BubR1 N terminus acts as a soluble inhibitor of cyclin B degradation by APC/C(Cdc20) in interphase. Developmental cell *16*, 118-131.
Mangiola, A., Lama, G., Giannitelli, C., De Bonis, P., Anile, C., Lauriola, L., La Torre, G., Sabatino, G., Maira, G., Jhanwar-Uniyal, M*., et al.* (2007). Stem cell marker nestin and c-Jun NH2-terminal kinases in tumor and peritumor areas of glioblastoma multiforme: possible prognostic implications. Clin Cancer Res *13*, 6970-6977.
Mao, Y., Desai, A., and Cleveland, D.W. (2005). Microtubule capture by CENP-E silences BubR1-dependent mitotic checkpoint signaling. J Cell Biol *170*, 873-880.
Marcotte, R., Brown, K.R., Suarez, F., Sayad, A., Karamboulas, K., Krzyzanowski, P.M., Sircoulomb, F., Medrano, M., Fedyshyn, Y., Koh, J.L*., et al.* (2012). Essential gene profiles in breast, pancreatic, and ovarian cancer cells. Cancer discovery *2*, 172-189.
Maresca, T.J., Groen, A.C., Gatlin, J.C., Ohi, R., Mitchison, T.J., and Salmon, E.D. (2009). Spindle assembly in the absence of a RanGTP gradient requires localized CPC activity. Curr Biol *19*, 1210-1215.
Marumoto, T., Tashiro, A., Friedmann-Morvinski, D., Scadeng, M., Soda, Y., Gage, F.H., and Verma, I.M. (2009). Development of a novel mouse glioma model using lentiviral vectors. Nature medicine *15*, 110-116.
Mason, D.X., Keppler, D., Zhang, J., Jackson, T.J., Seger, Y.R., Matsui, S., Abreo, F., Cowell, J.K., Hannon, G.J., Lowe, S.W*., et al.* (2006). Defined genetic events associated with the spontaneous in vitro transformation of ElA/Ras-expressing human IMR90 fibroblasts. Carcinogenesis *27*, 350-359.
Mellor, J. (2006). It takes a PHD to read the histone code. Cell *126*, 22-24.
Mizui, Y., Sakai, T., Iwata, M., Uenaka, T., Okamoto, K., Shimizu, H., Yamori, T., Yoshimatsu, K., and Asada, M. (2004). Pladienolides, new substances from culture of Streptomyces platensis Mer-11107. III. In vitro and in vivo antitumor activities. The Journal of antibiotics *57*, 188-196.

Moore, M.J., Wang, Q., Kennedy, C.J., and Silver, P.A. (2010). An alternative splicing network links cell-cycle control to apoptosis. Cell *142*, 625-636.
Musacchio, A., and Salmon, E.D. (2007). The spindle-assembly checkpoint in space and time. Nat Rev Mol Cell Biol *8*, 379-393.
Musselman, C.A., and Kutateladze, T.G. (2009). PHD fingers: epigenetic effectors and potential drug targets. Molecular interventions *9*, 314-323.
Musselman, C.A., and Kutateladze, T.G. (2011). Handpicking epigenetic marks with PHD fingers. Nucleic acids research *39*, 9061-9071.
Nakajima, H., Hori, Y., Terano, H., Okuhara, M., Manda, T., Matsumoto, S., and Shimomura, K. (1996). New antitumor substances, FR901463, FR901464 and FR901465. II. Activities against experimental tumors in mice and mechanism of action. The Journal of antibiotics *49*, 1204-1211.
Neshat, M.S., Mellinghoff, I.K., Tran, C., Stiles, B., Thomas, G., Petersen, R., Frost, P., Gibbons, J.J., Wu, H., and Sawyers, C.L. (2001). Enhanced sensitivity of PTEN-deficient tumors to inhibition of FRAP/mTOR. Proceedings of the National Academy of Sciences of the United States of America *98*, 10314-10319.
Nichols, W.W., Murphy, D.G., Cristofalo, V.J., Toji, L.H., Greene, A.E., and Dwight, S.A. (1977). Characterization of a new human diploid cell strain, IMR-90. Science (New York, NY *196*, 60-63.
Oltra, E., Pfeifer, I., and Werner, R. (2003). Ini, a small nuclear protein that enhances the response of the connexin43 gene to estrogen. Endocrinology *144*, 3148-3158.
Oltra, E., Verde, F., Werner, R., and D'Urso, G. (2004). A novel RING-finger-like protein Ini1 is essential for cell cycle progression in fission yeast. Journal of cell science *117*, 967-974.
Paddison, P.J., Silva, J.M., Conklin, D.S., Schlabach, M., Li, M., Aruleba, S., Balija, V., O'Shaughnessy, A., Gnoj, L., Scobie, K.*, et al.* (2004). A resource for large-scale RNA-interference-based screens in mammals. Nature *428*, 427-431.
Park, D.M., and Rich, J.N. (2009). Biology of glioma cancer stem cells. Mol Cells *28*, 7-12.
Parsons, D.W., Jones, S., Zhang, X., Lin, J.C., Leary, R.J., Angenendt, P., Mankoo, P., Carter, H., Siu, I.M., Gallia, G.L.*, et al.* (2008). An integrated genomic analysis of human glioblastoma multiforme. Science (New York, NY *321*, 1807-1812.
Paulsen, R.D., Soni, D.V., Wollman, R., Hahn, A.T., Yee, M.C., Guan, A., Hesley, J.A., Miller, S.C., Cromwell, E.F., Solow-Cordero, D.E.*, et al.* (2009). A genome-wide siRNA screen reveals diverse cellular processes and pathways that mediate genome stability. Molecular cell *35*, 228-239.
Peterson, T.R., Laplante, M., Thoreen, C.C., Sancak, Y., Kang, S.A., Kuehl, W.M., Gray, N.S., and Sabatini, D.M. (2009). DEPTOR is an mTOR inhibitor frequently overexpressed in multiple myeloma cells and required for their survival. Cell *137*, 873-886.
Phillips, H.S., Kharbanda, S., Chen, R., Forrest, W.F., Soriano, R.H., Wu, T.D., Misra, A., Nigro, J.M., Colman, H., Soroceanu, L.*, et al.* (2006). Molecular subclasses of high-grade glioma predict prognosis, delineate a pattern of disease progression, and resemble stages in neurogenesis. Cancer Cell *9*, 157-173.
Picard, D. Picard Lab Website, Department of Cell Biology

University of Geneva.
Piccirillo, S.G., Reynolds, B.A., Zanetti, N., Lamorte, G., Binda, E., Broggi, G., Brem, H., Olivi, A., Dimeco, F., and Vescovi, A.L. (2006). Bone morphogenetic proteins inhibit the tumorigenic potential of human brain tumour-initiating cells. Nature *444*, 761-765.
Pollard, S.M., Yoshikawa, K., Clarke, I.D., Danovi, D., Stricker, S., Russell, R., Bayani, J., Head, R., Lee, M., Bernstein, M.*, et al.* (2009). Glioma stem cell lines expanded in adherent culture have tumor-specific phenotypes and are suitable for chemical and genetic screens. Cell stem cell *4*, 568-580.
Pylayeva-Gupta, Y., Grabocka, E., and Bar-Sagi, D. (2011). RAS oncogenes: weaving a tumorigenic web. Nature reviews *11*, 761-774.

Quintana, E., Shackleton, M., Sabel, M.S., Fullen, D.R., Johnson, T.M., and Morrison, S.J. (2008). Efficient tumour formation by single human melanoma cells. Nature *456*, 593-598.
R Development Core Team (2011). R: A language and environment for statistical computing (Vienna: R Foundation for Statistical Computing).
Raynaud, F.I., Eccles, S., Clarke, P.A., Hayes, A., Nutley, B., Alix, S., Henley, A., Di-Stefano, F., Ahmad, Z., Guillard, S*., et al.* (2007). Pharmacologic characterization of a potent inhibitor of class I phosphatidylinositide 3-kinases. Cancer research *67*, 5840-5850.
Robinson, J.T., Thorvaldsdottir, H., Winckler, W., Guttman, M., Lander, E.S., Getz, G., and Mesirov, J.P. (2011). Integrative genomics viewer. Nature biotechnology *29*, 24-26.
Robinson, M.D., McCarthy, D.J., and Smyth, G.K. (2010). edgeR: a Bioconductor package for differential expression analysis of digital gene expression data. Bioinformatics *26*, 139-140.
Robinson, M.D., and Oshlack, A. (2010). A scaling normalization method for differential expression analysis of RNA-seq data. Genome biology *11*, R25.
Robinson, M.D., and Smyth, G.K. (2007). Moderated statistical tests for assessing differences in tag abundance. Bioinformatics *23*, 2881-2887.
Robinson, M.D., and Smyth, G.K. (2008). Small-sample estimation of negative binomial dispersion, with applications to SAGE data. Biostatistics *9*, 321-332.
Rzymski, T., Grzmil, P., Meinhardt, A., Wolf, S., and Burfeind, P. (2008). PHF5A represents a bridge protein between splicing proteins and ATP-dependent helicases and is differentially expressed during mouse spermatogenesis. Cytogenetic and genome research *121*, 232-244.
Sabatini, D.M. (2006). mTOR and cancer: insights into a complex relationship. Nature reviews *6*, 729-734.
Sanai, N., Alvarez-Buylla, A., and Berger, M.S. (2005). Neural stem cells and the origin of gliomas. The New England journal of medicine *353*, 811-822.
Santaguida, S., and Musacchio, A. (2009). The life and miracles of kinetochores. Embo J *28*, 2511-2531.
Sawin, K.E., LeGuellec, K., Philippe, M., and Mitchison, T.J. (1992). Mitotic spindle organization by a plus-end-directed microtubule motor. Nature *359*, 540-543.
Schadt, E.E., Lamb, J., Yang, X., Zhu, J., Edwards, S., Guhathakurta, D., Sieberts, S.K., Monks, S., Reitman, M., Zhang, C*., et al.* (2005). An integrative genomics approach to infer causal associations between gene expression and disease. Nat Genet *37*, 710-717.
Schadt, E.E., Molony, C., Chudin, E., Hao, K., Yang, X., Lum, P.Y., Kasarskis, A., Zhang, B., Wang, S., Suver, C*., et al.* (2008). Mapping the genetic architecture of gene expression in human liver. PLoS Biol *6*, e107.
Scholl, C., Frohling, S., Dunn, I.F., Schinzel, A.C., Barbie, D.A., Kim, S.Y., Silver, S.J., Tamayo, P., Wadlow, R.C., Ramaswamy, S*., et al.* (2009). Synthetic lethal interaction between oncogenic KRAS dependency and STK33 suppression in human cancer cells. Cell *137*, 821-834.
Schwarz, G. (1978). Estimating the dimension of a model. Ann Statist *6*, 461-464.
Shaw, R.J., and Cantley, L.C. (2006). Ras, PI(3)K and mTOR signalling controls tumour cell growth. Nature *441*, 424-430.
Shultz, J.C., Goehe, R.W., Wijesinghe, D.S., Murudkar, C., Hawkins, A.J., Shay, J.W., Minna, J.D., and Chalfant, C.E. (2010). Alternative splicing of caspase 9 is modulated by the phosphoinositide 3-kinase/Akt pathway via phosphorylation of SRp30a. Cancer research *70*, 9185-9196.
Silva, J.M., Li, M.Z., Chang, K., Ge, W., Golding, M.C., Rickles, R.J., Siolas, D., Hu, G., Paddison, P.J., Schlabach, M.R*., et al.* (2005). Second-generation shRNA libraries covering the mouse and human genomes. Nature genetics *37*, 1281-1288.
Silva, J.M., Marran, K., Parker, J.S., Silva, J., Golding, M., Schlabach, M.R., Elledge, S.J., Hannon, G.J., and Chang, K. (2008). Profiling essential genes in human mammary cells by multiplex RNAi screening. Science (New York, NY *319*, 617-620.

Sims, R.J., 3rd, Millhouse, S., Chen, C.F., Lewis, B.A., Erdjument-Bromage, H., Tempst, P., Manley, J.L., and Reinberg, D. (2007). Recognition of trimethylated histone H3 lysine 4 facilitates the recruitment of transcription postinitiation factors and pre-mRNA splicing. Molecular cell *28*, 665-676.
Singh, S.K., Clarke, I.D., Terasaki, M., Bonn, V.E., Hawkins, C., Squire, J., and Dirks, P.B. (2003). Identification of a cancer stem cell in human brain tumors. Cancer Res *63*, 5821-5828.
Singh, S.K., Hawkins, C., Clarke, I.D., Squire, J.A., Bayani, J., Hide, T., Henkelman, R.M., Cusimano, M.D., and Dirks, P.B. (2004). Identification of human brain tumour initiating cells. Nature *432*, 396-401.
Smyth, G.K., Michaud, J., and Scott, H.S. (2005). Use of within-array replicate spots for assessing differential expression in microarray experiments. Bioinformatics *21*, 2067-2075.
Solimini, N.L., Luo, J., and Elledge, S.J. (2007). Non-oncogene addiction and the stress phenotype of cancer cells. Cell *130*, 986-988.
Son, M.J., Woolard, K., Nam, D.H., Lee, J., and Fine, H.A. (2009). SSEA-1 is an enrichment marker for tumor-initiating cells in human glioblastoma. Cell stem cell *4*, 440-452.
Sonoda, Y., Ozawa, T., Hirose, Y., Aldape, K.D., McMahon, M., Berger, M.S., and Pieper, R.O. (2001). Formation of intracranial tumors by genetically modified human astrocytes defines four pathways critical in the development of human anaplastic astrocytoma. Cancer Res *61*, 4956-4960.
Stiles, C.D., and Rowitch, D.H. (2008). Glioma stem cells: a midterm exam. Neuron *58*, 832-846.
Stupp, R., Mason, W.P., van den Bent, M.J., Weller, M., Fisher, B., Taphoorn, M.J., Belanger, K., Brandes, A.A., Marosi, C., Bogdahn, U*., et al.* (2005). Radiotherapy plus concomitant and adjuvant temozolomide for glioblastoma. N Engl J Med *352*, 987-996.
Sudakin, V., and Yen, T.J. (2007). Targeting mitosis for anti-cancer therapy. BioDrugs *21*, 225-233.
Sun, Y., Pollard, S., Conti, L., Toselli, M., Biella, G., Parkin, G., Willatt, L., Falk, A., Cattaneo, E., and Smith, A. (2008). Long-term tripotent differentiation capacity of human neural stem (NS) cells in adherent culture. Molecular and cellular neurosciences *38*, 245-258.
Takahashi, K., Tanabe, K., Ohnuki, M., Narita, M., Ichisaka, T., Tomoda, K., and Yamanaka, S. (2007). Induction of pluripotent stem cells from adult human fibroblasts by defined factors. Cell *131*, 861-872.
Tang, Z., Bharadwaj, R., Li, B., and Yu, H. (2001). Mad2-Independent inhibition of APCCdc20 by the mitotic checkpoint protein BubR1. Dev Cell *1*, 227-237.
TCGA (2008). Comprehensive genomic characterization defines human glioblastoma genes and core pathways. Nature *455*, 1061-1068.
Tran, L.M., Zhang, B., Zhang, Z., Zhang, C., Xie, T., Lamb, J.R., Dai, H., Schadt, E.E., and Zhu, J. (2011). Inferring causal genomic alterations in breast cancer using gene expression data. BMC Syst Biol *5*, 121.
Trapnell, C., Pachter, L., and Salzberg, S.L. (2009). TopHat: discovering splice junctions with RNA-Seq. Bioinformatics *25*, 1105-1111.
Trapnell, C., Roberts, A., Goff, L., Pertea, G., Kim, D., Kelley, D.R., Pimentel, H., Salzberg, S.L., Rinn, J.L., and Pachter, L. (2012). Differential gene and transcript expression analysis of RNA-seq experiments with TopHat and Cufflinks. Nat Protoc *7*, 562-578.
Trappe, R., Ahmed, M., Glaser, B., Vogel, C., Tascou, S., Burfeind, P., and Engel, W. (2002). Identification and characterization of a novel murine multigene family containing a PHD-finger-like motif. Biochemical and biophysical research communications *293*, 816-826.
Uchida, K.S., Takagaki, K., Kumada, K., Hirayama, Y., Noda, T., and Hirota, T. (2009). Kinetochore stretching inactivates the spindle assembly checkpoint. J Cell Biol *184*, 383-390.
van der Houven van Oordt, W., Diaz-Meco, M.T., Lozano, J., Krainer, A.R., Moscat, J., and Caceres, J.F. (2000). The MKK(3/6)-p38-signaling cascade alters the subcellular distribution of hnRNP A1 and modulates alternative splicing regulation. The Journal of cell biology *149*, 307-316.
van Roon, A.M., Loening, N.M., Obayashi, E., Yang, J.C., Newman, A.J., Hernandez, H., Nagai, K., and Neuhaus, D. (2008). Solution structure of the U2 snRNP protein Rds3p reveals a knotted zinc-finger motif. Proceedings of the National Academy of Sciences of the United States of America *105*, 9621-9626.

Veiseh, M., Gabikian, P., Bahrami, S.B., Veiseh, O., Zhang, M., Hackman, R.C., Ravanpay, A.C., Stroud, M.R., Kusuma, Y., Hansen, S.J.*, et al.* (2007). Tumor paint: a chlorotoxin:Cy5.5 bioconjugate for intraoperative visualization of cancer foci. Cancer research *67*, 6882-6888.
Verhaak, R.G., Hoadley, K.A., Purdom, E., Wang, V., Qi, Y., Wilkerson, M.D., Miller, C.R., Ding, L., Golub, T., Mesirov, J.P.*, et al.* (2010). Integrated genomic analysis identifies clinically relevant subtypes of glioblastoma characterized by abnormalities in PDGFRA, IDH1, EGFR, and NF1. Cancer Cell *17*, 98-110.
Vescovi, A.L., Galli, R., and Reynolds, B.A. (2006). Brain tumour stem cells. Nature reviews *6*, 425-436.
von Mering, C., Huynen, M., Jaeggi, D., Schmidt, S., Bork, P., and Snel, B. (2003). STRING: a database of predicted functional associations between proteins. Nucleic acids research *31*, 258-261.
Wang, E.T., Sandberg, R., Luo, S., Khrebtukova, I., Zhang, L., Mayr, C., Kingsmore, S.F., Schroth, G.P., and Burge, C.B. (2008). Alternative isoform regulation in human tissue transcriptomes. Nature *456*, 470-476.
Wang, J.C., and Dick, J.E. (2005). Cancer stem cells: lessons from leukemia. Trends in cell biology *15*, 494-501.
Wang, Q., He, J., Lynn, B., and Rymond, B.C. (2005). Interactions of the yeast SF3b splicing factor. Molecular and cellular biology *25*, 10745-10754.
Wang, Q., Liu, T., Fang, Y., Xie, S., Huang, X., Mahmood, R., Ramaswamy, G., Sakamoto, K.M., Darzynkiewicz, Z., Xu, M.*, et al.* (2004). BUBR1 deficiency results in abnormal megakaryopoiesis. Blood *103*, 1278-1285.
Wang, Q., and Rymond, B.C. (2003). Rds3p is required for stable U2 snRNP recruitment to the splicing apparatus. Molecular and cellular biology *23*, 7339-7349.
Wang, X., Babu, J.R., Harden, J.M., Jablonski, S.A., Gazi, M.H., Lingle, W.L., de Groen, P.C., Yen, T.J., and van Deursen, J.M. (2001). The mitotic checkpoint protein hBUB3 and the mRNA export factor hRAE1 interact with GLE2p-binding sequence (GLEBS)-containing proteins. J Biol Chem *276*, 26559-26567.
Weg-Remers, S., Ponta, H., Herrlich, P., and Konig, H. (2001). Regulation of alternative pre-mRNA splicing by the ERK MAP-kinase pathway. The EMBO journal *20*, 4194-4203.
Wendel, H.G., Silva, R.L., Malina, A., Mills, J.R., Zhu, H., Ueda, T., Watanabe-Fukunaga, R., Fukunaga, R., Teruya-Feldstein, J., Pelletier, J.*, et al.* (2007). Dissecting eIF4E action in tumorigenesis. Genes & development *21*, 3232-3237.
Whitesell, L., and Lindquist, S.L. (2005). HSP90 and the chaperoning of cancer. Nature reviews *5*, 761-772.
Will, C.L., Urlaub, H., Achsel, T., Gentzel, M., Wilm, M., and Luhrmann, R. (2002). Characterization of novel SF3b and 17S U2 snRNP proteins, including a human Prp5p homologue and an SF3b DEAD-box protein. The EMBO journal *21*, 4978-4988.
Wood, K.W., Lad, L., Luo, L., Qian, X., Knight, S.D., Nevins, N., Brejc, K., Sutton, D., Gilmartin, A.G., Chua, P.R.*, et al.* (2010). Antitumor activity of an allosteric inhibitor of centromere-associated protein-E. Proc Natl Acad Sci U S A *107*, 5839-5844.
Yang, X., Boehm, J.S., Yang, X., Salehi-Ashtiani, K., Hao, T., Shen, Y., Lubonja, R., Thomas, S.R., Alkan, O., Bhimdi, T.*, et al.* (2011a). A public genome-scale lentiviral expression library of human ORFs. Nature methods *8*, 659-661.
Yang, X., Deignan, J.L., Qi, H., Zhu, J., Qian, S., Zhong, J., Torosyan, G., Majid, S., Falkard, B., Kleinhanz, R.R.*, et al.* (2009). Validation of candidate causal genes for obesity that affect shared metabolic pathways and networks. Nat Genet *41*, 415-423.
Yang, X., Tu, Z., and Zhu, J. (2011b). Systems Biology Approaches to Studying Diet x Genome Interactions. In Nutritional Genomics (CRC Press), pp. 63-76.
Yu, J., Vodyanik, M.A., Smuga-Otto, K., Antosiewicz-Bourget, J., Frane, J.L., Tian, S., Nie, J., Jonsdottir, G.A., Ruotti, V., Stewart, R.*, et al.* (2007). Induced pluripotent stem cell lines derived from human somatic cells. Science (New York, NY *318*, 1917-1920.

Yuan, B., Xu, Y., Woo, J.H., Wang, Y., Bae, Y.K., Yoon, D.S., Wersto, R.P., Tully, E., Wilsbach, K., and Gabrielson, E. (2006). Increased expression of mitotic checkpoint genes in breast cancer cells with chromosomal instability. Clin Cancer Res *12*, 405-410.
Zecevic, M., Catling, A.D., Eblen, S.T., Renzi, L., Hittle, J.C., Yen, T.J., Gorbsky, G.J., and Weber, M.J. (1998). Active MAP kinase in mitosis: localization at kinetochores and association with the motor protein CENP-E. J Cell Biol *142*, 1547-1558.
Zheng, H., Ying, H., Yan, H., Kimmelman, A.C., Hiller, D.J., Chen, A.J., Perry, S.R., Tonon, G., Chu, G.C., Ding, Z.*, et al.* (2008a). p53 and Pten control neural and glioma stem/progenitor cell renewal and differentiation. Nature *455*, 1129-1133.
Zheng, H., Ying, H., Yan, H., Kimmelman, A.C., Hiller, D.J., Chen, A.J., Perry, S.R., Tonon, G., Chu, G.C., Ding, Z.*, et al.* (2008b). Pten and p53 converge on c-Myc to control differentiation, self-renewal, and transformation of normal and neoplastic stem cells in glioblastoma. Cold Spring Harbor symposia on quantitative biology *73*, 427-437.
Zhu, J., Lum, P.Y., Lamb, J., GuhaThakurta, D., Edwards, S.W., Thieringer, R., Berger, J.P., Wu, M.S., Thompson, J., Sachs, A.B.*, et al.* (2004). An integrative genomics approach to the reconstruction of gene networks in segregating populations. Cytogenet Genome Res *105*, 363-374.
Zhu, J., Wiener, M.C., Zhang, C., Fridman, A., Minch, E., Lum, P.Y., Sachs, J.R., and Schadt, E.E. (2007). Increasing the power to detect causal associations by combining genotypic and expression data in segregating populations. PLoS Comput Biol *3*, e69-e69.
Zhu, J., Zhang, B., Smith, E.N., Drees, B., Brem, R.B., Kruglyak, L., Bumgarner, R.E., and Schadt, E.E. (2008). Integrating large-scale functional genomic data to dissect the complexity of yeast regulatory networks. Nat Genet *40*, 854-861.
Zhu, Y., Guignard, F., Zhao, D., Liu, L., Burns, D.K., Mason, R.P., Messing, A., and Parada, L.F. (2005). Early inactivation of p53 tumor suppressor gene cooperating with NF1 loss induces malignant astrocytoma. Cancer cell *8*, 119-130.

Curriculum Vitae

Christopher G. Hubert 19916 19th Ave. NE, Apt #202, Shoreline, WA 98155
(203) 545-3640
cghubert@u.washington.edu

EDUCATION

Ph.D., Molecular and Cellular Biology
University of Washington and Fred Hutchinson Cancer Research Center
Seattle, WA
November 2012
Research Advisors: James M. Olson (primary mentor)
Patrick J. Paddison (co-mentor)
Thesis title:
Identification of Cancer-Specific Essential Genes in Glioblastoma Multiforme
Dissertation Title:
Genome-wide RNAi screens in human brain tumor isolates reveal a cancer-specific requirement for PHF5A

B.S., Biomedical engineering
The Johns Hopkins University
Baltimore, MD
May 2003
Computer Engineering Concentration
Business and Entrepreneurship Minor

RESEARCH EXPERIENCE

Graduate Research Assistant
University of Washington and Fred Hutchinson Cancer Research Center
Seattle, WA
September 2006 – November 2012
Research Advisor: James M. Olson, MD, PhD

Research Assistant I, II
Brigham and Women's Hospital and Harvard Medical School
Boston MA
June 2003 – August 2006
Research Advisor: Jonathan A. Fletcher, MD

Research Assistant
The Johns Hopkins Medical Institute, Anesthesiology & Critical Care Medicine
Baltimore, MD
Sept 2000 – May 2003
Research Advisor: Randal O. Dull, PhD, MD

Undergraduate Research

The Johns Hopkins University, Biomedical Design Team Member
Baltimore, MD
Sept 1999 – May 2003
Research Advisor: Robert Allen, Ph.D.

SCIENTIFIC RESEARCH PUBLICATIONS

Hubert CG[†], Bradley RK[†], Ding Y, Toledo CM, Skutt-Kakaria K, Girard EJ, Davison J, Berndt J, Corrin P, Basom R, Delrow JJ, Webb TR, Pollard SM, Lee JW, Olson JM*, Paddison PJ*
Genome-wide RNAi screens in human brain tumor isolates reveal a novel viability requirement for PHF5A.
Manuscript submitted, Cancer Cell. 2012.

Ding Y, **Hubert CG**, Corrin P, Vazquez J, Baysom R, Zhang B, Risler JK, DeLuca J, Pollard SM, Delrow J, Zhu J, Olson JM, Paddison PJ.
A cancer-specific requirement for BUB1B/BubR1 in human brain tumor isolates and genetically transformed cells?
Cancer Discov. 2012 Nov 15. [Epub ahead of print] PMID: 23154965

Ou WB, **Hubert C**, Corson JM, Bueno R, Sugarbaker DJ, Fletcher JA.
Targeted Inhibition of Multiple Receptor Tyrosine Kinases in Mesothelioma.
Neoplasia. 2011 Jan;13(1):12-22.

Jarjour J, West-Foyle H, Certo MT, **Hubert CG**, Doyle L, Getz MM, Stoddard BL, Scharenberg AM.
High-resolution profiling of homing endonuclease binding and catalytic specificity using yeast surface display.
Nucleic Acids Research. 2009 Sept; doi:10.1093/nar/gkp726

Hubert CG, McJames S, Mecham I, Dull RO.
Digital Imaging System and Virtual Instrument Platform for Measuring Hydraulic Conductivity of Vascular Endothelial Monolayers.
Microvasc. Res. 2006 Mar; 71(2):135-40.

Dull RO, DeWitt BJ, Dinavahi R, Schwartz L, **Hubert C**, Pace N, Fronticelli C.
Quantitative assessment of hemoglobin-induced endothelial barrier dysfunction.
J. Appl. Physiol. 2004 Nov; 97(5):1930-7.

ABSTRACTS and PRESENTATIONS

Hubert CG, Hansen S, Stroud M, Olson JM
Tumor Paint distinguishes tumor from normal tissue in mouse models of skin cancer.
Joint Meeting of IPOS 14th World Congress and COSA's 39th Annual Scientific Meeting, Brisbane 2012

Hubert CG, Ding Y, Toledo CM, Berndt J, Olson JM[†], Paddison PJ[†]

A functional genetic approach in patient-derived glioblastoma stem cells reveals pre-mRNA splicing components to be cancer-lethal gene targets.
International Society of Pediatric Neuro-Oncology Meeting, Toronto 2012

Hubert CG,, Ding Y, Toledo CM, Berndt J, Olson JM†, Paddison PJ†
A functional genetic approach in patient-derived glioblastoma stem cells reveals pre-mRNA splicing components to be cancer-lethal gene targets.
American Association for Cancer Research, Annual Meeting, Chicago 2012

Hubert CG.
Identification of Synergistic Combination Therapies for Glioblastoma.
***Speaker** - Bear Necessities Pediatric Cancer Research Symposium 2010*
University of Chicago Medical Center, Chicago, Illinois

Hwang WY (student), **Hubert CG** (mentor), Paddison PJ, Olson JM.
Spindle check point targeted therapy for Glioblastoma.
National Conference on Undergraduate Research (NCUR)

Bauer S., **Hubert CG**., Oliveira A., Demetri GD., Fletcher JA.
MDM2 Therapeutic Potential in Soft Tissue Sarcoma.
12th Annual CTOS meeting, Venice, 2006.

Bauer S., Heinrich M., **Hubert CG**, Cohen R, Bertagnolli M, Demetri GD., Fletcher JA.
KIT hyperactivation in imatinib-resistant GIST: Implications for salvage therapies.
American Society of Clinical Oncology annual meeting, Orlando, 2005.

Hubert CG., Fletcher JA.
Oncogenic Signaling Inhibition of Imatinib-Resistant Gastrointestinal Stromal Tumors.
***Speaker:** BWH Pathology Research Seminar, 2004 Dec.*

Duensing A., Joseph N., Liu C., **Hubert CG**., Smith F., Heinrich M., Corless C., Fletcher CD., Fletcher JA.
Protein Kinase C Theta (PKCθ) is selectively expressed and constitutively phosphorylated in GISTs.
American Association for Cancer Research annual meeting, Orlando, 2004.

Hubert CG., Dull RO.
Design of a Computer Controlled Device for the In-Vitro Measurement of Transendothelial Fluid Flux.
Howard Hughes Summer Research Fellowship poster session, JHMI, Baltimore, 2002

Hubert CG., Dull RO.
Redesign of an In-Vitro System for Transendothelial Fluid Flux Measurement.
Howard Hughes Summer Research Fellowship poster session, JHMI, Baltimore, 2001

TEACHING AND MENTORING EXPERIENCE

Undergraduate Research Mentor
Fred Hutchinson Cancer Research Center

FHCRC Cancer Research Internship Program
Woong Hwang, Rochester University - Summer 2010 – Award winner
Mac Staben, Middlebury College - Summer 2010
Stephanie Silva del Toro, University of Puerto Rico - Summer 2011 – Award winner

Science and Education Partnership
Fred Hutchinson Cancer Research Center
Madonna Brinkman, SEP teaching partner
Summer 2008

Teaching Assistant
University of Washington
Foundations in Molecular Cell Biology
Professor: Merrill B. Hille, PhD
Fall 2007

GRANTS AND FELLOWSHIPS

NIH Interdisciplinary Training Grant in Cancer Research, *2011 – 2012.*
NIH Interdisciplinary Training Grant in Cancer Research, *2009 – 2011.*
Howard Hughes Summer Research Fellowship, *2002.*
Howard Hughes Summer Research Fellowship, *2001.*

GENERAL SCIENCE PUBLICATIONS

Hubert CG.
Tumor Painting - A toxin from scorpion venom combined with a fluorescent beacon specifically lights up a variety of cancers.
Northwest Science & Technology, Fall 2008, www.nwst.org

Hubert CG.
A Tiny Bit of Caution - A look at the potential hazards of nanotechnology.
Northwest Science & Technology, Fall 2008, www.nwst.org

HONORS AND AWARDS

Research Finalist - Bear Necessities Pediatric Cancer Foundation - 2010
Dean's List academic honors, The Johns Hopkins University - Fall 2002, Spring 2003
Eagle Scout, Assistant Scoutmaster - Boy Scouts of America